Order Number 9312191

A near-infrared faint galaxy survey: Evolution and the cosmological geometry from K band photometry

Gardner, Jonathan Perry, Ph.D.

University of Hawaii, 1992

U·M·I

300 N. Zeeb Rd.
Ann Arbor, MI 48106

A NEAR-INFRARED FAINT GALAXY SURVEY: EVOLUTION AND THE COSMOLOGICAL GEOMETRY FROM K BAND PHOTOMETRY

A DISSERTATION SUBMITTED TO THE GRADUATE DIVISION OF
THE UNIVERSITY OF HAWAII IN PARTIAL FULFILLMENT OF
THE REQUIREMENTS FOR THE DEGREE OF

DOCTOR OF PHILOSOPHY
IN
ASTRONOMY

DECEMBER 1992

By
Jonathan Perry Gardner

Dissertation Committee:

Lennox L. Cowie, Committee Chair
Esther M. Hu
Kenneth C. Chambers
Alan Tokunaga
Paul G. Lucey

Acknowledgments

The relationship between a student and his thesis advisor is a very close one, involving guidance both in the professional and personal domains. I have had the very good fortune to share this relationship with two very intelligent and kind hearted men, beginning with Simon Lilly from 1987 to 1990, and continuing with Len Cowie who saw me through to the completion of this project. I thank them both.

I would like to thank Alan Stockton for being on my committee from the beginning to just a few months before my defense. I wish to acknowledge the contributions of Richard Wainscoat who is a co-investigator on the Hawaii Wide Survey project. We spent many cold nights together observing on Mauna Kea and I have come to think of him as a friend as well as a colleague. Observing on large telescopes is made infinitely easier with the help of competent telescope operators, and I would like to thank Dave Woodworth, Steve Massey and Frank Cheigh of the UH 2.2 meter telescope for all the help they have given me. While very little data taken on UKIRT has made it into this thesis, I have very fond memories of observing with Delores Walther in the early days of the Hawaii Deep Survey. I have used the *zodiac* image processing package to process my data, and I owe a tremendous debt to George Miyashiro, who wrote the package and has kept it running through thick and thin. I also would like to thank Pui Hin Rhoads for keeping the computers running smoothly.

The secretaries at the Institute For Astronomy have always demonstrated the highest levels of professionalism, and several times have stood between me and disaster. By doing everything from helping me to track down Len to replacing my plane tickets when my backpack was stolen, they have contributed immensely to my

success here. I would particularly like to thank Georgette Albert, Diane Tokumura, Nancy Lyttle, Barbara Flaska and Craig Drose. Jill Kajikawa-Kent has also always been a smiling face in the hallways.

The greatest contribution to this thesis and to my life here for the last six years has come from my friends, classmates and officemates, Mike Rigler and Jim Annis. We have spent countless hours, day and night, discussing everything from cosmology to our latest girlfriend problems, and doing everything from sharing computer code to brewing beer. Together we have changed from naive gradlings to professional astronomers, suffering through starvation wages, crazy roommates, and uncaring professors, while sharing the joys of pure intellectual discovery.

And last but by no means least, I would like to thank the many other people who have chosen to share their lives with me during my stay in Hawaii, including: Alex Storrs, Angel Gardner, Barbara Polk, Barbara Wong, Beth Clark, Bev Neese, The Cast-Offs, Christa Gardner, Dan Gardner, Danger Mouse, Daniel Cole and Stephen Fleming, Dave Wall, Dawn Pang and Kip McAtee, Debbie and Larry Ward, Dick and El Burson, Didi-Sprite --,-'-<@, Doug Bergerson, Doug Simons, Ed Rosenthal, Elbereth, Erin Bennett, Gillian Nan, Hua Chen, Inge Heyer, Janet Moelzer, Jim Deane and Debbie Maraziti, Joe Piscitelli, Joyce Terashima and Ray Baker, Kathleen Robertson, Katrina Porter, Keoni Wagner, kitten, Lauri Saiki, Lesley Friedman, Lily Cheng, Marcia Kemble, Marcia Nelson, Matt Penn, Merritt and Ruth Ann Gardner, Mike Pierce, Mike Ressler, Patty Iwamoto, Phil Hidalgo, Ron Fitch, Russ Lavery, Stephanie Pang, Terry Friedman, Tim Gardner and Michelle Rago, TJ, and Tom and Lisa Brady.

Abstract

The results of four K band surveys of the extragalactic sky are presented. Each survey was designed to balance depth with area of coverage, and a sufficient number of galaxies was studied at each magnitude from K = 12 to K = 22 to provide good statistics. Each survey area was also observed in the B and I bands. Methods for making long exposures in the near-infrared and optical are described. The K band number counts are compiled. The excess seen in the B band number counts is not seen in the K band number counts, and a change in slope is seen in the K counts at K = 17. The number count data are shown to be consistent with the measured B-K color, as the K band selected sample becomes rapidly bluer after turning over at K = 17. The I-K colors are presented and it is argued that there is a deficiency of galaxies with the colors of unevolved ellipticals at z = 1. The B-K colors are shown to move away from the no-evolution model beginning at K = 17. The position of the galaxies on the B-I vs I-K plot are consistent with these arguments. The surface brightness of the galaxies is analyzed and it is argued that variation in surface brightness causes no systematic bias in the number count data. Various aspects of the data are compared with models of primeval galaxies and galaxy evolution. The K band number counts are compared with a model of pure luminosity evolution, a cosmological constant model and a merging model. It is argued that the merging model is the best explanation for all of the data, although the model needs to be modified before it will provide a good fit to the number counts.

Table of Contents

List of Tables

List of Figures

Preface

Kumulipo

O ke au i ka huli wela ka honua,
O ke au i ka huli lole ka lani,
O ke au i kuka'iaka ka la,
Ho'omalamalama i ka malama,
O ke au o Makali'i i ka po,
O ka walewale ho'okumu honua,
O ke kumu o ka lipo, i lipo ai,
O ke kumu o ka po, i po ai,
O ka lipolipo, o ka lipolipo,
O ka lipo o ka la, o ka lipo o ka po,
Po wale ho'i hanau ka po,
Hanau Kumulipo i ka po, he kane,
Hanau Po'ele i ka po, he wahine.

At the time when the Earth became hot,
At the time when the Heavens turned about,
At the time when the sun was darkened,
To cause the moon to shine,
At the time of the rising of the Pleiades,
The slime, this was the source of the Earth,
The source of the darkness that made darkness,
Darkness of the sun, darkness of the night,
Nothing but night, the night gave birth,
Born was Kumulipo in the night, a man,
Born was Po'ele in the night, a woman.

Chapter 1: Introduction

From the first person who rose above the struggle of day to day existence and looked up at the stars, mankind has sought to find the meaning and history of life in the universe. Although the explanations in the past were frequently wrong, the quest for answers has satisfied a yearning that is a fundamental part of our psychological makeup. While the answers and explanations that scientists come up with today may be no more closer to fundamental truth than those of the past, they nonetheless have a profound impact upon the philosophical life of humanity.

The question of how the universe came into being and how it evolved into its present state is one of the most important problems on which an astronomer can work. The study of the early universe is the realm of the particle physicists, the relativity theorists, and satellites such as COBE which probe the sky for the faint cold remnants of the big bang. The evolution of the universe from the time that the first galaxies formed until the present day can be studied from the ground. Studying distant galaxies is also the way to measure the cosmological geometry, for the very early universe is too uniform for measurements to be made, and the galaxies of the local universe are not uniform enough for the subtle effects of geometry to be seen.

Field galaxies hold the key to understanding galaxy evolution, and the near-infrared holds the key to understanding field galaxies. While objects such as radio galaxies and quasars can be found and studied at very high redshifts, their unusual nature makes it difficult to draw conclusions about the universe as a whole. Similarly, the environment within clusters of galaxies dominates larger scale effects, and the study of the galaxies within clusters, while important, is not the way to describe the average properties of the universe.

Field galaxies, defined to be those galaxies which are not part of rich clusters, do not have unusual radio emission, and are not dominated by quasar

nuclear activity, make up the bulk of the universe. They are common enough that one can point a telescope anywhere out of our galaxy and get large numbers of objects in a relatively short time. However, field galaxies are generally fainter than the unusual objects mentioned above, and are thus more difficult to find and to observe at high redshift. To potentially reach field galaxies at the high redshifts at which radio galaxies and quasars are routinely studied requires exposures of many hours on the world's largest telescopes.

Studies of galaxy evolution and the cosmological geometry are statistical in nature, and it is critical that the data be uniform and free from selection biases. Ideally one wants a similarly selected sample that spans a wide range in redshift, so that one can compare the properties of high redshift galaxies with those of low redshift galaxies selected in the same way. In practice this is difficult to do, as the very effects one wishes to study can bias the sample selection. The goal thus becomes to select the sample on the basis of properties which are expected to change very little with time. Radio power and quasar nuclear activity occur on very short timescales, and the alignment effect observed between the optical and the radio axes in radio galaxies indicates that many of the properties of these objects are directly affected by these short timescale processes. (Chambers, *et al.*, 1987).

Similarly, light emitted in the blue and ultraviolet is dominated by short-lived massive stars. A burst of star formation can change the blue and ultraviolet brightness of a galaxy in a few million years, and the evolution of the massive stars will continue to change the color as time goes on. The light in the near-infrared, for non-starburst galaxies, is produced by stars similar to our sun, which have lifetimes comparable to the age of the galaxy. Thus a sample selected in the near-infrared changes little with time, and objects at high redshift can be compared to those at low redshift with little selection bias.

At high redshift, the near-infrared samples the well-understood rest frame optical part of the spectrum, while at high redshift the optical samples the poorly understood rest frame ultraviolet. In the near-infrared, the *K* corrections (the changes to measured broad-band magnitudes due to the redshift of the spectral energy distribution,) are much smoother and better understood than in the optical. (Coleman, *et al.*, 1980). The expectations for galaxy evolution provided by the models of chemical evolution in galaxies show that the near-infrared evolution is smoother and operates on a longer time scale than that of the optical. (Arimoto and Yoshii, 1986). Thus the ideal field galaxy survey selects the objects for study based upon their near-infrared magnitudes, and then examines the optical and optical-infrared colors of this sample for the effects of evolution. Follow-up studies obtaining spectroscopic redshifts are also important for separating the effects of evolution and cosmological geometry.

Until the arrival of array detectors it was very difficult to do a near-infrared survey. Most early field galaxy survey work was done in the optical, beginning with photographic plates, (*e.g.*, Koo, 1981, Shanks *et al.*, 1984), and continuing to very faint levels with CCD cameras, (*e.g.* Tyson, 1988, Lilly *et al.*, 1991). This survey work was followed up by spectroscopic redshift surveys of samples selected in the blue. (Peterson *et al.*, 1986, Broadhurst *et al.*, 1988, Colless *et al.*, 1990, Cowie *et al.*, 1991). One notable exception to the early work in the optical was the work of Mobasher *et al.*, (1986), who observed a sample of objects selected in the optical with near-infrared single point detectors. This survey, however, was limited to relatively bright galaxies, and while the data is useful in tying down the local near-infrared properties of galaxies such as the luminosity function, it does not go deep enough to observe any cosmological effects. Currently, however, using infrared array detectors, it is possible to conduct a survey of objects selected in the near-infrared.

This thesis presents the results from four surveys designed to cover the magnitude range from the near-infrared completeness limit of the Mobasher *et al.*, (1986) data to the faintest limits that have yet been observed. Each survey is limited at the bright end by the small number of bright galaxies in the area covered, and at the faint end by the photometric effects of noise. The four surveys are the Hawaii Wide Survey (HWS), which covers 1.58 square degrees to a depth of K = 15, the Hawaii Medium Wide Survey (HMWS), which covers 580 square arcminutes to a depth of K = 17, the Hawaii Medium Deep Survey (HMDS), which covers 170 square arcminutes and goes as deep as K = 19, and the Hawaii Deep Survey (HDS) which covers 16.5 square arcminutes and goes as deep as K = 23. The HDS results have been presented elsewhere (Cowie *et al.*, 1992); the results of the other three surveys are being presented here for the first time. These four surveys, taken together with the Mobasher *et al.*, (1986) data, provide a sufficient number of galaxies for good statistics in each magnitude bin from K = 10 to K = 23, and represent a comprehensive examination of the near-infrared extragalactic sky.

The K band, centered at 2.2 μm wavelength, cuts off just shortward of the thermal infrared, and thus is the reddest band at which is it possible to work without very high background levels. It is also redward of the majority of the atmospheric OH emission which dominates the J and H bands. The redness of most galaxies makes it possible to observe to greater distances in the K band than in J and H. The filters selected for the HWS, the HMWS and HMDS, B (4400 ± 980 Å), I (9000 ± 2400 Å), and K' (2.11 ± 0.18 μm, Wainscoat and Cowie, 1992), cover nearly the whole optical-infrared atmospheric window and are evenly spaced in wavelength. The HDS used U' (3400 ± 150 Å), B, V (5500 ± 890 Å), I and K'. The HWS was done on the University of Hawaii's 0.6 meter Planetary Patrol telescope, with a NICMOS3 256x256 infrared detector, and an optical CCD camera. The

HMWS and the HMDS were done with the UH 2.2 meter telescope, with the same equipment. The HDS is an ambitious observational program begun in 1987, using optical CCDs and the NICMOS3 camera on the UH 2.2 meter telescope and CFHT, and IRCAM on UKIRT. In addition, observations have been made on one of the HDS fields with the Hubble Space Telescope.

In this thesis I will begin in chapter 2 by giving a detailed review of other field galaxy surveys, both photometric and spectroscopic. As field galaxy survey work was often motivated by the search for primeval galaxies, I will also review the theoretical models of primeval galaxies. Then I will discuss the early results of the HDS, leading up to the report in Lilly *et al.*, (1991) of the optical survey results. I will describe in chapter 3 the selection of the fields for the Hawaii surveys, the observations for the HMWS and the HMDS, the image processing techniques, the object identification and catalog preparation, and the star/galaxy separation. I will report in chapter 4 the HDS K band and spectroscopic redshift survey results. I will discuss in chapter 5 the K band number counts, in the light of B band counts and spectroscopic redshift survey results. In chapter 6, I will analyze the survey color data, discuss the effects of surface brightness on the sample selection, and discuss various theoretical models of the number count and color data. Finally I will discuss how future observations could further increase our understanding of galaxy evolution and the cosmological geometry.

References for Chapter 1

Arimoto, N., and Yoshii, Y., 1986, *Astron. Astrophys.*, **164**:260.

Broadhurst, T.J., Ellis, R.S., and Shanks, T., 1988, *M.N.R.A.S.*, **235**:827.

Chambers, K.C., Miley, G.K., and van Breugel, W., 1987, *Nature*, **329**:604.

Coleman, G.D., Wu, C.-C., and Weedman, D.W., 1980, *Ap. J. Supp.*, **43**:393.

Colless, M., Ellis, R.S., Taylor, K., and Hook, R.N., 1990, *M.N.R.A.S.*, **244**:408.

Cowie, L.L., Songaila, A., and Hu, E.M., 1991, *Nature*, **354**:460.

Cowie, L.L., Gardner, J.P., Hu, E.M., Wainscoat, R.J., Hodapp, K.W., 1992, *Ap. J.*, *submitted.*

Koo, D.C., 1981, *Ph.D.* thesis, University of California, Berkeley.

Lilly, S.J., Cowie, L.L., and Gardner, J.P., 1991, *Ap. J.*, **369**:79.

Mobasher, B., Ellis, R.S., and Sharples, R.M., 1986, *M.N.R.A.S.*, **223**:11.

Peterson, B.A., Ellis, R.S., Efstathiou, G., Shanks, T., Bean, A.J., Fong, R., and Zen-Long, Z., 1986, *M.N.R.A.S.*, **221**:233.

Shanks, T., Stevenson, P.R.F., Fong, R., and MacGillivray, H.T., 1984, *M.N.R.A.S.*, **206**:767.

Tyson, J.A., 1988, *A.J.*, **96**:1.

Wainscoat, R.J., and Cowie, L.L., 1992, *A. J.*, **103**:332.

Chapter 2: Historical Overview

Until the advent of infrared array detectors, studying the statistical properties of galaxies in the infrared was a difficult task. Random surveys are prohibitively expensive in telescope time when done with single point detectors, unless objects of interest are sufficiently well separated that very low spatial resolution can be used. While this is true for galaxies in the radio, and to some extent in the far infrared, in the near infrared the high density of stars relative to galaxies at the magnitudes in which a low resolution random survey can be done means that it is not a very useful exercise. Thus, with the exception of the attempts by Collins and Joseph (1988) and by Boughn *et al.* (1986), all early work studied the infrared properties of samples selected at other wavelengths.

Lilly and Longair (1982, 1984) measured the K magnitudes of a complete sample of radio galaxies from the 3C catalog. Their most surprising and important result was that the infrared Hubble diagram, K magnitude vs. redshift had very low dispersion, only 0.4 magnitudes, over a range of 6 magnitudes in K and from $z = 0.05$ to $z = 1.7$. Others (*e.g.* Lilly *et al.*, 1985, Rigler *et al.*, 1992) have extended this work to lower power radio sources, and to higher redshifts, and find that the low dispersion continues. However, there are indications that this is part of the nature of radio galaxies, and not an aspect of galaxies in general. The radio source in a galaxy is a very short-lived phenomenon, and there is interaction between the radio source and the stars, as is evidenced by the alignment between the radio emission and the optical, and to a lesser extent, the infrared light. While radio galaxies are worthy of study in their own right, and while they do represent the most distant stellar populations currently visible, their very specialized nature makes it difficult to draw cosmological conclusions. To determine the overall properties of the

universe, it is necessary to pursue the much more difficult task of finding and studying field galaxies.

In the optical, even prior to the advent of CCD cameras, photographic plates could be used with Schmidt cameras to cover large areas. An early project which managed to study a sample of field galaxies in the near infrared was the work of Mobasher *et al.* (1986). They obtained J, H, and K magnitudes of a complete sample of 194 galaxies selected at B = 17, and having the tremendous additional advantage of measured redshifts (Peterson *et al.*, 1986). They primarily analyzed the infrared and optical-infrared color-luminosity relations; however, their data contains several other results which are of interest to the present work. The sample is selected in B, but contains every galaxy brighter than the B limit, and is a complete K sample up to the limit of the reddest galaxy in B-K. The reddest galaxy in the K selected sample of the Hawaii Wide Survey at K < 13 has B-K ≈ 4.86, and thus one can consider the Mobasher *et al.* (1986) sample as a nearly complete K selected sample to K = 12.5. Analyzed in this way, there are several interesting results in the data which have not been discussed. Number counts are easily constructed, and are useful in the region from K = 10 to K = 12.5. This is discussed in Chapter 5. In addition, by combining the redshift data with the measured infrared magnitudes it is possible to construct an infrared luminosity function. And finally, the color information (B-K) can be used to establish the bright end of the trends seen in my data. In all, although it has not yet been analyzed as such, the Mobasher *et al.* (1986) data set is a K band selected sample, approximately 85% complete, covering 41.56 square degrees to a depth of K = 12.5.

I. Primeval Galaxy Models and Observational Searches

Early survey work was motivated by a theoretical model of dust-free protogalaxies developed by Partridge and Peebles (PP, 1967). Eggen, Lynden-Bell and Sandage (1962) analyzed the orbits and metallicities of old stars in our galaxy and argued that the majority of the stars formed in a very short period of time. PP extended this argument to construct a general model for forming galaxies, and to determine how forming galaxies would appear in observations. In the PP model, galaxies form through the collapse of overdense regions, pass through a very luminous phase in which the majority of the stars are formed, and appear as large, bright objects at high redshift. The earliest searches for these objects were conducted by Partridge (1974) and Davis and Wilkinson (1974). They searched 5.5 square arcminutes in the optical red wavelength region 6200-8900 Å for objects 10 to 30 arcseconds in diameter, but found none to a depth of 40 Jy, or approximately R = 19.5. These data ruled out models in which galaxies formed at $z < 6$, although they did not test modifications of this theory in which galaxies have smaller angular sizes and luminosities.

Koo and Kron, (1980) conducted a Lyman α search using slitless spectroscopy, again in the 6000-9000 Å wavelength region, looking for the expected bright Lyman α line at a redshift of $z = 4$ to $z = 6$. They also had a negative result, with a much stronger limit (4 μJy, corresponding approximately to R = 22), and also ruled out compact objects fitting the model. Pritchet and Hartwick (1990) used a narrow band (100 Å) filter tuned to detect Lyman α at a redshift of $z = 1.9$, combined with broad band U to cover 360 square arcminutes. They also had a negative result to a detection depth of 27.6 mag arcsec^{-1}, for a pure emission line source, and about 2.5 magnitudes brighter for a source similar to the emission-line radio galaxy 3C326.1. This survey, although tuned to a very narrow redshift region, is

nonetheless sensitive to a wide range of galaxy formation models, because galaxies that began to coalesce as early as $z = 7.5$ could still be in their luminous phase at $z = 1.9$. There are two possible conclusions that can be drawn from this data. If the majority of galaxy formation is at very low redshift, i.e., $z < 2$, or at very high redshift, $z > 7.5$, then this survey would not have detected it. The other, more likely explanation, is that Lyman α emission from primeval galaxies is not observable, either because it is not being produced, or because it is being absorbed by dust. While radio galaxies have strong Lyman α emission at these redshifts, it could be directly related to the radio emission and therefore not present in primeval field galaxies. (For discussions of the alignment effect between the radio jets and the Lyman α emission, see *e.g.* Chambers *et al.* 1987, and Rigler *et al.*, 1992). The Lyman α emission could also be absorbed by dust either in the galaxy, or in the intergalactic medium. This will be discussed below.

Thompson *et al.* (1992) have begun a Lyman α survey using a Fabry-Perot interferometer tuned to four different wavelength regions, corresponding to $z = 2.6$, $z = 3.3$, $z = 4.4$ and $z = 4.8$ for Lyman α. They have made no detections yet, although they have only surveyed about 100 square arcminutes in more than one redshift region. They are also pursuing an additional survey by examining the off-source regions of long slit spectroscopic frames for serendipitous discoveries. Although the field coverage is small, typically a slit coverage of 2 arcseconds by 2 arcminutes per exposure, the piggy-back nature of this survey results in a lot of data being examined. They have so far examined about 50 one-hour exposures and found a dozen objects, mostly moderate redshift star forming or mildly active galaxies, possibly corresponding to the faint blue galaxy population discussed by Tyson (1988), Cowie *et al.* (1991, 1992) and in this thesis.

Several other techniques have been used in attempts to detect large red PP primeval galaxies in the optical. Matilla (1976) used a dark cloud in our galaxy to provide a foreground reference against which to observe the unresolved background radiation at 4000 Å. His results caused much excitement as they suggested that primeval galaxies could be as bright as B < 20, however, further studies by Dube, *et al.*, (1977, 1979), Spinrad and Stone (1978), and Toller (1983), using similar and different techniques showed that Matilla's (1976) measurement was an order of magnitude too high. The later experiments reached an upper limit of 3×10^{-8} W, which is below the predictions of formation models with $z_{form} < 5$.

With low redshift PP protogalaxies seemingly ruled out (Koo, 1986a), attention then turned to the infrared, as PP had predicted that protogalaxies would have their peak emission in the 1 to 3 μm wavelength region, because of high redshift of formation. If the protogalaxies are dark in the Lyman continuum, galaxy formation at redshifts greater than 8 would not be detected in the visible region, but Lyman α would not pass out of the K band, for example, unless z > 20. Collins and Joseph, (1988) searched two optically blank fields totalling 0.36 square arcminutes in J and K with a photometer for ultrared extended objects. Reaching 33 μJy, or K = 16.2, they detected a single object having the colors of a normal spiral galaxy. This negative result began to constrain the PP model in the infrared. A very similar survey was conducted at about the same time by Boughn, *et al.*, (1986), which achieved a very similar negative result.

It is interesting to consider the large red primeval galaxy model of PP in light of the current K band number counts. Early researchers often used a very optimistic set of assumptions to justify surveys using their limited capabilities. Lilly and Cowie (1987), however, constructed a model which is fairly independent of assumptions of cosmological geometry and timescale of star formation by assuming that a primeval

galaxy will have the flat spectrum ($f\nu \propto \nu^{-1}$) characteristic of an unreddened young stellar population.

In the initial star bursting phase of the PP model, the majority of the metals in the universe were produced, and this metal production by stellar nucleosynthesis would have produced a surface brightness on the sky of

$$S_{bol} = ((0.007)\ \rho_L\ c^3\ \Delta x)\ /\ (4\ \pi\ (1+z_{form}))\ ergs^{-1}\ cm^{-2}\ sr^{-1},$$

where z_{form} is the redshift of galaxy formation, ρ_L is the density of material processed by fusion to produce a mass fraction Δx of metals. Assuming that the primeval galaxies have a flat spectrum, the K band surface brightness is independent of z_{form} unless $z_{form} > 20$ and Lyman α has passed out of the K band. The K surface brightness is then

$$S_K = 7.2 - 2.5\log(\Omega_L/0.1) - 2.5\log(\Delta x/0.01)\ magnitudes\ deg^{-2},$$

where Ω_L corresponds to ρ_L, and Δx has been normalized. This surface brightness defines a line on the number count diagram along which an appropriate luminosity function would slide, depending upon the specifics of the model, such as z_{form}, the cosmological geometry, and the duration of the starbursting phase. Geometry gives the number density of the progenitors of objects with present density n_0 for $q_0=0.5$:

$$N(deg^{-2}) \approx 625\ (1+z_{form})\ (n_0/(0.002\ Mpc^{-3}))\ h^2\ (\Delta t/10^8\ yr)$$

where h is H_0 in units of 100 km s^{-1} Mpc^{-1}. Figure 2.1 is the K band galaxy number counts, discussed in greater detail in Chapter 5, with this model plotted.

In this model, the predicted number of primeval galaxies is lower than the number of normal galaxies for $K < 20$, and so a very important consideration is whether we can recognize them for what they are. In the surveys discussed in this thesis, there are no large ultrared objects of the kind predicted by PP to be primeval galaxies at high redshifts ($z > 7$). If we assume that this failure to find primeval galaxies means that they are not there (i.e., primeval galaxies do not appear to have

the colors of normal galaxies or stars), then we have placed a much stronger constraint on the model. Also plotted in Figure 2.1 are the upper limits implied by the failure to find primeval galaxies in the area covered at each magnitude bin.

One assumption of the PP model as commonly used, is that primeval galaxies are relatively dust free. There are several reasons for the plausibility of this assumption, including the fact that quasars are relatively unobscured to high redshift. Radio galaxies show strong Lyman α emission at high redshift, and show little evidence for dust. The first stars to form must have formed in a dust free environment, for it takes stars to make the metals which make up the dust, although this phase could have been as short as the lifetime of massive stars, 2-5 x 10^7 years. However, the failure of optical and near infrared surveys to find primeval galaxies of the PP model type could be because they are totally enshrouded by dust. This would cause them to emit most or all of their energy as a blackbody at 30K, with the peak being at 100 μm in the rest frame. Most, or all, of the low redshift starburst regions are dusty (Djorgovski, 1992), although IRAS starbursters show multiple nuclei, and thus are probably collisions of pre-existing enriched galaxies, rather than low-redshift analogs of primeval galaxies.

Djorgovski (1992) analyzed the possibility that primeval galaxies are radiating all of their energy in the far infrared, due to obscurement by dust. The energy produces a surface brightness on the sky which would be approximately 1% of the cosmic microwave background radiation (CMBR) at the wavelengths sampled by the COBE FIRAS experiment. The upper limit which COBE has currently set on such an excess is < 0.3%, and will be extended to < 0.1% when all of the expected data has been analyzed. Even with the most liberal assumptions, that the excess due to primeval galaxies mimics the shape of the CMBR in these wavelengths and does not have a distinctive peak, the maximum energy density allowed just barely

fits the estimated density from primeval galaxies. Under more realistic assumptions, the model is ruled out. Thus it appears unlikely that primeval galaxies are entirely enshrouded by dust. However, the possibility remains that they are partially enshrouded, or that some, but not all primeval galaxies are entirely enshrouded.

It may appear from this recitation of upper limits and negative results that primeval galaxies do not exist, despite the fact that this is an absurd statement. However, it must be emphasized that the results are often very model dependent, and models exist which are not ruled out by the present data. The optical identification of the radio galaxy 3C326.1 at z = 1.8 (McCarthy *et al.*, 1987) caused much excitement as it was thought to be a protogalaxy candidate. While the K band photometry now shows there to be a substantial old star population (Lilly and McLean, 1989), the original discovery that the Lyman α emission represented a star formation rate of 300 M_{sol} prompted Baron and White (1987) to construct an inhomogeneous dissipative collapse model which would produce protogalaxies which looked like 3C326.1. Their model has two significant deviations from the previous models. First, they cut off the bright phase of star formation at the time of collapse, rather than beginning it there, causing the primeval galaxy to be fainter. Secondly, the inhomogeneous nature of their model causes primeval galaxies to be clumpy and extended, as is 3C326.1, resulting in low surface brightness, and the likelihood that the primeval galaxy would be mistaken for a small cluster of galaxies rather than a single one.

Cowie (1988) constructed a simple model representing the faintest apparent magnitude that a flat spectrum primeval galaxy could be by calculating the luminosity resulting from metal production as a function of star formation rate. The equations he used were:

$$F_\nu = 2.5 \times 10^{29} \text{ ergs/s Hz } ((dM/dt)/100\ M_{sol}\ yr^{-1})$$

$$m_K = 2.5 \log (F_\nu(1+z)/4\pi\, d_l^2\, f_{\nu 0K})$$

where (dM/dt) is the star formation rate, d_l is the luminosity distance (Lang, 1980):

$$d_l = (cz/H_0)(1 + z(1-q_0) \,/\, [(1+2q_0)^{1/2}+1+q_0 z])$$

and $f_{\nu 0K} = 6.5 \times 10^{-21}$ ergs s^{-1} cm^{-2} Hz^{-1} is the K band zero point.

These equations are plotted in figure 2.2, for (dM/dt) = 100 M_{sol}/yr, and for the minimum flux case where 10^{11} h^{-2} M_{sol} are produced in the Hubble time at that epoch, $t(z)h^{-1}$. Cowie (1988) took this figure to be encouraging, arguing that in the flat universe, low H_0 case primeval galaxies are sure to appear in the Hawaii Deep Survey (HDS), and that even with a more pessimistic choice of parameters it is likely that the HDS I band images would contain them. However, another point that can be taken from this figure is that the apparent magnitude of a primeval galaxy is very dependent upon q_0 and H_0, and that there is a wide choice of models in which they are too faint to be observed. Additionally, as Cowie (1988) points out, because the magnitude varies slowly with redshift, the colors of a high z population might be difficult to distinguish from a low z population, at least until Lyman α passes through the bandpass. This is particularly true for q_0=0.5. In this case, a population of high redshift primeval galaxies could have already been observed at the faintest levels, but not yet been identified.

In summary, there are a wide range of primeval galaxy models, predicting everything from bright extended red objects to faint compact blue ones. However, various observational programs, including this one, are beginning to put strong constraints on some of the models, and it appears likely that the field is close to making an unambiguous discovery of a population of primeval galaxies. This will come either through the spectroscopic identification of a flat spectrum object at high redshift, or, more subtly, through statistical arguments about a moderately high redshift active star forming population.

II. Photometric and Spectroscopic Surveys

Early optical photometric surveys, and indeed all photometric surveys seeking to cover large areas, use photographic plates on Schmidt telescopes. Photographic plates, although suffering from small dynamic range and non-linearity effects, have a much higher resolution than CCD cameras, and can therefore cover a much wider area without resorting to mosaicing. Digital scanning of the plates allows the data to be subsequently analyzed by computer, thus removing the bias which arises when human perception is involved. Photometric surveys are also often done as a preliminary step to obtaining data at other wavelengths, such as infrared or radio, and to obtaining spectroscopic redshifts. Although current CCD technology allows observers to go much deeper photometrically than spectroscopically, this was not always true for early observers.

The widest field surveys are the all-sky compilations of bright galaxies, such as the *Third Reference Catalogue of Bright Galaxies* (de Vaucouleurs *et al.*, 1991,) in which data on galaxies selected by analysis of the Palomar all-sky survey are compiled from the literature. Next comes the catalogs of galaxies still selected by scanning the Palomar survey, but for which additional data has been taken. The *Nearby Galaxies Catalog* (Tully, 1988) is an example of this, and was construction to aid in the measurement of H_0. Next there is the Center For Astrophysics redshift survey (CFA, Huchra *et al.*, 1983), which covered 2.7 steradians of the northern sky to a detection depth of 14.5, and obtained redshifts for about 2400 galaxies. This survey is useful for the investigation of large-scale structure, and the construction of the nearby luminosity function.

Two early photometric/spectroscopic surveys are the Durham-AAT redshift survey (DARS, Peterson *et al.*, 1986), and the survey of Kirshner *et al.* (KOS, 1978.

1979, 1983). These surveys, extending to approximately B = 17, and covering 70 and 12 square degrees, respectively, for the first time reached beyond the large local inhomogeneities to sample the statistical properties of the universe as a whole, while not yet reaching far enough to be effected by evolution. Thus they were ideally suited to determine the non-evolved luminosity functions for various types of galaxies in various bandpasses. Efstathiou *et al.*, (1988) determined that both the DARS data and the KOS data fit a Schechter luminosity function when analyzed with a maximum-likelihood estimator for a spatially inhomogeneous distribution where luminosity is uncorrelated with position. They determined, however, that the CFA data do not fit a Schechter function, and attributed this to errors of order 0.4 magnitudes in the photometry.

The Schechter luminosity function for galaxies has the form

$$\phi(L)dL = (\phi^* L^{\alpha})\exp(-L/L^*)dL$$

where ϕ^*, α, and L^* are free parameters. It is also written as a function of M^*, the absolute magnitude corresponding to L^*, or, equivalently, B^* or K^*, representing the absolute magnitude in a particular bandpass. Efstathiou *et al.* (1988) fit the luminosity function for all galaxies in the DARS B band data with a Schechter function of $B^* = -19.68 \pm 0.10$, $\alpha = -1.07 \pm 0.05$, and $\phi^* = (1.56 \pm 0.34)\times10^{-2}$ h^3 Mpc^{-3} for $H_0 = 100h$ km/sec/Mpc. Loveday *et al.*, (1992), analyzing the Stromlo-APM redshift survey data got a slightly lower value for ϕ^*, and, significantly, measured very different functions for E/S0 galaxies than for spirals. For E/S0, they measured $\alpha = 0.20 \pm 0.35$, $B^* = -19.71 \pm 0.25$; and for spirals they measured $\alpha = -0.80 \pm 0.20$, and $B^* = -19.40 \pm 0.16$. Their normalization for all galaxies is $\phi^* = (1.40 \pm 0.17)\times10^{-2}$ h^3 Mpc^{-3}. Although Efstathiou *et al.* (1988) saw some evidence for different luminosity functions for E/S0 galaxies and for spirals, their data were not extensive enough to measure it.

Kron (1980), Tyson and Jarvis (1979), Shanks *et al.*, (1984), and Koo (1986b) were some of the groups which used photographic plates to get photometry deeper than the Palomar sky survey, and to analyze the number counts of faint galaxies. In the mid 1980s an excess in the number of galaxies over the models was seen beginning at B=21 and continuing with no turnover to as faint as was then being observed. This trend continues even in the faintest counts made today, at B=27. (Tyson, 1988, Lilly *et al.*, 1991). This excess will be discussed in more detail, and in the light of new data, in chapters 4, 5 and 6.

With the advent of CCD array cameras which are linear over a large dynamic range it became possible to coadd exposures taken on different nights, and thus to reach unprecedented depths photometrically. Tyson (1988) conducted a survey of 130 square arcminutes in B, R and I that reached a high signal-to-noise galaxy detection depth of B=27, and deduced some information about galaxies at B = 28, although at this level he made use of very large correction factors and the data are somewhat unreliable. In addition he detected some large-scale structure which he initially proposed might be PP protogalaxy clouds, but later determined to be the optical signature of the IRAS galactic cirrus at B = 30 TO B = 31.

Tyson (1988) extended the optical number counts to B=27, showing that the excess of galaxies over the simplest models discovered at brighter levels, continues to this limit, and becomes even more significant. He also showed that the galaxies making up this excess are blue, approaching (B-R) = 0, (R-I) = 0.8 in the faint limit. He ruled out a $q_0 = 0.5$ universe, if the blue galaxy counts are due to the evolution of a single population of galaxies. He determined that there must be very active evolution, for his measurements of the extragalactic background light due to the resolved galaxies, essentially an integral over the number counts, were more than twice the passive-evolution predictions.

While Tyson (1988) discussed the possibility of the excess blue counts being due to a population of dwarf galaxies, he argued that a low redshift population, at $z < 0.2$, would produce nearly Euclidean (q_0=0.5) number counts, and that the colors of the excess blue galaxies are different from nearby morphologically classified dwarf galaxies. In addition, he claims that follow-up spectroscopy on some of the faint blue galaxies revealed that none of them are at $z < 0.6$. These data were not published, however, and the faint blue galaxies have few emission or absorption lines, and are very hard to identify. (Lilly *et al.*, 1991, also, the one remaining unidentified object in Cowie *et al.*, 1991 despite a 20 hour integration is one of the 3 flat spectrum objects discussed in Cowie *et al.*, 1988.) Those which have been identified have proven to be at $z < 0.5$, and Colless *et al.* (1990) make strong arguments against the faint blue galaxies being a high redshift population. If Tyson (1988) was basing this claim on a large number of unidentified galaxies, rather than a number of galaxies identified to be at $z > 0.6$, this claim is not very reliable. Published spectroscopic redshift data reaches the opposite conclusion, i.e., that there are very few galaxies with $z > 0.6$ at these levels. (Broadhurst *et al.*, 1988, Colless *et al.*, 1990, Cowie *et al.*, 1991). In addition, he was considering a more restricted definition of dwarf galaxies than later observers who support this explanation (Broadhurst *et al.*, 1988, Cowie *et al.*, 1992), confining them to being $M_B \leq -16$, and $z < 0.2$. While these properties are those of local dwarfs, Tyson does qualify his conclusion of low q_0 with the statement that the blue counts could be due to the evolution of a single population.

Tyson (1988) detected no distinct primeval galaxy candidates. His measurement of large, low surface brightness structure was later found to be correlated with the infrared galactic cirrus found by IRAS, and was therefore not the detection of a collapsing PP protogalactic cloud. He considered the possibility that

the faint blue galaxies are a population of primeval galaxies somewhat obscured by dust, either in the galaxies themselves, or in the intervening region, however, these would then be more extended than he has observed. He would have detected pregalactic Lyman α emission clouds of size less than 100 kpc and mass of 10^{11} M_{sol}, but detected only one object with the correct colors and morphology, despite the prediction of a confusion limit of such objects. His conclusion, that the primeval galaxy population is hiding, unidentified, among the faint blue galaxies, remains one of the most likely explanations at present.

At the same time that Tyson (1988) was conducting his optical survey, Elston (1988) was conducting the first near-infrared galaxy survey using array detectors. Motivated by the PP primeval galaxy model he observed 10 square arcminutes in K and in R, searching for very red objects in R-K, which could be interpreted as objects in which Lyman α has passed out of the R band, at $z > 6$. He found several objects which fit these criteria, 2 objects which had $K < 17$ and $(R-K) > 5$, and several more which had $K \approx 18$, and were undetected at $R = 22.3$, and thus have $(R-K)>4.3$ (Elston *et al.*, 1988). He argued that because they are above the envelope either for several models of evolving galaxies or for a non-evolving brightest cluster member elliptical galaxy, they must represent a new population, presumably the primeval galaxies for which he was searching. Subsequent spectroscopic observations, however, revealed that the objects were relatively nearby ellipticals with a near-infrared excess. (Lilly *et al.*, 1988, Elston *et al.*, 1989). Other surveys, however, including the surveys which comprise this thesis, have found no evidence for this population.

It is important to understand where Elston *et al.* (1988) went wrong. First, when trying to identify objects by their colors, one must realize that this only works well for normal objects. While it is possible, as Elston *et al.* (1988) attempted, to

argue that a particular object cannot be fit by any normal SED at any redshift, and therefore must be unusual, this does not mean that the object necessarily fits a particular theoretical model. When searching for primeval galaxies, or other types of objects at high redshift, one can only find candidates; a redshift should not be claimed without spectroscopic identification. Secondly, the most extreme members of any population are statistically more noisy then the objects nearer the mean. Every population will have 32% of the objects more than 1 sigma away from where they are supposed to be, and 4.5% of the objects more than 2 sigma away. By examining the most extreme member of a population, one is selecting for the noisier objects. The objects selected by Elston *et al.* (1988) were approximately 2 sigma away from the brightest cluster member elliptical galaxy line, and therefore their colors could be simply due to noise. Deeper survey observations, including those in this thesis, have not seen the turn-up in the red envelope at Elston's magnitude limit, but instead have seen a turn-up at their, fainter, magnitude limits. This is simply one of the effects of noise.

Jenkins and Reid (1991) measured the K band galaxy number counts by means of a statistical technique that relied on the deviations of flux densities of random observations from that produced by noise and by a model of the predicted star counts. They used a photometer on UKIRT, and had a noise limit per observation of K=18. However, by means of this statistical technique they estimated the number counts as faint as K=20. It must be noted, however, that they did this by fitting a power law to the counts, and thus the turnover seen in chapter 5 at K $\approx$ 17 would cause their counts at the faint end to be an overestimate. Another source of error in their measurement is the unreliability of their star count model.

A spectroscopic redshift survey, by positively identifying each object within its selected magnitude range and to the 80-90% completeness limit achievable

provides much more information than a photometric survey. Number counts and even color analysis can hide, or imply when it is not present, a substantial amount of evolution. The results can be interpreted in a much less model-dependent manner, and the effects of cosmological geometry and galaxy evolution can be more easily separated. In addition, the strength of the detected emission lines provide a measure of the rate of star formation. While spectroscopy, of course, cannot be done with the ease, and to the same magnitude limits that photometric surveys can be done, it is possible in a spectroscopic survey to identify and investigate a minority population in detail at a magnitude range in which it is only just beginning to appear in the number counts and color analysis of a photometric survey. With the intent of investigating the population of faint blue galaxies which were just beginning to appear at B=21, Broadhurst *et al.* (BES, 1988) conducted a spectroscopic redshift survey of over 200 galaxies selected at B=20 to B = 21.5.

The most surprising discovery of BES was that the faint blue galaxy population did not appear at high redshift in their data, and the data were fit by a no-evolution model. This seemed to imply that the excess galaxies lie in the redshift range expected from the objects observed in local field surveys with brighter limits. This was in direct contradiction to the simplest explanation for the blue number counts, that evolution caused galaxies to be more luminous in the past. Bruzual (1983) proposed two models for galaxy evolution, the c-model, similar to the PP primeval galaxy models, in which an initial burst of star formation occurs, followed by passive evolution of the main sequence as the more massive stars die out, and the μ-model, in which star formation is extended in duration, and gradually declines towards the present epoch. (The current rate of star formation is not sufficient to make the number of stars in nearby galaxies over the Hubble time, and therefore all models include star formation rates which were higher in the past.)

BES drew several conclusions from the data. The Bruzual (1983) c-model, when applied to all galaxies in the same manner, can be ruled out by the number counts alone, as it predicts an observable hump, or turnover, in the counts. The μ-model, is not consistent with both the number counts and the redshift distribution, for it would predict a substantial high-redshift tail at B = 21, which was not observed. Thus the standard models, in which all galaxies are derived from populations having the same evolutionary history, were inconsistent with the data, and luminosity evolution does not have a very strong effect upon galaxies at $z < 0.5$.

If the number count data were modelled with an excess population of faint dwarfs, the redshift distribution would have a low redshift excess over the standard no-evolution model, and there would have been several very low-redshift objects ($z < 0.03$) detected in the survey. The data are incompatible at the low-redshift end either with an additional population following a Schechter function with $B^* = -17$, (approximately 2.5 magnitudes fainter than the measured local B^*,) and a space density 20 times that of the standard population (as is required to fit the very large excess in the number counts), or with a luminosity function that follows the Schechter form with $\alpha = -1.25$ at the bright end, but steepens to $\alpha = -2$ at the intrinsically faint end. Both of these models, when adjusted to fit the number counts, would produce a low-redshift excess over the redshift survey data.

BES proposed a model in which luminosity evolution is luminosity dependent, that is, intrinsically fainter galaxies undergo bursts of star formation at moderate redshifts. This model was supported by two things. In their analysis of the strengths of the [OII] 3727 Å emission line, they discovered that objects with strong emission were much more numerous in their survey than in the DARS survey (Peterson *et al.*, 1986) done at brighter levels. While the strength of the [OII] 3727 Å line is not strictly a measure of the star-formation rate, as it depends also upon the

excitation level, it is an indication of star-formation activity. BES also drew an analogy to the Butcher-Oemler effect (Butcher and Oemler, 1978) which is an excess of star formation activity in seen in the galaxies of clusters of similar redshift to their survey. Considering the difference in environments between the cluster galaxies and the field galaxies, it is remarkable that a very similar model of star formation activity can explain both sets of data. Although their model provided a very convincing fit to the data, BES failed to consider other possible explanations, including a cosmological geometry in which there is more volume at low redshift due to a non-zero cosmological constant Λ, or number evolution of galaxies due to merging, the disruption of dwarf galaxies by supernovae, or simply having the starforming galaxies burn out and become too faint to be observed.

Colless *et al.* (LDSS, 1990) conducted a redshift survey using their multi-slit Low Dispersion Survey Spectrograph with a sample selected between B = 21 and B = 22.5, extending the results of BES by over a magnitude. Their sample consisted of 169 faint objects selected solely by geometric instrumental considerations and by magnitude on photographic plates and without regard to star/galaxy classification. Of these objects, 20 were excluded from consideration either because their spectra could not be extracted, or because no spectra could be identified. The latter were believed to be plate defects. There were 87 galaxies identified, 33 stars, and 29 objects which were not identified. They considered this to be an 81% identification rate, including the stars, which is acceptable when their failure rate is similar for stars and galaxies. Using morphological star/galaxy classification, this is true, as they had an identification rate of 78% for objects classified morphologically as galaxies. This identification rate is similar to the 85% rate of BES. Of the spectroscopically identified objects, they determined that the morphological misidentification rate was approximately 15%, which would result in a 5% deficit in

the galaxy number counts at these magnitudes. However, at brighter magnitudes, where stars comprise a much higher percentage of the total objects, this could significantly bias the galaxy number counts.

The LDSS results were similar to those of BES. Although their entire sample was inconsistent with the no-evolution model at the 98% probability level, when their three fields were considered independently, this was true for only one field. The remaining two fields were consistent with the no-evolution model. LDSS interpreted this as due to clustering in the inconsistent field, and indeed the histogram for that field shows the majority of the excess to be clumped around $z = 0.4$. Although they consider the possibility that most or all of their unidentified objects are galaxies at high redshift, (it is quite likely that the identification failure rate is a function of redshift, and they make the point that at $z > 0.8$ the [OII] 3727 Å line passes out of their spectroscopic bandpass), the excess in the number counts is a factor of 2 at $B = 22.5$, and so at least 50% of the excess galaxies have been identified as being at $z < 0.5$.

The conclusion that the redshift distribution fits the no-evolution model, even when the excess in the number counts is a factor of two, provides additional evidence against the claim that the excess is due to uniform luminosity evolution of the entire galaxy population. LDSS supported the BES conclusion that there is luminosity dependent luminosity evolution, and that low luminosity galaxies go through a brief, intense period of star formation at moderate ($z < 0.6$) redshifts.

III. The Hawaii Deep Survey

In 1987, Lilly and Cowie (1987) proposed an ambitious deep survey (HDS) in the optical and near-infrared, on the Canada-France-Hawaii Telescope, the United Kingdom Infrared Telescope, and the University of Hawaii's 2.2 meter telescope,

which would make CCD exposures comparable in depth to those of Tyson (1988), while taking advantage of the better seeing available at Mauna Kea, and go to unprecedented depths in the K band. The bandpasses, UBVIK, were selected to provide maximal wavelength coverage, from the atmospheric cutoff of a specially constructed U' filter, to just before the thermal infrared beyond K. The intermediate filters provided a roughly constant interval in log(λ). The purpose of the survey was to investigate galaxy formation and evolution in the infrared, to attempt to fit the cosmological geometry, and to search for primeval galaxies. Brown dwarfs are unlikely to be detected in a survey of this small area. Survey work, however, always provides the possibility that unexpected discoveries will be made.

The field selection and data reduction are discussed in chapter 3, as the techniques used are similar to those in this thesis. The first result from the HDS was the identification of a population of flat-spectrum objects. (Cowie *et al.*, 1987) These objects, comprising a subset of the faint blue galaxies identified by Tyson (1988), begin to appear at $B \approx 24$, and have an SED which is flat from B through K. The HDS identified three of these objects in the SSA-22 field. The SED of these objects cannot be fit by a non-evolved SED of a normal galaxy type at any redshift. Their colors appear similar to a starburst spectrum (Johansson, 1988).

The redshift of a flat spectrum object cannot be estimated from broad band colors, (this estimation relies upon the leverage provided by continuum features; flat spectrum objects do not have any such features, while all non-evolved galaxy types do show these features), however, Cowie *et al.* (1987) argued that the surface brightness produced by this population represented the production of $40h^{-2}\%$ of the metals present in the local universe, where h is H_0 in units of 50 km/sec/Mpc. This result is independent of most model parameters, including the redshift of the objects, the cosmological geometry, the assumed form of the initial mass function of

stars, and the duration of the starburst. Subsequent spectroscopy has identified one of the three objects as a z = 0.13 extragalactic HII region whose broad band colors were dominated by strong emission lines (thus once again showing the dangers of relying upon photometric identification of individual objects), the remaining two objects have resisted spectroscopic identification. Although the surface brightness arguments are weakened by this identification, it remains that the flat-spectrum objects are responsible for producing a significant fraction of the metals in the universe.

When more K band data became available, attention in the HDS project turned to the K band number counts, and to individual objects selected by their colors. Cowie *et al.*, (1990) reported number counts to K = 21.4 (a more up-to-date version of these counts is discussed in chapter 5.) They also reported the color distribution of the sample, and brought attention to a population of very red galaxies. These galaxies, having (I-K) colors as red as 5.1, have colors which could be fit by the SED of an unevolved spiral galaxy at a redshift of z = 2. While it is unlikely that anything at a redshift of 2 is unevolved, the existence of an object this red can be combined with galaxy evolution models to constrain the geometry of the universe, and the redshift of galaxy formation z_{form}.

Figure 2.3 is a plot of I-K vs redshift for a variety of models. The solid lines are the no-evolution models for 4 types of galaxies, ellipticals, Sbc's, Scd's, and Magellanic irregulars. While an elliptical galaxy can become much redder than this at high redshift (z > 1.5), and a spiral galaxy can become this red at a redshift of z = 2, simply due to the *K* correction, as was stated by Cowie *et al.*, (1990), the models of galaxy evolution will at some point take over, and we would expect high redshift objects to be blue. In this figure, there are also plotted 4 models of Chambers and Charlot (1990). These models were developed to explain the colors of

high redshift radio galaxies, and represent the minimum time in which a galaxy can evolve to be as red as observed radio galaxies. This time, combined with the redshift of formation, and a selected cosmological geometry, gives the colors of the object as a function of redshift. The evolutionary track of an object in figure 2.3 will, at high redshift, join one of the evolutionary tracks, follow it up until it intersects one of the no-evolution tracks (in the reddest case, the Elliptical galaxy track), then return down to the present day galaxy color of I-K ≈ 2. The existence of an ultra-red object can rule out some of the models; those which do not ever reach that red. Of course, if $z_{form} >> 5$, as is the case with the Partridge and Peebles (1967) models, and Lyman α is redshifted beyond the I band ($z > 8$), then objects could be much redder than this in any cosmology. Turning this argument around, the minimum z_{form} for any cosmology, based upon the existence of an object with I-K = 5.1 is $z_{form} > 1.7$.

Lilly *et al.* (LCG, 1991) analyzed the optical and spectroscopic results of the deep survey. LCG, using an I band selected sample, showed that the B-I color becomes bluer as one goes to fainter magnitudes, going from B_{AB}-I_{AB} = 1.9 at $I_{AB} < 22.5$, to B_{AB}-I_{AB} = 1.2 for $24.5 < I_{AB} < 25.5$. The flat spectrum objects, in the Absolute Bolometric system (Oke, 1974) have B_{AB}-$I_{AB} < 0.8$, and appear just fainter than $I_{AB} = 25.5$. The fraction of flat spectrum objects increases to fainter magnitudes, however, there are no objects with B_{AB}-$I_{AB} < 0$ at more than the 1 sigma level. Tyson (1988) had found many such objects, and indeed at $25 < R < 26$ his mean $(B_J\text{-}R)_{AB} \approx -0.2$. LCG interprets this difference to be due to the corrections that Tyson applied to his data to remove systematic errors in his isophotal magnitudes, because his uncorrected colors are similar to the LCG aperture photometry colors, which do not need those corrections.

The number counts in the B and I bands measured by LCG agree well with those of Tyson (1988) at all but the very faintest magnitudes. Again, however, the B

band corrections applied to correct for object non-detection, cause this difference, as the uncorrected values agree well between the two surveys. These corrections, determined in each case by placing false objects of known magnitudes on the images and rerunning the object detection programs, calculate the accuracy of the object detection routines, and are an important part in the measurement of the number counts at faint levels. The biggest advantage LCG had over Tyson (1988) was in the seeing achievable from Mauna Kea. Their data typically have FWHM < 1" in the best images, compared to Tyson's FWHM ≈ 2". They determined that a large fraction of the faintest objects have very compact cores, corresponding to a radius of 5 kpc at cosmological distances. Thus the main trend of the data of LCG is that at faint magnitudes there is an excess of compact, blue galaxies over the no-evolution models. The LCG results have recently been confirmed by Peterson (1992, private communication) who confirms that the Tyson (1988) I band photometry is incorrect at the faint end.

LCG turned their attention to three questions which could be addressed by their data. The first concerns the nature of the brighter galaxies in their survey, with $B_{AB} < 24$, for which spectroscopic observations had begun. (Spectroscopic data on the B < 24 sample have now been completed at the 95% level, and is reported in Cowie *et al.*, 1991.) At this magnitude, the B band number counts already show an excess of a factor of 3 over the no-evolution prediction. The second is a discussion of the nature of the flat spectrum objects identified by Cowie *et al.* (1988), and finally there is a discussion of the nature of the faintest galaxies at $B_{AB} \approx 26$.

The galaxies at $B_{AB} < 24$ continue to display the effects seen at B = 22.5 by LDSS, that is, despite the excess over the no-evolution model seen in the number counts, the redshift distribution is fit by this model, with neither a low-redshift excess, caused by a low-luminosity excess in the luminosity function, nor a high-

redshift excess, caused by uniform luminosity evolution. LCG used the redshift information of the HDS, LDSS, and BES to construct a "back-counting" model of the no-evolution number counts. This technique was used to determine if the model had been significantly biased by uncertainties in the local luminosity function. There were two interesting conclusions from this analysis. While it was impossible to fit the counts at $B_{AB} \approx 24$ with a no-evolution model determined from the brighter data, the counts fainter than this were consistent with the $B_{AB} \approx 24$ counts and no further evolution. Thus the population at $B_{AB} \approx 24$ has undergone significant evolution, of some type, relative to the LDSS population at $B_{AB} \approx 22.5$, but most of this population is at relatively low redshift. Simple luminosity evolution, or evolution in M^*, with a fixed ϕ^* is not sufficient, there must be some number or density evolution, or evolution in ϕ^*. This does not necessarily mean non-conservation of galaxy number, for evolution of the type proposed by BES would cause lower luminosity galaxies to become brighter for a while, changing the number of M^* galaxies while not changing the total number of galaxies. An additional possibility is merging, characterized by a constant product ϕ^*L^*, maintaining the total brightness of the galaxy population.

Each of these models has both advantages and problems. Conventional evolution in M^* will increase the number counts by bringing galaxies at greater distances into the apparent magnitude range, and thus allowing one to sample greater volumes. However, this will increase the mode (or median, which is easier to determine for small samples) redshift beyond that which has been measured. As an aside, comparing the mean redshift of the data to model predictions is very unreliable, as the mean for most models is dominated by the high redshift end, where uncertainties in the redshift of formation and early evolution play a larger role. In addition, the mean measured redshift can be very uncertain due to

incomplete identification of the object sample, while the median could be determined simply by assigning unidentified objects to arbitrarily high redshift. Evolution in ϕ^*, as is produced either by density evolution or by an evolutionary bursting model, will increase the number counts, but have little effect on the median redshift. A merging model with constant ϕ^*L^* will produce little change in the number counts, but will decrease the median redshift. As we are seeing high number counts, and no-evolution redshift distributions, this would tend to argue for evolution in ϕ^* with constant L^*.

Merging has two problems in explaining the evolution in ϕ^*. The first is that it would be difficult to produce the large number of galaxies at $z \approx 0.4$, and the second is that this large amount of merging would tend to disrupt the disk systems of spiral galaxies, and produce bluer populations in elliptical galaxies. Since the total number of galaxies must be reduced by a factor of 2, the merging model requires the post-merging production of both spirals and ellipticals. However, the galaxies are very small, and it is possible that a galaxy such as ours could absorb a $0.1L^*$ galaxy and not lose its disk. Another argument against the merging model comes from the 2 point correlation function (Guhathakurta, 1992, Efstathiou *et al.*, 1991) which shows that the faint blue galaxies are too weakly clustered to be the progenitors of the nearby galaxy population. Melott (1992), however, argues that they made overly restrictive assumptions about the growth of clustering, and thus the merging model is not inconsistent with the correlation function data. LCG shows that the galaxies in their redshift sample are not preferentially at the same redshift. While there are not enough galaxies in this sample to do a proper three dimensional correlation analysis, this is further evidence against the merging hypothesis.

Broadhurst *et al.*, (1992) argue that the merging hypothesis best fits the data. They construct a simple merging model in which the product $L^*\phi^*$ is conserved

and the star formation rate is higher in the past. This last comes from the measurements of BES and LDSS of the equivalent width of the [OII] 3727 Å line, which is greater for fainter galaxies. Non-merging models with higher star formation rates in the past run into the problem that the predicted mean redshift is too high. Working strictly from the number counts and redshift survey data, Broadhurst *et al.*, (1992) make a good case for the merging model. They argue that the angular correlation studies are subject to errors in the boundary conditions which are comparable to the measured correlation, and that more studies are needed. However, they do not address the problems of stability of the disks, or the red colors of elliptical galaxies.

The BES model of starbursts in low-luminosity galaxies boosting them up to L^* for a short duration will have the effect of evolution in ϕ^*, however, this model also has some difficulty in producing the large excess seen in the number counts at B = 24. While this model works well for the small excess seen by BES and by LDSS, to produce an enhancement of a factor of 2 in galaxies brighter than M_B = -19, one must integrate down to M_B = -17.5., and to produce a factor of 3 (which is needed if one adopts the low ϕ^* value of Efstathiou *et al.*, 1988), one must integrate down to M_B = -16. However, the colors of the galaxies, which get bluer as one goes to fainter limits, show evidence for enhanced star formation, lending support to this interpretation. LCG also considers two alternative proposals, a larger volume element produced by a flat universe with a cosmological constant, and the prospect that we may be seeing galaxies at B = 24 which have disappeared by the present epoch, that is, true number evolution. These proposals will be discussed in light of the deep K band number counts of Cowie *et al.*, (1992) in chapter 4.

LCG discusses the nature of the bluest galaxies, both the trend towards the blue of the general population at fainter levels, and the distinct population of flat-

spectrum objects which cannot be fit by the SEDs of normal galaxies at any redshift at $z < 1$. These unclassifiable objects comprise only 15% of the population at $B_{AB} < 24$, and therefore are not the explanation for the excess in the number counts. LCG revises the earlier estimates of the contribution of these flat-spectrum objects to the production of metals in the universe to about 10%. The spectra of the three flat-spectrum objects discussed by Cowie *et al.*, (1987) show that 1 is an extra-galactic HII region at redshift $z = 0.13$, and the other 2 resist identification, even with very long (20 hour) exposures. Their spectra show no emission lines to a limit of an equivalent width of 20 Å. They are extended and elongated, and show a marked difference from the extragalactic HII region, which is compact with strong lines. (The strong lines dominate the broad band colors, mimicking a flat spectrum.)

The combination of the very blue colors and the lack of strong lines in the flat spectrum objects is difficult to explain. Blue colors in a galaxy is an indication of active star formation, but star formation often produces strong emission lines. One of the galaxies has a flat spectrum through to the U' at 3400 Å, making it unlikely to be at redshift $z > 2$, where the Lyman break and the Lyman α forest would begin to be seen. The other galaxy has a redder U'-B color, but similar arguments place it at $z < 3.5$. The SED's, including a rise in the K band reminiscent of the radio galaxy 0902+34 at $z = 3.4$, and the absence of emission lines are suggestive of high redshift, but are by no means conclusive. Redshifts of $z > 2$ would place the Lyman α line in the region of the spectra, and would mean that this line is unexpectedly weak.

At 26th magnitude, the very faintest levels in the LCG survey, the galaxies are interesting, but it is difficult to draw firm conclusions from them. The noise in the photometry makes photometric classification unreliable, and they are too faint for spectroscopy without long exposures on a 10 meter class telescope. The majority

of the objects are probably normal galaxies at a wide range of redshifts. The most remarkable aspect of galaxies at these magnitudes is their number density. To $B_{AB} \approx 26.5$, there are 2.5×10^5 galaxies deg^{-2}, and there are indications that the integrated number density to fainter magnitudes might be as high as 10^6, from deep slit profiles obtained in the spectroscopy program (Cowie and Lilly, 1990.) Because of the good seeing of the Hawaii Deep Survey, confusion is not a factor at $B_{AB} = 26$, where the average separation is 8 arcseconds, but may become a factor at a number density of 10^6, where the average separation is 4 arcseconds, approaching the typical size of large galaxies.

That the large excess of galaxies seen at B = 21.5 and B = 24 continues without abating to B = 26 stretches to its limits the explanation of BES for the excess. The low luminosity bursting would have to apply over the whole cosmological timescale sampled at these faint levels. In order for the galaxy to end up as a present-day 0.01 L^* galaxy, it would have to have an IMF heavily weighted towards high-mass stars, and have a method for removing the metals produced by these high-mass stars. The low q_0 explanation for the high number counts also falls short at the faintest levels. While wholescale merging of smaller units into larger ones remains a possibility, subject to the drawbacks mentioned above, it remains clear that the excess in the optical number counts represents a fundamental aspect of the universe and is not simply an effect of the models used to fit the data.

It seems likely that, barring wholescale merging from z = 0.4 to the present, that the excess population of compact blue galaxies has little to do with the production of the present day population of L^* galaxies. They are of too low luminosity, and too high number density. The deficiency of $0.5 < z < 1.0$ galaxies in the blue selected sample suggests that there has been only modest evolution of massive galaxies since this epoch. The infrared observations of the HDS, by

selecting the older, more massive galaxies, is better suited for finding the high redshift progenitors of the nearby population.

The physical cause of the excess blue population remains unclear. LCG argues that no one explanation is satisfactory, and thus a combination of several explanations seem likely. These explanations include bursts in low-luminosity galaxies, the merging of dwarf galaxies into larger units, and a possible high-redshift component that resists identification. This high-redshift component could be represented by the flat-spectrum objects for which attempts at spectroscopic identification have largely remained unsuccessful. The HDS K band observations will be discussed in chapter 4, as well as, in the context of new data, throughout this thesis.

References for Chapter 2

Boughn, S.P., Sauson, P.R., and Uson, J.M., 1986, *Ap. J.*, **301**:17.

Broadhurst, T.J., Ellis, R.S., and Shanks, T., 1988, *M.N.R.A.S.*, **235**:827.

Broadhurst, T.J., Ellis, R.S., and Glazebrook, K., 1992, *Nature*, **355**:55.

Bruzual, G., 1983, *Ap. J.*, **273**:105.

Butcher, H., and Oemler, A., 1978, *Ap. J.*, **273**:105.

Chambers, K.C., Miley, G.K., van Breugel, W., 1987, *Nature*, **329**:604.

Chambers, K.C., and Charlot, S., 1990, *Ap. J. Lett.*, **348**:L1.

Colless, M., Ellis, R.S., Taylor, K., and Hook, R.N., 1990, *M.N.R.A.S.*, **244**:408.

Colless, M., Ellis, R.S., Taylor, K., and Shaw, G., 1992, preprint.

Collins, C.A., and Joseph, R.D., 1988, *M.N.R.A.S.*, **235**:209.

Cowie, L.L., 1988, in *The Post-Recombination Universe*, eds. N. Kaiser and A. Lasenby, Kluwer:Dordrecht, p. 1.

Cowie, L.L., Lilly, S.J., Gardner, J., and McLean, I.S., 1987, *Ap. J. Lett.*, **332**:L29.

Cowie, L.L., Gardner, J.P., Lilly, S.J., and McLean, I., 1990 *Ap. J.*, **360**:L1.

Cowie, L.L., and Lilly, S.J., 1990, in *The Evolution of the Universe of Galaxies*, ed. R.G. Kron, A.S.P Conference Series:San Francisco, pg. 212.

Cowie, L.L., Songaila, A., and Hu, E.M., 1991, *Nature*, **354**:460.

Cowie, L.L., Gardner, J.P., Hu, E.M., Wainscoat, R.J., Hodapp, K.W., 1992, *Ap. J.*, *submitted.*

Davis, M., and Wilkinson, D.T., 1974, *Ap. J.*, **192**:251.

de Vaucouleurs, G., de Vaucouleurs, A., Corwin, H.G.Jr., Buta, R.J., Paturel, G., and Fouque, P., 1991, *Third Reference Catalogue of Bright Galaxies*, Vol. I-III, (New York:Springer).

Djorgovski, S., 1992, to appear in *Cosmology and Large-Scale Structure in the Universe*, ed. R.R. de Carvalho, A.S.P. Conference Series, *in press.*

Dube, R.R., Wickes, W.C., and Wilkinson, D.T., 1977, *Ap. J. Lett.*, **215**:L51.

Dube, R.R., Wickes, W.C., and Wilkinson, D.T., 1979, *Ap. J.*, **232**:333.

Efstathiou, G., Ellis, R.S., and Peterson, B.A., 1988, *M.N.R.A.S.*, **232**:431.

Eggen, O.J., Lynden-Bell, D., and Sandage, A.R., 1962, *Ap. J.*, **136**:748.

Elston, R.J., 1988, Ph.D. Thesis, University of Arizona.

Elston, R., Rieke, G.H., Rieke, M.J., 1988, *Ap. J. Lett.*, **331**:L77.

Elston, R., Rieke, M.J., Rieke, G.H., 1989, *Ap. J.*, **341**:80.

Guhathakurta, P., 1992, in *The Early Observable Universe From Diffuse Backgrounds*, ed. B. Rocca-Volmerange, J.M. Deharveng and J. Tran Thanh Van, Cedex:Editions Frontiers, pg. 155.

Huchra, J., Davis, M., Lathan, D., and Tonry, J., 1983, *Ap. J. Supp.*, **52**:89.

Jenkins, C.R., and Reid, I.N., 1991, *A. J.*, **101**:1595.

Johansson, L., 1988, *Astr. Ap.*, **191**:29.

Kirshner, RP., Oemler, A. Jr., Schechter, P.L., 1978, *A.J.*, **83**:1549.

Kirshner, RP., Oemler, A. Jr., Schechter, P.L., 1979, *A.J.*, **84**:951.

Kirshner, RP., Oemler, A. Jr., Schechter, P.L., Schectman, S.A., 1983, *A.J.*, **88**:1285.

Koo, D.C., and Kron, R.G., 1980, *PASP*, **92**:537.

Koo, D.C., 1986a, in *The Spectral Evolution of Galaxies*, eds. C. Chiosi and A. Renzini, Dordrecht:Reidel, pg. 419.

Koo, D.C., 1986b, *Ap. J.*, **311**:651.

Kron, R.G., 1980, *Ap. J. Supp.*, **43**:305.

Lang, K.R., 1980, *Astrophysical Formulae*, 2nd edition, (Springer:New York).

Lilly, S.J., and Longair, M.S., 1982, *M.N.R.A.S.*, **199**:1053.

Lilly, S.J., and Longair, M.S., 1984, *M.N.R.A.S.*, **211**:833.

Lilly, S.J., Longair, M.S., and Allington-Smith, J.R., 1985, *M.N.R.A.S.*, **215**:37.

Lilly, S.J., and Cowie, L.L., 1987, in *Infrared Astronomy with Arrays*, eds. C.G. Wynn-Williams and E.E. Becklin, Honolulu:Univ. Hawaii), p. 473.

Lilly, S.J., Gardner, J.P., Cowie, L.L., and McLean, I.S., 1988, *Ap. J. Lett.*, **332**:L59.

Lilly, S.J., and McLean, I.S., 1989, *Ap. J. Lett.*, **346**:L65.

Lilly, S.J., Cowie, L.L., and Gardner, J.P., 1991, *Ap. J.*, **369**:79.

Loveday, J., Peterson, B.A., Efstathiou, G., and Maddox, S.J., 1992, *Ap. J.*, **390**:338.

Matilla, K., 1976, *A.A.*, **47**:77.

McCarthy, P.J., Spinrad, H., Djorgovski, S., Strauss, M.A., van Breugel, W., and Liebert, J., 1987, *Ap. J. Lett.*, **319**:L39.

Mobasher, B., Ellis, R.S., and Sharples, R.M., 1986, *M.N.R.A.S.*, **223**:11.

Oke, J.B., 1974, *Ap. J. Supp.*, **27**:21.

Partridge, R.B, and Peebles, P.J.E., 1967, *Ap. J.*, **148**:377.

Partridge, R.B., 1974, *Ap. J.*, **192**:241.

Peterson, B.A., Ellis, R.S., Efstathiou, G., Shanks, T., Bean, A.J., Fong, R., and Zen-Long, Z., 1986, *M.N.R.A.S.*, **221**:233.

Pritchet, C.J., and Hartwick, F.D.A., 1990, *Ap. J. Lett.*, **355**:L11.

Rigler, M.A., Lilly, S.J., Stockton, A., Hammer, F., Le Fèvre, O., 1992, *Ap. J.*, **385**:61.

Shanks, T., Stevenson, P.R.F., Fong, R., and MacGillivray, H.T., 1984, *M.N.R.A.S.*, **206**:767.

Spinrad, H., and Stone, R.P.S., 1978, *Ap. J.*, **226**:609.

Toller, G.N., 1983, *Ap. J. Lett.*, **266**:L79.

Thompson, D.J., Djorgovski, S., and Trauger, J., 1992, to appear in *Cosmology and Large-Scale Structure in the Universe*, ed. R.R. de Carvalho, A.S.P. Conference Series, *in press*.

Tully, R.B., 1988, *Nearby Galaxies Catalog*, (Cambridge:Cambridge Univ. Press).

Tyson, J.A., and Jarvis, J.F., 1979, *Ap. J. Lett.*, **230**:L153.

Tyson, J.A., 1988, *A.J.*, **96**:1.

Yoshii, Y., and Takahara, F., 1988, *Ap. J.*, **326**:1.

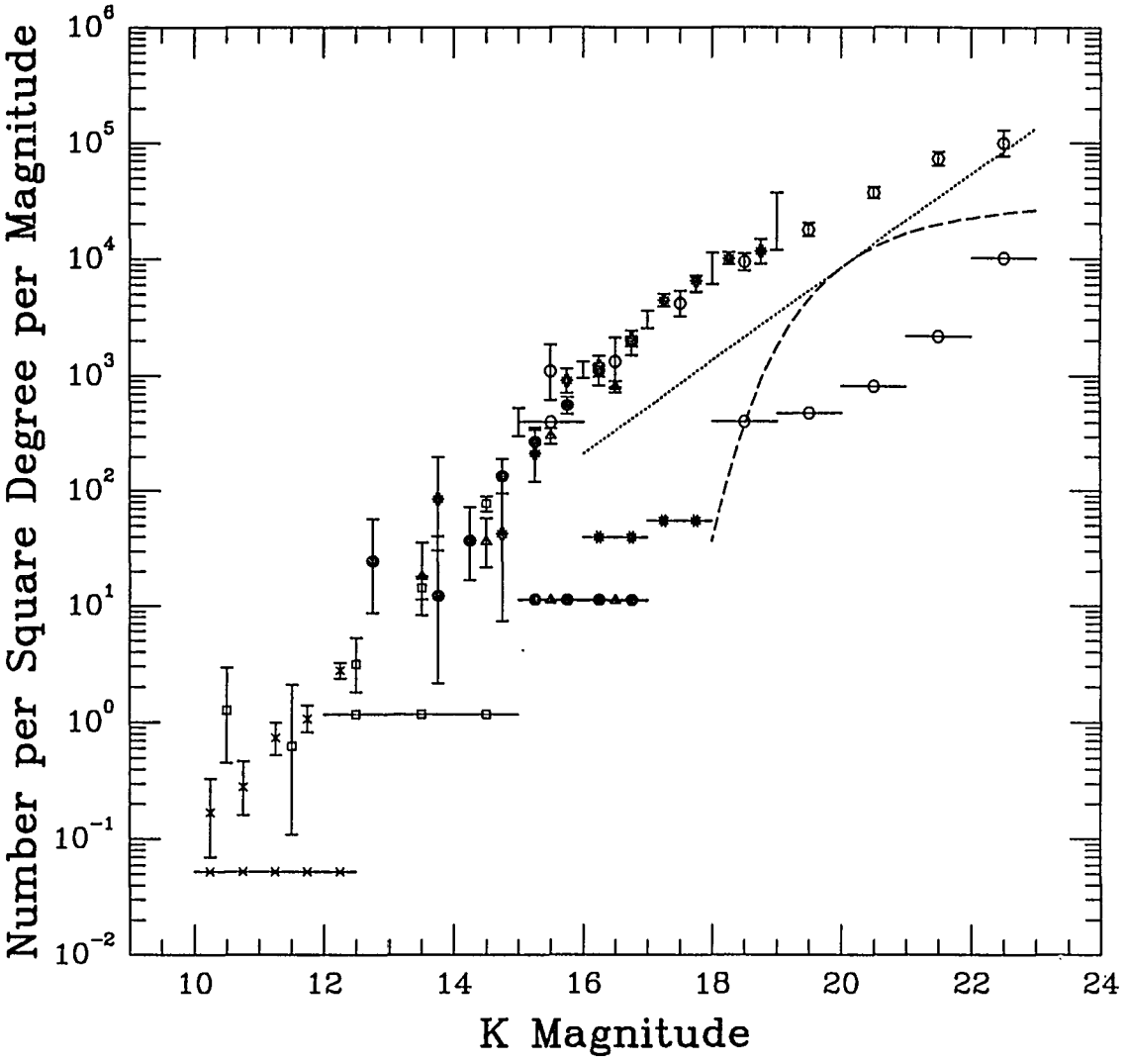

Figure 2.1: The K band number counts from chapter 5 plotted with a simple model for primeval galaxies. The symbols represent the various surveys, and are the same as in figure 5.1. The dotted line provides a locus along which a suitable luminosity function, the dashed line, will slide. Also plotted are the upper limits on the density of objects which could be identified, but are not detected, for each of the surveys. Since the primeval galaxy model is above the upper limits on undetected objects, it is likely that primeval galaxies are hiding within the survey catalogs, but have the same colors as normal galaxies, and remain unidentified.

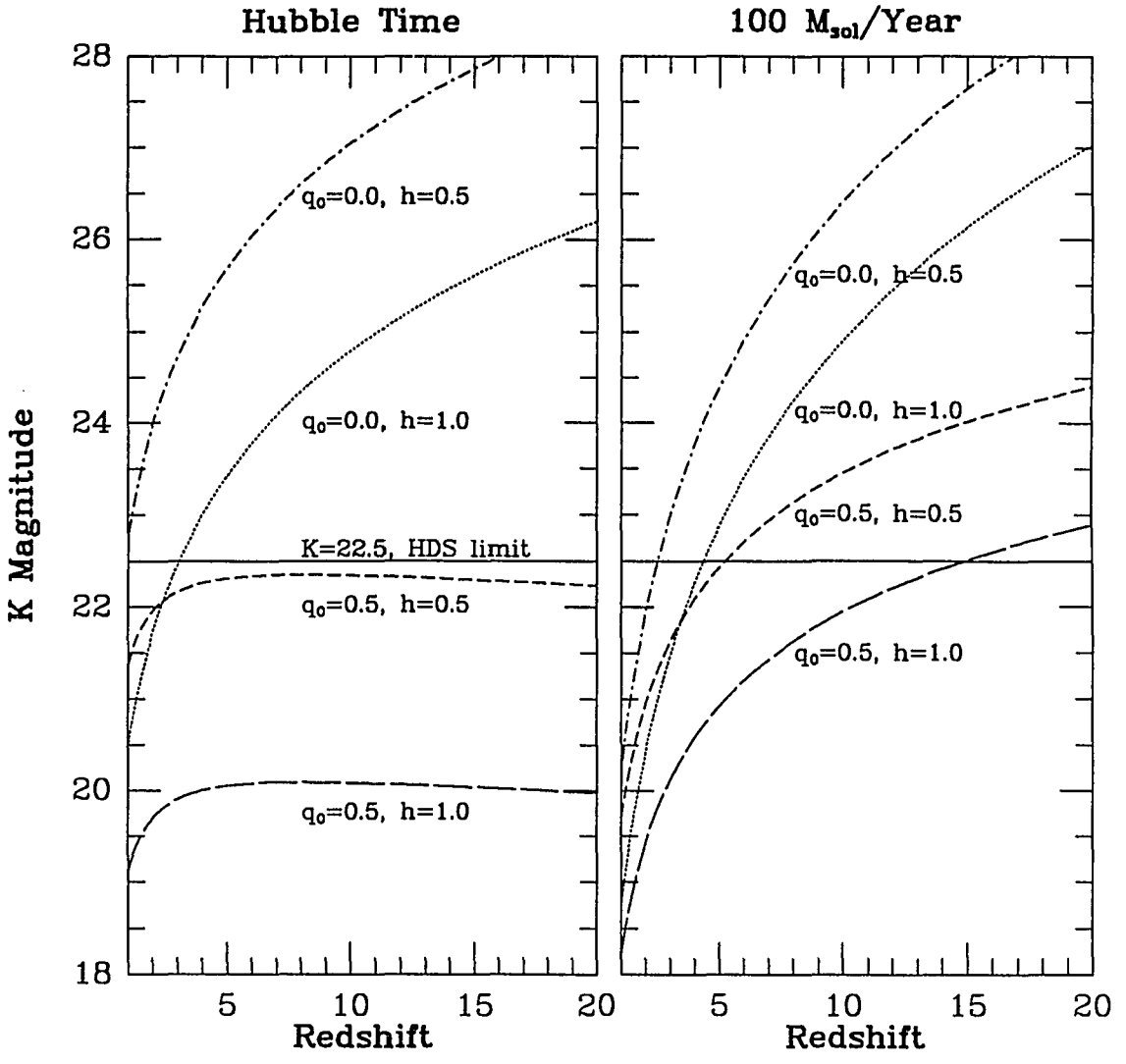

Figure 2.2: The expected K magnitude of primeval galaxies for a variety of models based upon the surface brightness caused by the production of the metals in the universe. The Hubble time model assumes that the star formation rate is such that $10^{11}h^{-2}M_{sol}$ stars are produced in the Hubble time at that epoch, where H_0 = 100 h km/sec/Mpc. The other model has a star formation rate of 100 M_{sol}/Year. Also plotted is the K = 22.5 detection limit of the Hawaii Deep Survey. There are a wide variety of models which would not have been observed by the HDS.

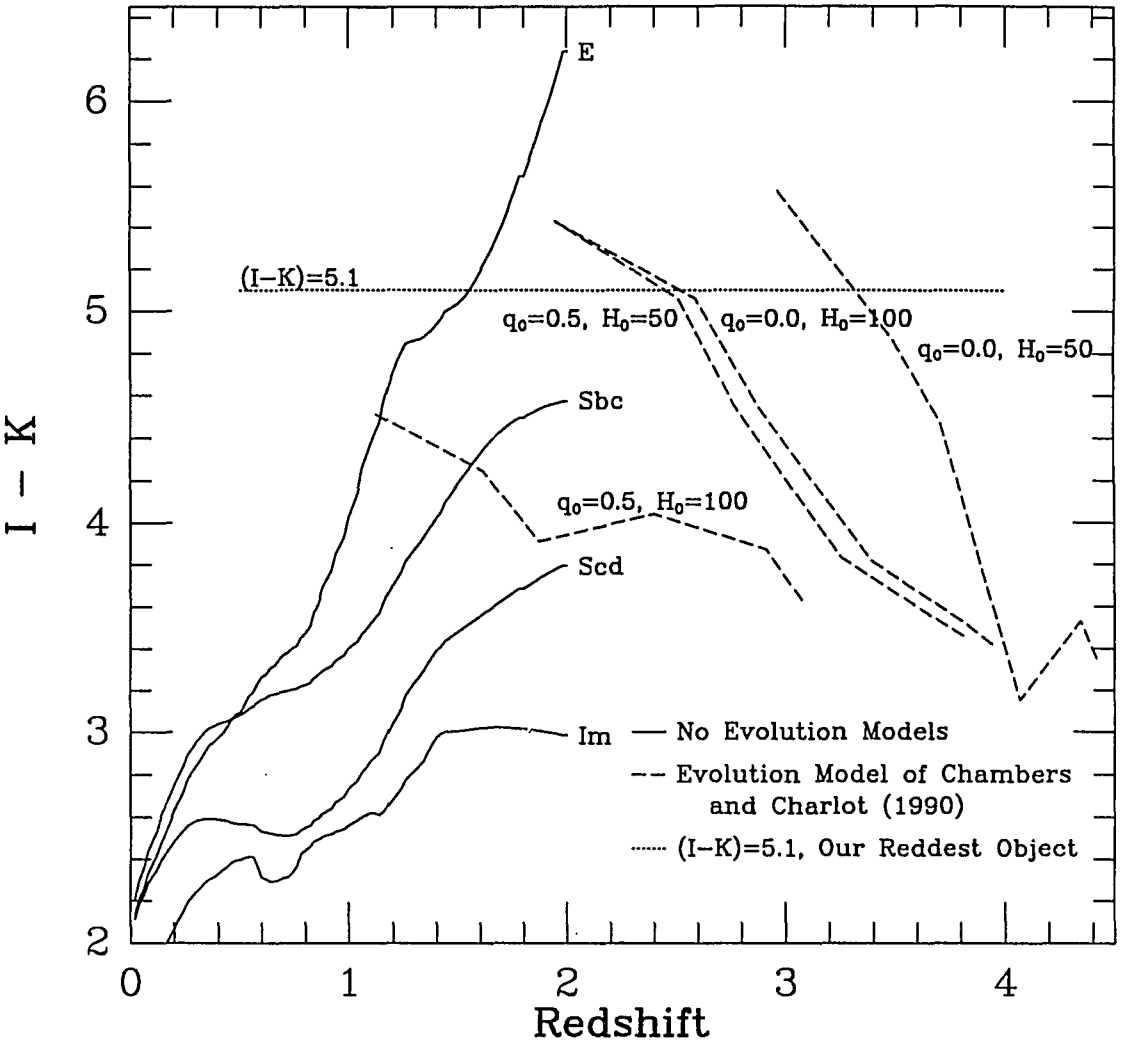

Figure 2.3: A plot of the I-K color vs redshift for the model predictions of Chambers and Charlot (1990), and the non-evolved model of 4 types of galaxies. In a closed, very short timescale universe (q_0 = 0.5, H_0 = 100 km/sec/Mpc) one would not expect a galaxy to reach (I-K)=5.1, which is the reddest object in the HDS.

Chapter 3: Data Reduction

In this chapter I will describe the methods of field selection, observations, image processing, object identification and catalog preparation, and star/galaxy separation for the two surveys which comprise the new data in this thesis. The two surveys are the Hawaii Medium Wide Survey (HMWS), and the Hawaii Medium Deep Survey (HMDS). The HMWS covers 580 square arcminutes to a depth of K = 17, and the HMDS covers 170 square arcminutes to a depth of K = 18. Each area has been observed to a comparable depth in I and B. These two surveys are discussed in the context of a wider, brighter survey, the Hawaii Wide Survey (HWS), and a smaller but deeper survey, the Hawaii Deep Survey (HDS).

I. Field Selection

The fields were selected in two different ways. For the HMDS, 4 of the fields were taken from the fields chosen for the HDS. This field selection was summarized in Lilly *et al.* (1990), but I will describe it in more detail here. First, 18 positions were selected, each more than 30 degrees away from the galactic plane, at the intersection between each hour of Right Ascension, with a multiple of 10 degrees of Declination, between 0 degrees and 50 degrees reachable from Mauna Kea Observatory. Then the Palomar Observatory Sky Survey (POSS) prints were searched. Near each potential position, a field was selected which lay on the intersection between the lines of 5 minutes of Right Ascension and each degree of Declination, and was free from visible objects in a 3 arcminute square region centered on the coordinate position. An attempt was made to avoid positions within Zwicky clusters, although 3 of the 18 selected areas did fall within clusters. However, no observations have been made on these fields; all observations are thus free of nearby bright clusters. The 4 HDS fields, SSA-04, SSA-13, SSA-17, and SSA-

22, were taken from this list, and lie at 4 hours, 13 hours, 17 hours and 22 hours respectively. The 3 HMDS fields, SSA-04, SSA-17, and SSA-22 coincide with and include the HDS fields. The HMDS field SSA-08 was taken from the list of fields selected for the HDS, although no HDS observations of this field have been made.

The fields were selected at more than 30 degrees galactic latitude so as to avoid problems of galactic extinction, and to avoid having most of the fields occupied by bright stars. At the same time, we did not select the heavily observed regions near the north galactic pole, so as to provide an independent check upon the work proceeding in that region (e.g. Broadhurst *et al.*, 1992). Work done at a single location can be biased to an unknown extent by clustering. The fields were selected to lie on the intersection of coordinate lines so as to be demonstrably random. The coordinates are based upon features of the Earth, with the equator, north and south poles defining Declination, and the position of the Greenwich meridian at the Vernal equinox defining right ascension. These coordinates are arbitrary for extra-galactic science, and therefore the exact position of the fields is unbiased. The positions of the fields are listed in table 3.1 and are plotted in galactic coordinates in figure 3.1.

The selection of the fields to be free of objects on the POSS prints potentially introduces a bias against bright objects. Because the HDS was not meant to study bright objects, this was deemed to be an acceptable bias. The selection criteria was intended to avoid having a significant part of the field covered by uninteresting bright objects. Objects are visible on the POSS prints to a depth of approximately B = 20. Because the bluest objects observed in any of the surveys are the flat spectrum objects, and a flat spectrum object has B-K = 2.06, any observations at K > 18 are unbiased by this effect. Flat spectrum objects are unknown at this bright magnitude, and the avoidance of objects in the fields was not perfect at the faintest

magnitudes. In addition, objects are more likely to be selected by eye when they are compact with high surface brightness, that is, stars. Thus it is likely that this bias is not significant for galaxies with K > 16. The HDS has but a single object at this magnitude. Brighter than this, there is the potential that this bias can affect some of the statistical conclusions of the HMDS. For the HWS, this effect is minimized, because the area subject to this bias is small compared to the total area observed, less than 0.3%. For the HMWS, 3 of the fields which were subject to this bias were offset by 5 arcminutes so as not to include the original selected field. The other 2 fields, coinciding with the HMDS SSA-04 and SSA-08, result in 3% of the area covered being biased. This was deemed acceptable.

During the course of data reduction and subsequent analyses, two ways in which the selection of fields could have been improved have arisen. The observations, both in the infrared and in the optical, are composed of multiple exposures coadded together to make a final image. These exposures, for reasons explained below, are offset from each other by 10 to 20 arcseconds. After the initial reduction process, in which each frame is flattened by the median sky flat process, the frames must then be shifted and coadded. These shifts can be most accurately determined from the data itself, but only if there are objects which can be seen on each individual exposure. If the objects have sufficient signal to noise, subpixel shifts can be determined by cross-correlation techniques. Thus it would be useful at this stage for the selected fields to have at least one bright star in the field, and because a bright star is likely to be saturated in one or more of the colors, it would be useful to have several stars.

This effect was worst in the early HDS images made with IRCAM on UKIRT, in which it often happened that there were no objects visible, even in a coadded exposure of an hour. While on UKIRT the offsets input into the guide camera were

accurate enough to coadd the data taken within a given night, it often was a very difficult process to coadd data from successive nights in an observing run. Later exposures made with the NICMOS camera on the UH 2.2 meter telescope were easier to co-register, because the large field of view made the exposures more likely to include bright objects. However only about half of the fields had sufficient signal to noise in the cross correlation to allow automatic co-registration. The remainder were done by selecting an object by eye and co-registering the maximum pixel. This process did not allow sub-pixel registration, and the final images did not ever have resolutions better than 2 pixels. An additional reason for having one or more bright objects in the fields is that it makes it easier for subsequent spectroscopic observations.

The three remaining fields of the HMDS were selected to coincide with the fields of the Durham LDSS redshift survey (LDSS: Colless *et al.*, 1990). These are the Dur-00, the Dur-10, and the Dur-13 fields, corresponding to the LDSS 00.2, 10.2, and 13.2 fields. The 00.2 field is near the South Galactic Pole. The remaining two fields are on the equator. Because the LDSS had already obtained spectroscopic redshifts for a subset of the objects in a $B < 22.5$ selected sample, there was the potential to serendipitously analyze the K band photometry of a spectroscopic survey sample. Although the field of view of the HMDS allowed coverage of only about a quarter of the LDSS objects, subsequent observations have been made on the remainder of the objects, and will be discussed elsewhere. (Gardner, in preparation.)

Three of the HMWS fields were selected to coincide with the HMDS fields Dur-00, SSA-04 and SSA-08. These HMWS fields include the HMDS fields, and this provides a check on the calibration. As has been discussed above, the bright-end bias affecting the HMDS fields compromises only a small part of the area of the

HMWS. The remaining 3 fields of the HMWS were taken from the HDS selected areas, SSA-00, SSA-01, and SSA-02, but were offset by 5 arcminutes so as not to include the area that was selected to be free of bright objects. Each HMWS field is a strip 3 arcminutes by 30 arcminutes, and like the HMDS fields, have been observed in B, I, and K.

II. Observations

While the initial proposal called for the infrared observations to be done with IRCAM on UKIRT, bad weather prevented observations during the six nights I was granted in February and May 1990. The NICMOS camera was available on the University of Hawaii's 2.2 meter telescope for the next observing season in September 1990, and I used this camera to make all of the infrared observations reported in this thesis. The majority of the optical observations were made using a Texas Instruments 800^2 CCD camera on the 2.2 meter telescope, using focal reduction to achieve a 5 x 5 arcminute field of view. In the fall of 1991 I switched to a Tektronics 1024^2 CCD for the optical observations. In direct mode this detector gave a 3 x 3 arcminute field of view.

Observations were begun in July 1989, and B and I exposures of 2 of the HMDS fields, SSA-17 and SSA-22 were made, along with a short U band exposure of SSA-22. In October 1989 several more exposures were made, some of which were non-photometric due to clouds. In December 1989, I had two nights in which I did the majority of my optical observations, observing the Dur-00, SSA-04, SSA-08, Dur-10, and Dur-13 fields. In February 1990, I was given two nights during which I was not able to observe in the west because of wind. As the majority of my fields were west in February, I was only able to get useful data on the Dur-13 and SSA-17

fields. The optical observations for the HMDS were completed in October 1990, with data on the SSA-22, Dur-00 and SSA-04 fields.

The K band observations of the HMWS fields Dur-00, SSA-04 and SSA-08 were done during the September, 1990 observing run with the NICMOS camera. This fields were then observed in the I and B bands during the October 1990 observing run. An incorrect plate scale was used for the TI 800^2 CCD detector, and there are a few gaps in the optical coverage of these fields, comprising approximately 2% of the field of view. The HMWS fields SSA-00, SSA-01, SSA-02 and SSA-03 were observed in December, 1990 in the K band, and in October, 1991 with the Tektronics 1024^2 CCD. Because of time constraints, the SSA-03 field was not observed in the optical.

III. Image Processing

Image processing involves essentially three processes. The background coming from everything other than the objects of interest must be subtracted. The pixels of an array detector have a linear response to an incoming signal, but the linear response is a different one from pixel to pixel. The image must be flattened, that is, the linear response of each pixel must be calibrated to that of every other pixel, so that the response of the detector to a constant flux is a constant signal. Finally, the image must be calibrated to a known signal, so that absolute photometry is possible. Traditionally in the optical, these three processes are done by subtracting a dark frame, that is an exposure taken with the detector shutter closed, dividing by a dome flat, which is an exposure of a lighted, but blank part of the telescope dome, and finally by calibrating the images with exposures of standard stars of known magnitudes. In the infrared, where the backgrounds from the telescope and the sky are much higher, and dominate other effects, an image of a

blank part of the sky is subtracted, and the images are calibrated with standard stars.

When one is making exposures of very faint objects, the traditional methods of image processing do not work well enough. A technique of using the images themselves for self-flattening, or more properly, using images to flatten their near neighbors was developed by Tyson (1986), and refined for the Hawaii Deep Survey (HDS), and in the present work. A dome flat is able to flatten an image to about 1%, that is, the residual pixel-to-pixel response differs by 1%. It is possible, however, to improve on this and flatten an image to a few parts in 10^5. The technique, called median sky flatting, involves taking a series of exposures, each offset from the other. The majority of the image is not occupied by objects, but is an exposure of the sky, or background, which is assumed to be constant over the field of view. When the images are stacked into a cube, the modal response of each pixel is the response of that pixel to this constant background. Because the noise is reduced by the square root of the number of images used to determine the mode, the result is a low-noise, highly accurate flat field image. In practice, the median is used as an estimator of the mode, because there are rarely enough images to determine the true mode. In the infrared, this technique can be used to construct a highly accurate background image to be subtracted. It has the advantage over traditional infrared chopping techniques that 100% of the exposure time is spent on the object of interest, rather than 50%.

The images were all made with a series of exposures, each offset from the other in a grid pattern with a spacing of 10 arcseconds. The exposure was determined by a balance between the need for as many exposures as possible to accurately determine the sky, and the need to fill the well so as to be sky noise limited. There were images with as few as 4 individual exposures, particularly in B,

and as many as 25 per point, or 100 per field in the K band. (To cover the full HMDS field in the K band it was necessary to use a 4x4 mosaic of images. In the optical, the focal reduction was sufficient to cover the field of view in a single exposure.) Because 4 exposures is not enough to determine the flat field, exposures from different fields were combined, in the optical, to determine the small-scale flat field fluctuations, while the large-scale fluctuations were determined with just the exposures of a given field. This was done with 7x7 point median smoothing, subject to the following formula:

finalflatA = [smooth(skyflatA)/smooth(skyflatABCD)]*skyflatABCD

In this formula, finalflatA is the flat field used for field A, skyflatA represents the median pixel response of this single field, where skyflatABCD represents the median pixel response of a whole night's data. In the infrared there were always enough exposures for each field that combining exposures from different fields was not necessary.

The NICMOS exposures did not have a significant dark current, so a dark frame was not subtracted. However, at the telescope, dark images were taken, and they were used, along with dome flats, to identify the bad pixels. The dome flats were coadded and normalized. Any pixel greater than 1.4, or less than 0.7 was considered bad. On the dark images, any pixel greater than 5 counts per second, or less than 1 count per second were considered bad. These criteria were determined empirically, by sorting the pixels in a dark or dome flat frame, and choosing a cutoff where the pixels begin to behave anomalously. Within these criteria, approximately 1% of the pixels were bad, and these criteria identified all pixels that appeared to be bad in a visual inspection of the images. The bad pixels were flagged in the images by a magic number, and were ignored in all further operations, until just before the

final expansion and coaddition, when they were replaced with the median response of other images to that position on the sky.

Dome flats were taken at the beginning and end of each night, by shining a lamp on the dome slit shutter and exposing the chip through the telescope. Because the dome flat lamp had an approximate black body temperature of 2-4000 K, close to the temperature of most of the observed objects, the dome flats are used as a multiplicative correction. In the K band, the background, or sky, comes from a combination of emission from the telescope, emission from the air inside the dome, and emission from the atmosphere. Very little of the background is true galactic or extragalactic background radiation. The background has a very different temperature than the objects, and thus it was used as an additive correction after being determined through the median sky flatting procedure.

Multiplicative and additive corrections are the same to first order, that is, the first order Taylor expansion of $1/(1-x) \approx 1-x$, when x is small. In very long exposures, where the corrections are smoothed by the coaddition of many frames, the difference becomes negligible, and in the HDS, both the dome flats and the sky flats were used as multiplicative corrections. However, in the HMDS and the HMWS, the distinction was made. The noise in the final images was determined to be the same whether the sky flats were divided or subtracted, and it was decided to use subtraction so as to preserve the photometric accuracy. The order of operations makes no difference algebraically, so subtracting the skyflat and then dividing by the domeflat is equivalent to dividing first and then subtracting. However, because of the importance of normalization in the construction of the skyflat, the images were always flattened with domeflats before the skyflats were constructed.

After the dome flats were divided into the images, the images were assembled into cubes and normalized. For the median sky flat procedure to work,

normalization is very important, for a slight difference in the background level from frame to frame will result in a biased median. For example, if the images have radically different background levels, the median could pull out a single image from the middle, which would then not have the benefit of reduction in noise by the square root of the number of images, and instead would have the effect of increasing the noise of each image by $\sqrt{2}$. The images were normalized to the mode determined by fitting a parabola to the logarithm of the histogram of the pixels of the image.

The sky flat was then constructed and subtracted from the images. The images were then co-registered with a two dimensional cross-correlation program, that cross-correlated each image with every other image, and used a least-squares analysis to determine all of the shifts. Because so many of the images in the HMDS lacked bright objects, there was not always sufficient signal to noise in the cross-correlation to accurately determine the registration (I used a minimum ratio of 4 for the peak to noise in the cross-correlation). When the resulting shifts did not match the original input shifts to better than 2 pixels, or when one or more images did not have meaningful shifts, the shifts were determined by choosing an object by eye, and centering on the maximum pixel in each image.

The images were then co-registered and coadded. A mask was then made, by taking every pixel above 3 sigma, and a 3x3 pixel square around every neighboring pixel above 2 sigma. This mask was unshifted and applied to every original, unsubtracted image. These images, with the objects masked out, were then normalized, and used to construct a second sky flat. The reason for this two-pass system is that objects in the images do affect the sky flat. While the images with the objects are not selected by the median, the objects bias the median because the pixels with the objects are always above the median, even if they "should" be below. Thus the median is slightly higher, by $1\sigma/\sqrt{n}$, where n is the number of images,

than it should be. This results in ghost images, or depressions around each object matching the offset grid pattern. Using two passes to eliminate objects from the frames going into the sky flat reduces this effect to an acceptable level.

Another problem with the median sky flat determination is that if the image to be flattened, or sky subtracted, is used in the median determination, approximately 1/n of the pixels will have been taken from that image. If the sky flat is then subtracted from the image, these pixels will all be set to 0, or if divided, they will be set equal to the normalization factor. While these pixels are, theoretically, part of the sky background, and not part of the objects, thus not affecting the photometry, they make it very difficult to accurately determine the noise of the image, and additionally might bias the local sky subtraction. Using the image in its own flattening adds no information, because it affects only the background pixels, and does not help with flattening the pixels that contain objects. It is the pixels that contain objects that must be flattened, after all, so using the image to be flattened in the sky flat will again only artificially lower the noise in the sky, while not affecting the objects. If computer time is at a premium, it can be necessary to construct but a single sky flat for all of the frames, and this was done in the early stages of this project for some of the optical data. However, most of the data was flattened with sky flats produced without the frame to be flattened, and individual sky flats were made for each frame.

In the optical and infrared two different procedures were followed at this point. The background in the K band varies much more than the background in the optical, and significant variation can be seen on the scale of hours. In the optical, while variation is seen from field to field within a single night, this is due to differences from point to point on the sky, such as from the moon, rather than a time variation. Thus in the infrared, the sky flat for each frame was produced from

12 frames on either side of the frame to be flattened. This corresponds approximately to data taken within 30 minutes of the frame to be flattened. This number was determined empirically, fewer than 24 frames resulted in the sky flats being noisy enough to add noise to the images, while with more than 24 frames the time variation of the detector increased the noise. In addition, with more than 24 frames, too much computer time was needed to calculate the median.

For the optical images, there were often too few frames on a single field in a single night to construct a median sky flat that would not add noise to the images. Thus all of the frames taken with the same filter on the same night were used to construct median sky flats. In addition, sky flats were constructed with the frames from a single field. With median filtering, the small scale pixel-to-pixel variations were taken from the sky flats from the whole night, and used to modulate the large-scale variations determined from the single field sky flats.

The optical images were then shifted and coadded as before. The infrared images, however, had 0.75 arcsecond pixels, with seeing of about 1 arcsecond, so they were expanded bilinearly 2x2. Before this was done, however, the cosmic rays and bad pixels were removed. The images were shifted so that the objects were aligned, and a median response was determined for each pixel. Every pixel more than 3 sigma away from the median was assumed to be a cosmic ray. These pixels, and every pixel which had previously been flagged with a magic number (the "bad" pixels) were then replaced with the median. The frames were then expanded, new cross-correlation shifts were determined, and the images were shifted and coadded.

The infrared images in the HMWS were treated similarly, however, cosmic rays were not filtered out, as each position on the sky was observed just 3 times in the infrared, and only 1 time in each optical filter. Cosmic rays were thus left in, and were removed at a later time. The optical images for the HMWS were not sky

flatted, but instead the dome flat was deemed to be good enough. The exposures in the B band were shorter than for the HMDS, so it was not feasible to use the HMDS images to flatten these images. However, due to the short exposures the majority of the noise comes from the photon noise of the background, and flat fielding with the dome flats to 1% was sufficient.

The calibration of the final images was done with standard stars of known brightness. In the optical these were taken from the list of Landolt, (1983). The standard star exposures were treated as much as possible in the same way as the field frames. The dome flat for each night was divided into the standard star exposures for that night. A sky flat chosen to be representative for that night was divided into the exposures. The photometry of the star was measured in a large (15 arcsecond) aperture, and the average of 4 similar apertures placed on the sky around the star was subtracted. In the infrared, the standard stars were taken from the list of Elias *et al.* (1982). Each star was observed successively at two places on the detector. The dome flat was divided into the two images, and then the two images were subtracted. This was done to simulate the subtraction of the sky flat from the field frames. Because of the time variation of the sky and the vastly different exposure times of the standard stars and the field frames, a real sky flat could not be used.

In the K band, the standard stars were checked for a color or airmass term, but these were not necessary. In the I band, an airmass term was calculated from different measurements of the same star on the same night at different airmasses. In the I band a color term was not necessary. In the B band, both airmass terms and colors terms were determined, the airmass term first from different measurements of the same star, and then the color term from measurements of different stars.

Noise determination in the final images was not a trivial process, since the noise measured on pixel scales was different than the noise measured on scales of the aperture used, and it is the latter which is the true noise of the photometry. Several methods were tried, including fitting a gaussian to the histogram of the data binned appropriately (actually, fitting a parabola to the log of the histogram), and doing an iterative three sigma clipping to the data, again binned appropriately, and then calculating the standard deviation. The problem with both these methods, however, is that when the data is binned on the scales of the aperture used, binning images of 1000^2 pixels by a factor of 15^2, the data does not have enough bins for accurate gaussian fitting, and it is heavily biassed by objects. A 5 arcminute squared image with of order 70^2 pixels at this depth could be considered confusion limited.

To determine the noise in the images at the scale of the objects a third method was used. Apertures, with local sky subtraction were placed at 100,000 random positions on the image. The edges of the images were blocked out, since the mosaicing procedure necessary for the median sky flatting results in the noise being higher at the edges, and the noise in the central region was being measured. The resulting measurements were then binned appropriately and the full width half max of the histogram was measured. The binning factor was determined iteratively at 100 bins in $\pm$ 3 σ, and the noise was determined at the 1/10 of a bin level.

Figure 3.2 is a plot of the noise in a typical image (HMDS SSA-22) as a function of the aperture used to measure it. In each case local sky subtraction was used, thus the small scale noise measurements do not include the larger scale noise.

The noise for each individual object in each filter in the HMDS was then calculated based upon the exposure at the position of the object. The noise for the

image measured in the manner described above was taken as the noise for the modal exposure for the image, and was scaled as the square root to the exposure in the aperture of the object. The varying exposure across the image resulted in varying levels of signal to noise at the same magnitude. However, for the number counts discussed in Chapter 5 the high noise regions at the edges of the images were excluded, so that the objects comprising the number counts to K = 18 do not go below 4 σ, and the majority of the objects are at 5 σ or higher. For the HMWS, the exposure across the images is relatively constant, so a single value of the noise was used for each image.

IV. Object Identification and Catalog Preparation

The object identification method is a critical part of the compilation of the number counts. While at the brighter, high signal to noise levels object identification is trivial, at the fainter levels the exact method can potentially bias the results. When number counts are compiled at the level of less than 5 σ the object identification method must be checked. Checking the object identification software is done by placing random known objects on the images and seeing if they are then recovered. Since this method only works if the object identification program results in an undercount of the objects, the parameters are usually set so that the program finds very few false objects, but instead errs on the side of failing to find real objects. The number counts are then corrected by the fraction of randomly placed known objects which the program fails to find. Object identification algorithms typically require correction when the noise in the objects falls below 5 σ, and at the 2 to 3 σ level the correction factors rapidly grow very large (Tyson, 1988, Lilly *et al.*, 1990). Thus at the K = 17 level for the HMWS and the K = 18 level for the HMDS, corresponding to approximately 5 σ no correction for object identification was used.

The catalog was prepared by a program which took every pixel in the images which were above a threshold, and traced it to the local maximum. These local maxima were then checked with the aperture photometry to see if they were above the threshold of image detection. The surface brightness threshold for potential objects was determined empirically, and was set to be approximately 2 σ. Images had several thousand local maxima above this limit, of which several hundred were objects above 5 σ. Several bright extended objects in the fields were checked, and it was determined that their peak surface brightness would be above the threshold if they were dimmed to the object detection level. Setting the levels higher than 2 σ resulted in the failure to detect known objects.

The aperture used was circular, but composed of whole pixels. All pixels which were even partially within the nominal circle were included, so the aperture is actually slightly larger than the diameter would indicate. However, all measurements which relied upon the area, such as for the noise, made use of the actual number of pixels in the aperture. The local sky was determined to be the median within an annulus surrounding the object. The aperture used in the infrared for both the HMWS and the HMDS had a diameter of 17 of the expanded pixels, or 6.375 arcseconds. The local sky was determined in an annulus with inner diameter of 8.625 arcseconds and an outer diameter of 11.625 arcseconds. Except for the brightest and largest extended objects, this was well outside the objects.

The flux limit in the aperture with local sky subtraction was taken nominally to be 5 σ, although this limit was adjusted slightly so as to provide a common limit for all the fields, and to provide even magnitude bins for the number counts. For the HMWS this limit was K = 17; for the HMDS it was K = 18, except for the Dur-13 and SSA-17 fields which were clipped off at K = 17 due to short exposures. For each field the catalog was prepared with a limit one half magnitude fainter than the final

cutoff, so that later corrections such as the aperture correction, and a minor adjustment to the photometric zero point did not require re-running the catalog program. The catalog was clipped to the 5 sigma levels only as a final step.

The catalog program had a tendency to produce double detections of the same object when a noise spike caused the object to have two local maxima. These were eliminated by a semi-automatic process that also corrected the photometry for contamination by nearby objects. Every object which had a neighbor within a certain limit (set to be 8 arcseconds for most objects, but larger for the brighter objects) was checked by eye. The fainter of the two objects was corrected for contamination, while the brighter object was left alone. If there was no third object in the way, the photometry of an aperture diagonally opposite the fainter object from the brighter object was subtracted. The subtracted value was not allowed to be negative, if it was then no correction was applied. If there was a third object in the way, another position was selected by eye for subtraction, subject to the constraint that it was an equal distance away from the brighter object as the fainter object. This effectively eliminated double identifications for single objects, as the two local maxima were typically separated only by a short distance. This resulted in a large correction factor being subtracted from the fainter local maxima, which put it lower than the detection cutoff, and eliminated it from the catalog. This algorithm worked well at eliminating all of the double identifications which were obvious to the eye.

Photometry in the optical filters was done by aligning the xy K image coordinates for each image, and measuring the aperture photometry. Initial alignment was done with two bright objects. The coordinates for the optical image of all the K selected objects were calculated and photometered. From this list the 10 to 20 brightest objects on the optical image were selected and a centroid was calculated for each. The alignment was then recalculated with a least squares fit.

The alignment consisted of 4 free parameters, the expansion factor, the rotation angle, and the x and y offsets. Thus two objects determines these parameters, and 10 to 20 objects overdetermines them sufficiently to overcome any uncertainties in the centroid. No further alignment was used for the individual objects, as this could cause errors for the fainter objects. The centroid of bright objects was rarely more than one or two 0.34 arcsecond pixels away from the calculated values, so this made little difference in the photometry measured in the 6 arcsecond aperture.

While the 6 arcsecond aperture includes almost all of the light for stars and compact objects, the galaxies are more extended than this. However, use of a larger aperture would increase the sky noise. Choosing the aperture size to use requires balancing the need for a consistent measurement of the total flux, even from objects of differing scale sizes, with the need to minimize the aperture sky noise. In the HMDS, use of a 6 arcsecond aperture corrected to 10 arcseconds by a constant offset for all extended objects was determined to be the optimal balance.

The photometric change with aperture size for a typical field is plotted in figure 3.3. The aperture correction was determined from the galaxies in the field which were relatively well-separated from other objects, and which were more than 1 magnitude brighter than the 5 σ detection limit. The median difference between the measurements at 6 arcseconds and the measurements at 10 arcseconds for these galaxies was then added to each galaxy in the field. The typical correction, determined individually for each image, was about 0.10 magnitudes for extended objects, and about 0.04 magnitudes for compact objects. For the HMWS, galaxies are typically bigger at brighter levels (simply because they are closer, and therefore subtend a larger angle for the same scale size.) Because of the small number of high signal to noise galaxies in the HMWS, the correction was determined from all of the

fields to be 0.20 magnitudes for galaxies. The HMWS fields had a similar correction for stars as the HMDS fields, as is expected for point sources.

The HDS (Lilly *et al.*, 1990, Cowie *et al.*, 1992) used a smaller aperture, 3.5 arcseconds in diameter and corrected this to 6 arcseconds. This use of a smaller aperture was justified as fainter galaxies are smaller because they are more distant, and therefore subtend smaller angles on the sky. The seeing in the HDS was better than in the HMDS and HMWS, being typically 1 arcsecond rather than 1.5 arcseconds. Finally the trend in galaxies to fainter levels is to become more compact. (Lilly *et al.*, 1990). This last is a result of the HDS, and was not known *a priori*. The use of different apertures, while justified, does introduce an offset when measurements of the objects in the overlap regions between the HMDS and the HDS are compared. This offset is an indication that the aperture corrections in the HDS are underestimated for the brightest objects, and the aperture corrections in the HMDS are overestimated for the faintest objects. There is a similar discrepancy between the measured magnitudes of the galaxies in the overlap regions between the HMWS fields and the HMDS fields, although the stars do not show a discrepancy. Each of these discrepancies are of order 0.1 magnitudes, which is the claimed accuracy of each of the surveys.

The K band observations for the HMDS and HMWS were all made during two observing runs, in September and December 1990. Only one field, SSA-08, was observed during both runs, and the data on this field were sufficiently well aligned that they could be combined into a single image. The optical data, however, were taken in 6 observing runs over a period of 26 months, from July 1989 until September 1991, and utilized two different detectors. Multiple measurements of the same field in the same filter were common in the HMDS, although the short exposures used in the HMWS made this unnecessary for that survey. The alignment

and plate scales of the different runs, even with the same detector and optics was not identical. Rather than resampling the data so that different images of the same field could be aligned, the fields were photometered independently, and these measurements were then combined. The observations for the HMDS and the HMWS are listed in tables 3.2 and 3.3 respectively.

Because the list of objects was prepared in the K band, it did not matter if an individual measurement of an object was low in signal-to-noise, if the final combined measurement was higher than the 2 σ cutoff used in the optical. Each observation of a field was independently aligned to the K band image, and the resulting positions were measured. The aperture corrections, measured independently for each HMDS observation were then applied. The different observations of the same objects were compared, and if there was a systematic discrepancy in the field, these were corrected to the image that was most likely to be photometric, based upon indications recorded in the observing logbook. The largest correction for non-photometric conditions which was applied was 0.14 magnitudes, and these corrections are listed in table 3.2. Exposures which required corrections larger than 0.2 magnitudes were not used. Observations for the HMWS were not made under non-photometric conditions, as there was no way to correct them. The measurements from different observing runs were then combined for each object weighted by the inverse square of the noise. The noise in the final photometry is listed in table 3.4, along with the area observed.

V. Star/Galaxy Separation

The problem of star/galaxy separation is not an easy one, but is critical at these magnitudes. Misidentification can have a tremendous effect upon the number counts even when it is random and not systematic, because of the great

preponderance of stars at the bright magnitudes. For color analysis, and follow-up studies, it is a bit less critical than for statistical studies, but misidentification can result in telescope time being wasted. However, the extreme colors which make a galaxy interesting and worthy of further study also make a star interesting. The number counts, for the most part, were determined in areas in which there was data in B, I, and K, so that a combination of morphology and color could be used to positively identify each object. Using morphology alone results in high galaxy counts because of the presence in the data of just barely resolved double stars, which appear morphologically to be galaxies. In addition, in the intermediate magnitudes of the HMDS, any morphological criteria has an area of ambiguity, and the cutoff between stars and galaxies has a tendency to be arbitrary. There is similarly a region of ambiguity on the color-color plot, particularly at relatively low signal-to-noise, and therefore color was used to identify objects, except for this region, where morphological criteria was used.

At the brightest levels, this is not a critical issue, for the galaxies are very large, and morphology is sufficient. At the faintest levels, the number of galaxies is far greater than the number of stars, and misidentification does not have as large of an effect. However, star/galaxy separation is critical in the HMWS and the HMDS, which comprise this thesis. To determine morphology the Kron r_{-2} criteria discussed in Kron (1980) was used. This is defined by

$$(1/r_{-2})^2 \equiv \int(1/x^2)g(x)dx \; / \; \int g(x)dx$$

The r_{-2} criteria weights the central light strongly, and is a measure of the compactness of the object. One advantage of this criteria is that every star (or at least every point source on the same image) has the same r_{-2} measure, independent of brightness. The noise in this measurement is dependent upon brightness, however. The result is small for stars and large for extended objects. The cutoff for

each field was determined empirically from the brightest objects, and then applied to all objects in the field.

The .75 arcsecond pixels were expanded by a factor of 8 in each direction, the centroid for each object was calculated and the inverse second moment in five annuli within a 6.4 arcsecond radius was determined. The local sky, as determined by the original photometry program was subtracted from each pixel, and this reduced the noise in the r_{-2} measure considerably. Because of the large expansion factor, excluding the center pixel (necessary because the data is discrete) had little effect.

To determine star/galaxy separation in color, the two regions on the B-I/I-K diagram corresponding to $2.5(I-K)-(B-I) \geq 2.0$ were used. This criteria is true for stars, and false for galaxies. Figure 3.4 is a plot on the B-I/I-K diagram of no-evolution models of four types of galaxies from $z = 0$ to $z = 1.5$, and the colors of three types of stars (dwarfs, giants and supergiants). The star/galaxy color criteria is plotted as a line. Also plotted is the data for a typical HMDS field. Figure 3.5 is a plot of the morphological criteria versus the color criteria for a typical HMDS field. Where there is conflict between the two criteria the color criteria was used where it is unambiguous, and the morphological criteria was used otherwise.

References for Chapter 3

Broadhurst, T.J., Ellis, R.S., and Glazebrook, K., 1992, *Nature*, **355**:55.

Colless, M., Ellis, R.S., Taylor, K., and Hook, R.N., 1990, *M.N.R.A.S.*, **244**:408.

Cowie, L.L., Gardner, J.P., Hu, E.M., Wainscoat, R.J., Hodapp, K.W., 1992, *Ap. J.*, *submitted.*

Elias, J.H., Frogel, J.A., Matthews, K., and Neugebauer, G., 1982, *A.J.*, **87**:1029.

Kron, R.G., 1980, *Ap. J. Supp.*, **43**:305.

Landolt, A.U., 1983, *A.J.*, **88**:439.

Lilly, S.J., Cowie, L.L., and Gardner, J.P., 1991, *Ap. J.*, **369**:79.

Tyson, J.A., 1986, *J. Opt. Soc. Am.*, **A 3**:2131.

Tyson, J.A., 1988, *A.J.*, **96**:1.

Field	R.A.	Dec.	b	l	POSS	Cluster	Near Star	Surveys
SSA-00	0:15:20	11°00'00"	-50°43'31"	109°44'58"	9	none	SAO 091816	HMWS
SSA-01	1:05:20	10°00'00"	-52°23'58"	129°27'50"	1274,635	none	SAO 092270	HMWS
SSA-02	2:05:20	12°00'00"	-46°30'14"	150°33'31"	209	none	SAO 092819	HMWS
SSA-03	2:55:20	-2°00'00"	-50°35'13"	178°19'49"	1453	none	SAO 130204	
SSA-04	3:54:57.3	1°01'00"	-37°05'09"	188°23'18"	232	none	SAO 111532	HDS,HMDS,HMWS
SSA-08	8:00:00	50°00'00"	31°46'11"	169°03'39"	1317	none	SAO 026649	HMDS,HMWS
SSA-09	9:00:00	41°00'00"	41°38'08"	181°08'02"	721	none	SAO 042659	
SSA-10	9:55:00	30°00'00"	51°58'54"	198°26'31"	1396	none	SAO 061783	
SSA-11	11:00:00	44°00'00"	62°33'13"	168°36'37"	1349	none	SAO 043583	
SSA-12	11:50:00	32°00'00"	76°24'04"	189°41'03"	1379	none	SAO 062740	
SSA-13	13:10:01.2	43°00'33"	73°49'47"	109°05'49"	133	none	SAO 044503	HDS,HWS
SSA-14	13:55:00	28°00'00"	75°23'24"	39°11'29"	86	1357.1+2836	SAO 083084	
SSA-15	15:00:00	40°00'00"	60°12'18"	66°29'22"	1371	none	SAO 064488	
SSA-16	15:40:00	28°00'00"	52°20'36"	44°10'37"	121	1539.1+2820	SAO 083949	
SSA-17	17:04:59.8	43°59'35"	36°50'41"	69°06'30"	1135	none	SAO 046500	HDS,HMDS,HWS
SSA-18	17:55:00	53°00'00"	29°29'22"	80°45'23"	1102	none	SAO 030625	
SSA-22	22:15:01.0	0°00'06"	-44°00'50"	63°03'23"	1146	none	SAO 145977	HDS,HMDS
SSA-23	23:10:00	-1°00'00"	-54°30'19"	76°52'01"	834	2312.5-0229	SAO 146564	
Dur-00	0:54:49.4	-27°43'53"	-88°16'43"	172°14'19"	21	----	SAO 166695	HMDS,HMWS
Dur-10	10:43'55.4"	0°05'33"	49°25'36"	250°03'09"	1397	none	SAO 118482	HMDS
Dur-13	13:41'57.3"	0°06'25"	59°53'32"	330°09'35"	465	1342.4+0016	SAO 120092	HMDS

Table 3.1: The HDS Small Selected Areas, and the three Durham fields of Colless *et al.*, (1990). The right ascension and declination are given, along with the galactic latitude b and longitude l, the Palomar Sky Survey plate number, the Zwicky clusters which contain the field, a nearby SAO star, and which surveys contain observations of the field.

Date	Field	Filter	Exposure	Phot.	Depth	P.C.	GAC	SAC
July 1989	SSA-17	I	18x5=90	Y	23.16	0.00	0.13	0.04
July 1989	SSA-22	I	15x5=75	Y	22.85	0.00	0.11	0.04
July 1989	SSA-17	B	9x10=90	Y	25.16	0.00	0.18	0.05
July 1989	SSA-22	B	9x10=90	N	25.24	0.13	0.15	0.03
Oct 1989	SSA-04	I	26x5=130	N	23.70	0.58	0.09	0.03
Oct 1989	SSA-08	I	12x5=60	no good				
Oct 1989	SSA-04	B	9x10=90	no good				
Oct 1989	SSA-08	B	3x10=30	no good				
Oct 1989	Dur-00	B	3x10=30	Y	24.58	0.10	0.09	0.05
Oct 1989	Dur-00	I	6x5=30	Y	22.79	0.00	0.14	0.04
Oct 1989	SSA-04	I	12x5=60	Y	23.18	0.00	0.13	0.05
Dec 1989	Dur-00	B	5x10=50	Y	24.86	0.03	0.10	0.03
Dec 1989	SSA-04	B	12x10=120	Y	25.40	0.03	0.25	0.03
Dec 1989	SSA-08	B	9x10=90	Y	25.26	0.00	0.08	0.03
Dec 1989	Dur-10	B	9x10=90	Y	25.10	0.00	0.20	0.04
Dec 1989	Dur-13	B	4x10=40	Y	24.33	0.00	0.23	0.04
Dec 1989	Dur-00	I	6x5=30	Y	22.26	0.06	0.07	0.03
Dec 1989	SSA-08	I	18x5=90	Y	23.13	0.00	0.09	0.03
Dec 1989	SSA-09	I	12x5=60	Y				
Dec 1989	Dur-10	I	18x5=90	Y	23.17	0.00	0.14	0.03
Dec 1989	Dur-13	I	11x5=55	Y	22.70	0.00	0.12	0.03
Feb 1990	SSA-17	B	5x10=50	Y	24.73	0.01	0.20	0.07
Feb 1990	SSA-12	B	9x10=90	Y				
Feb 1990	Dur-13	B	5x10=50	N	24.83	0.14	0.19	0.03
Sept 1990	Dur-00	K	62x1=62	Y	20.17	0.00	0.08	0.04
Sept 1990	SSA-04	K	56x1=56	Y	20.23	0.00	0.08	0.04
Sept 1990	SSA-08	K	27x1=27	Y	19.90	0.00	0.08	0.03
Sept 1990	SSA-17	K	9x1=9	Y	18.93	0.00	0.14	0.04
Sept 1990	SSA-22	K	92x1=92	Y	20.45	0.00	0.11	0.04
Oct 1990	SSA-22	B	9x10=90	Y	25.09	0.00	0.10	0.03
Oct 1990	SSA-22	I	18x5=90	no good				
Oct 1990	Dur-00	I	12x5=60	Y	23.08	0.00	0.11	0.03
Oct 1990	SSA-04	I	6x5=30	Y	22.91	0.00	0.09	0.03
Oct 1990	Dur-00	B	7x10=70	Y	24.88	0.00	0.08	0.02
Oct 1990	SSA-04	B	6x10=60	Y	24.98	0.00	0.07	0.03
Oct 1990	SSA-08	B	5x10=50	Y	24.75	0.01	0.07	0.01
Dec 1990	SSA-08	K	25x1=25	Y	19.86	0.00	0.08	0.03
Dec 1990	Dur-10	K	25x1=25	Y	20.02	0.00	0.16	0.08
Dec 1990	Dur-13	K	9x1=9	Y	19.37	0.00	0.18	0.03

Table 3.2: The observations of the HMDS fields. Listed are the date of the observing run; the field name; the filter; the number of exposures, the time of each exposure in minutes and the total exposure; whether or not the observation was photometric, with the photometric correction less than 0.10 magnitudes; the 1 σ depth in the 6 arcsecond aperture; the photometric correction; the aperture correction for the galaxies; and the aperture correction for the stars.

Date	Field	Filter	Exp.	Airmass	Depth	Gal.A.C.	Star A.C.
Dec 1990	SSA-00	K	3.	1.13	18.51	0.20	0.050
Sept 1991	SSA-00	I	5.	1.05	22.28	0.17	0.034
Sept 1991	SSA-00	B	5.	1.03	23.44	0.19	0.026
Dec 1990	SSA-01	K	3.	1.02	18.53	0.20	0.040
Sept 1991	SSA-01	I	5.	1.14	22.59	0.17	0.038
Sept 1991	SSA-01	B	5.	1.04	23.76	0.19	0.090
Dec 1990	SSA-02	K	3.	1.01	18.59	0.20	0.034
Sept 1991	SSA-02	I	5.	1.02	22.43	0.17	0.041
Sept 1991	SSA-02	B	5.	1.01	23.80	0.19	0.021
Dec 1990	SSA-03	K	3.	1.08	18.68	0.20	0.047
Sept 1990	SSA-04	K	3.	1.09	18.39	0.20	0.045
Oct 1990	SSA-04	I	5.	1.06	21.74	0.21	0.043
Oct 1990	SSA-04	B	5.	1.10	23.30	0.23	0.016
Sept 1990	SSA-08	K	3.	1.65	18.46	0.20	0.037
Oct 1990	SSA-08	I	5.	1.28	21.63	0.21	0.048
Oct 1990	SSA-08	B	5.	1.40	23.07	0.23	0.019
Sept 1990	Dur-00	K	3.	1.52	18.64	0.20	0.036
Oct 1990	Dur-00	I	5.	1.49	21.49	0.21	0.037
Oct 1990	Dur-00	B	5.	1.50	23.05	0.23	0.009
Dec 1990	Dur-00	K	3.	1.48	18.63	0.20	0.061

Table 3.3: The observations of the HMWS fields. Listed are the date of the observing run; the field name; the filter; the exposure in minutes; the airmass; the 1 σ depth in the 6 arcsecond aperture; the aperture correction for the galaxies; and the aperture correction for the stars.

Field	Survey	K depth	I depth	B depth	area	max
Dur-00	HMDS	20.17	23.35	25.28	24.86	17.23
SSA-04	HMDS	20.23	23.30	25.57	24.27	16.70
SSA-08	HMDS	20.26	23.37	25.41	24.37	15.15
Dur-10	HMDS	20.02	23.41	25.08	22.44	15.37
Dur-13	HMDS	19.37	22.90	24.90	23.46	16.27
SSA-17	HMDS	18.93	23.16	25.31	25.03	13.65
SSA-22	HMDS	20.45	22.85	25.47	23.23	12.99
SSA-00	HMWS	18.51	22.28	23.44	97.65	97.65
Dur-00	HMWS	18.64	21.49	23.05	97.65	97.65
SSA-01	HMWS	18.53	22.59	23.76	97.65	97.65
SSA-02	HMWS	18.59	22.43	23.80	97.65	97.65
SSA-04	HMWS	18.39	21.74	23.30	93.75	93.75
SSA-08	HMWS	18.46	21.63	23.07	97.65	97.65

Table 3.4: The depths and areas of the fields. Listed are the field name; the survey; the K band depth, 1 σ in a 6 arcsecond aperture; the I band depth; the B band depth; the area in square arcminutes which is covered in all three bands; and the area covered with the maximum exposure.

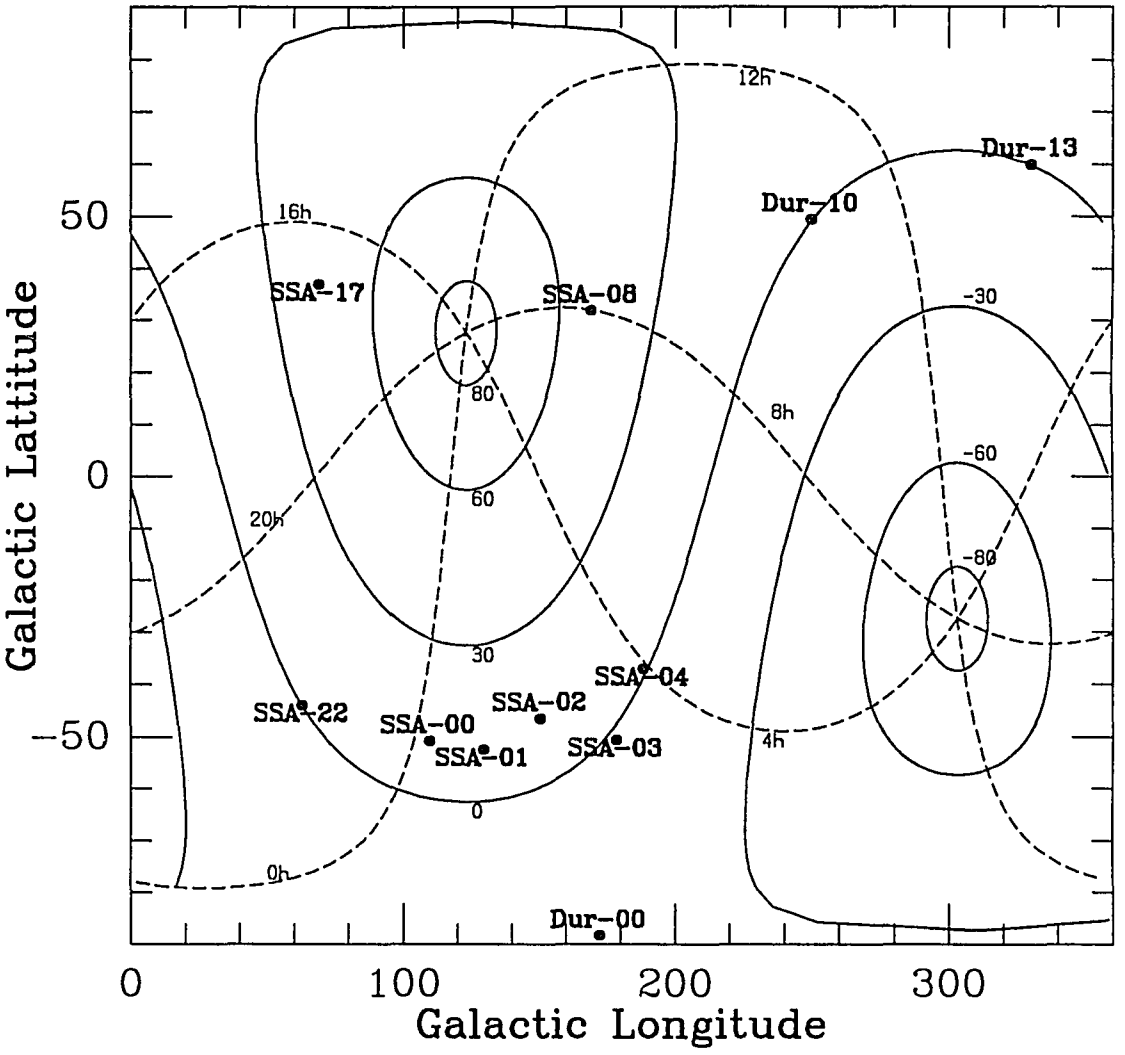

Figure 3.1: The positions in galactic coordinates of the fields in the HMDS and the HMWS. Also plotted are lines of constant declination (solid) and lines of constant right ascension (dashed).

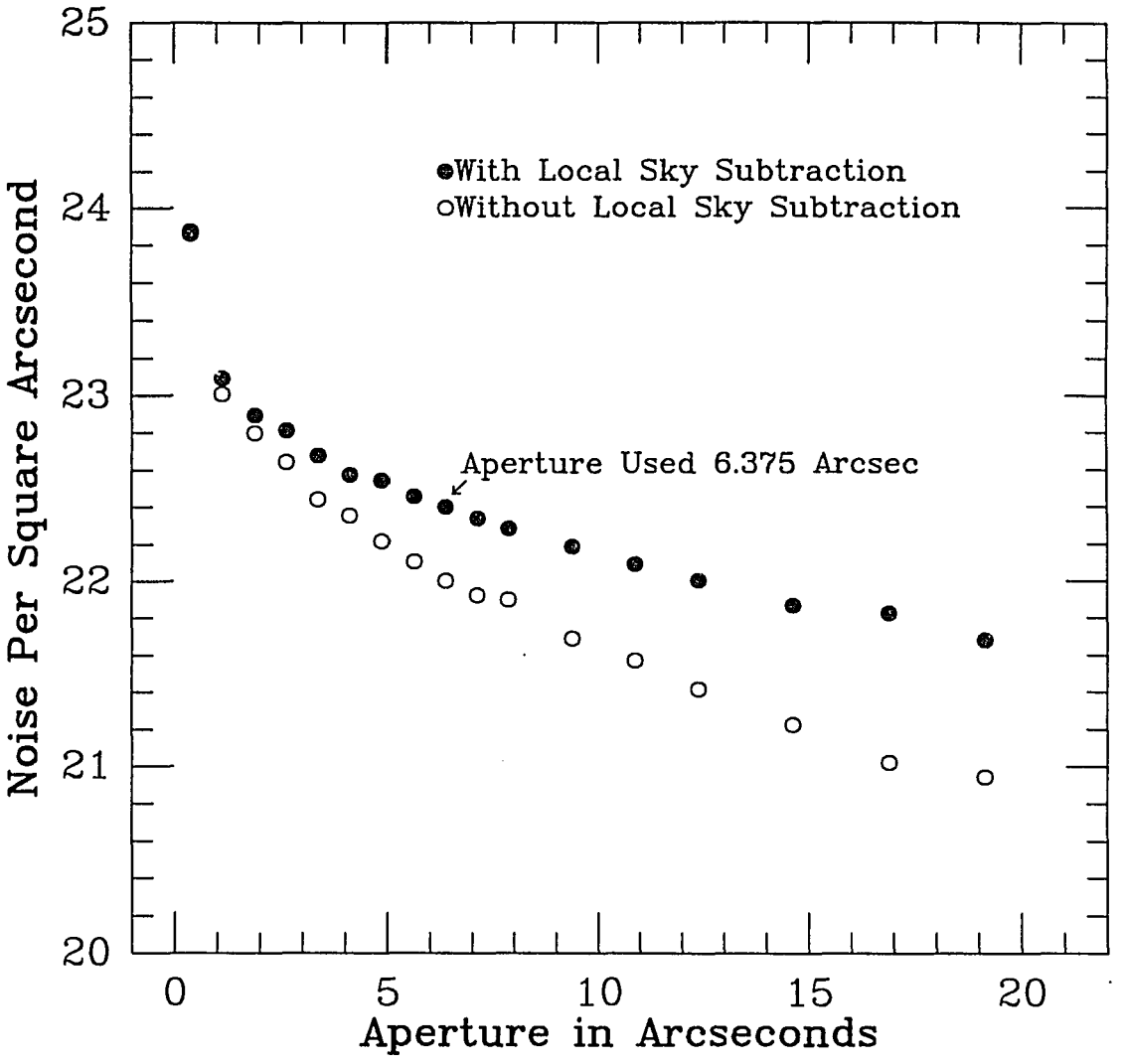

Figure 3.2: The noise measured in a typical image (HMDS SSA-22) as a function of the size of the aperture used to measure it. This is a measure of the scale of the noise. The large difference between a 1 pixel aperture and a 3 pixel aperture is due to the smoothing introduced by expanding the images by a factor of 2. The aperture used for objects in the HMWS and the HMDS is 6.375 arcseconds.

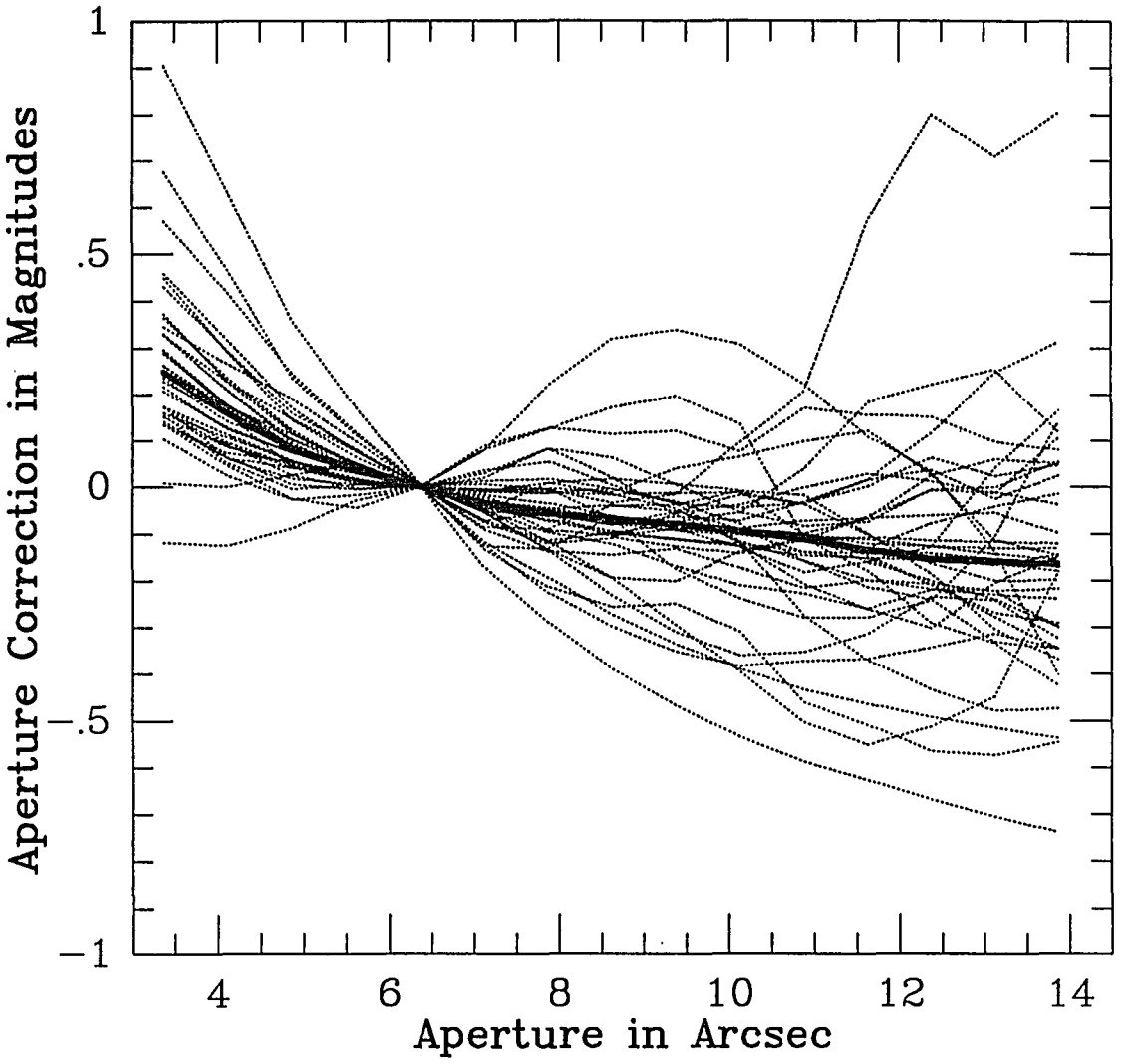

Figure 3.3: The measured photometry of galaxies as a function of aperture size plotted for a typical field in the HMDS (SSA-22). Only the galaxies which were well separated and are brighter than K = 18 are plotted, and the stars are not plotted. The solid line represents the median for each aperture size. All points have the magnitude in a 6 arcsecond aperture subtracted. The aperture correction used for this field is the point at 10 arcseconds, or 0.12 magnitudes.

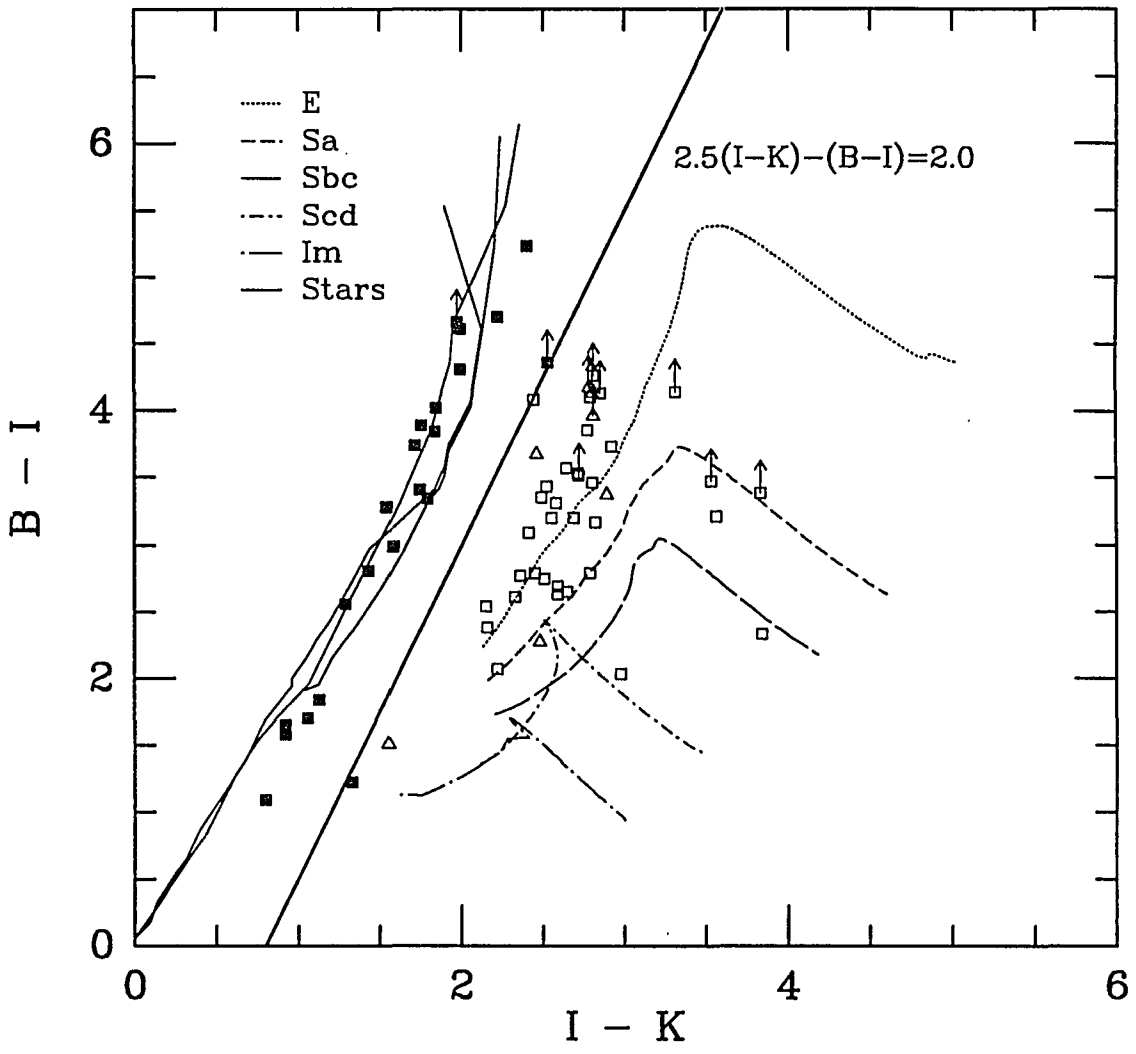

Figure 3.4: The color-color plot of a typical field in the HMDS (SSA-22). No-evolution models of four types of galaxies are plotted from z = 0 to z = 1.5. Models for three types of stars, dwarfs, giants and supergiants, are plotted. The star/galaxy color criteria 2.5(I-K)-(B-I) ≥ 2.0 is plotted as a solid line. The objects in the field are plotted as squares if the morphological criteria and the color criteria agreed, as triangle if they disagreed. Filled symbols denote stars, open symbols denote galaxies.

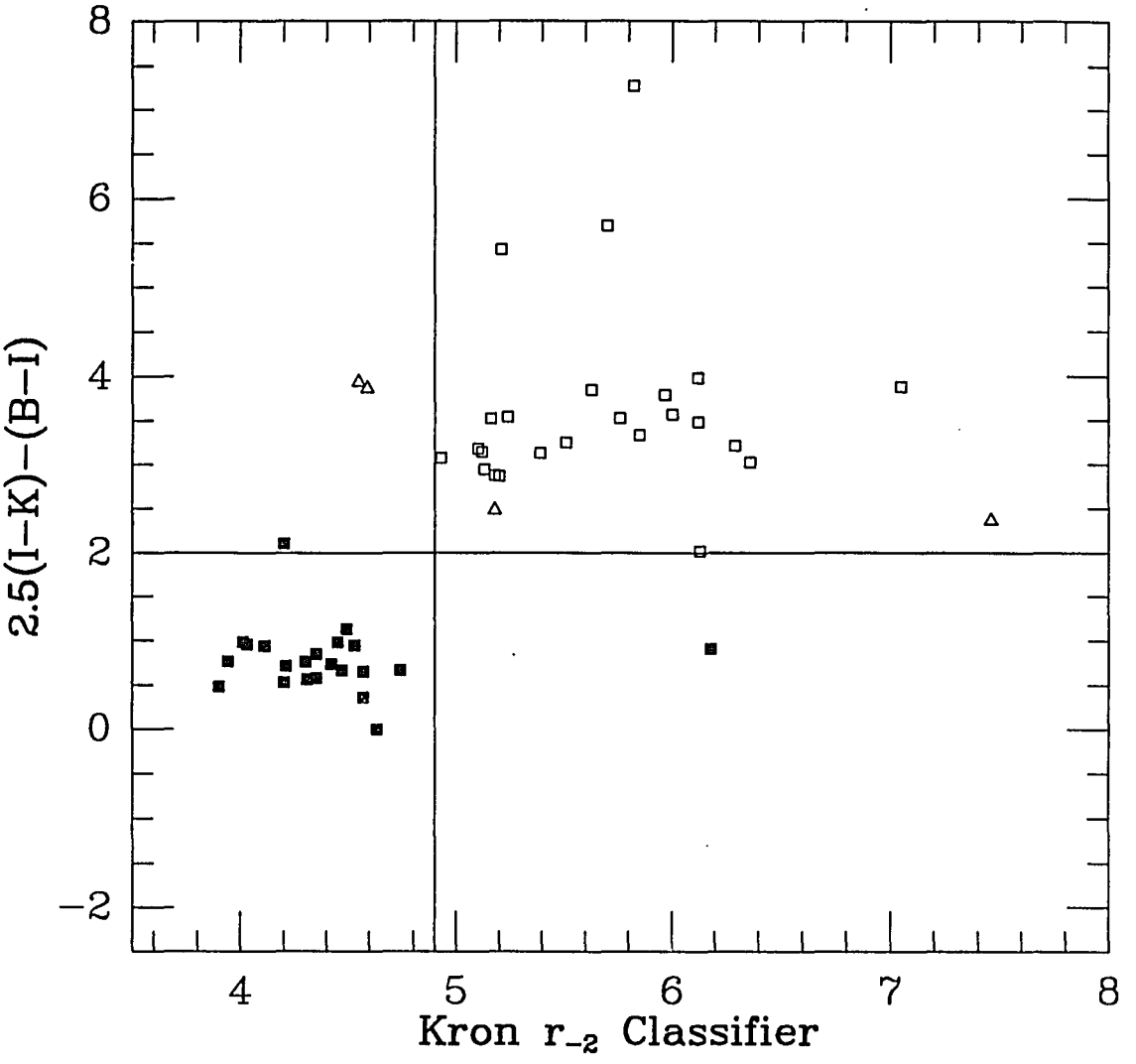

Figure 3.5: A comparison of the morphological r_{-2} criteria and the color criteria for star/galaxy separation for a typical HMDS field (SSA-22). The two criteria agree for objects in the lower left (stars) and upper right (galaxies) quadrants, and disagree for objects in the upper left and lower right quadrants. Objects in the upper left quadrant are mostly compact galaxies, and those in the lower right are double stars and saturated stars.

Chapter 4: The Hawaii Deep Survey K Band Observations

The Hawaii Deep Survey has obtained near-infrared faint galaxy counts to K = 23. The low number of galaxies making up these counts favors a $q_0 = 0.5$, $\Lambda = 0$ cosmological geometry. The B band number counts show a large excess of objects over this model. By combining spectroscopic redshift identifications with the K magnitudes, we show that this excess is caused by a population of faint blue dwarfs which is present at redshifts of $z \approx 0.4$, but is not counted in the local population. The dwarf galaxies contain as much K light as the normal galaxy population and may dominate the baryonic matter content of the universe.

I. Introduction

The cosmological deceleration parameter, q_0, can in principle be determined from galaxy number counts, but in practice luminosity and number evolution can easily dominate the geometrical effects. With samples selected in the radio and the optical evolution effects are strong because the nuclear activity producing the radio emission, and the massive stars producing the optical emission have short timescales relative to the age of the galaxy, and thus it is difficult to compare these samples to a present day population.

In the near-infrared, 2.2 microns or the K band, for non-starburst galaxies, the light is from near solar mass stars whose lifetimes are similar to the age of the galaxy. The evolutionary corrections are much smoother as these stars do not change quickly. At high redshifts the K band samples the well understood rest frame optical part of the spectrum, which is much flatter than the rest frame ultraviolet. Thus the cosmological dimming due to the K correction is less, allowing us to sample to large redshifts at brighter magnitudes.

When we reach faint enough levels to break through and sample the whole of the galaxy occupied volume, the number counts contain information about the geometry and the redshift of galaxy formation in the same way that star counts give us the structure and limits of our own galaxy.

II. The Hawaii Deep Survey

The Hawaii Deep Survey was designed to obtain deep K band galaxy samples with corresponding optical colors which can also be used as a basis for spectroscopic observations. We are using a Rockwell 256x256 HgCdTe array detector on the University of Hawaii's 2.2 meter telescope and on the Canada France Hawaii Telescope. We have K band galaxy counts to K = 23, and spectroscopic identifications are nearly complete for the B < 24 sample. We have begun spectroscopic work on a K band selected sample. In addition, work has begun on a wide field sample which will provide good signal to noise on the number counts from K = 14 to K = 20. Results obtained to date are reported in Cowie *et al.*, (1990), Lilly, *et al.*, (1991), and Cowie *et al.*, (1992).

The B band galaxy number counts, normalized to a simple power law, are plotted in Figure 4.1 against galaxy evolution models adapted from Yoshii and Takahara (1988). The models have numerous assumptions about the present population mix, the galaxy luminosity function, and galaxy evolution (younger galaxies being bluer and more luminous,) however, there are several model-independent conclusions which can be drawn. Up to B = 22, we can model the counts well. Beyond this the counts rise more rapidly than any of the models, even the extreme case with non-zero Λ. An open universe has more volume at high redshift than a closed universe, and a flat universe with $\Lambda = 0.9$ and $\Omega = 0.1$ has

even more volume, giving higher number counts at the faint end. These models do not, however, predict enough galaxies to fit the data.

Luminosity evolution has a stronger effect than geometry for the B selected sample. Because younger galaxies are expected to be brighter in the blue, they are seen to greater distance, and therefore more galaxies are counted. These galaxies should be at high redshift. Spectroscopic work has shown that this is not the case. Until the K band counts existed, there were two proposed explanations for the excess B counts, one cosmological and one astrophysical. The cosmological hypothesis was that we live in a flat universe with $\Lambda = 0.9$ and $\Omega = 0.1$, and there is moderate galaxy evolution (see, *e.g.*, Lilly, *et al.*, 1991). The B band number count data can be fit with this hypothesis, but they require a fairly low redshift of formation for the galaxies. The proposed astrophysical explanation is that there is a population of blue dwarf galaxies at redshifts of about 0.4 which is not included in the present day luminosity function (see *e.g.* Broadhurst *et al.*, 1988).

The K band counts are more sensitive to the cosmological geometry than the B band counts. At K = 17, the counts stop rising rapidly and flatten out to a much shallower slope. At this point we are no longer sampling to greater distances, but are seeing through to the end of the galaxy occupied volume. The count's slope is the faint end shape of the luminosity function averaged through this volume.

Thus the counts at the faint end favor a $q_0 = 0.5$, $\Lambda = 0.0$ geometry. This result is, of course, model dependent, but is more robust than it might seem at first. These curves represent models with redshift of galaxy formation of $z_{form} = 5$. However, to fit the open universe model to the faint K band counts, we would need to make z_{form} equal to 2, and for the more extreme non-zero Λ model, $z_{form} = 1.5$. In addition, this result is based upon a deficiency of galaxies, and this is much harder to explain away than the excess seen in B. Luminosity evolution makes galaxies

bright in the past and would increase the number counts. The same holds true for merging models. The stars which give off the K band light have been there since the galaxy formed, so it is very difficult to dim the galaxy relative to its current luminosity. The model independent conclusion to draw from the number counts is that there is no way to fit both the B band and the K band number counts with the same population. The difference between the B and K counts is essentially a color problem.

Figure 4.2 is a plot of the median B-K color vs. K magnitude. At the bright end we have B-K of 5 to 6, which is typical of a non-evolved galaxy population at moderate redshift. However, at the faint end B-K falls to 4, which is as blue as a local irregular. The surprise is that this happens in a K selected sample. The population must be dominated by starbursting galaxies. The blueness of the faint population is the cause of the discrepancy between the blue and the infrared number counts. What must be explained in any model is why there are so many faint blue galaxies.

III. The Spectroscopic Sample

We have spectroscopic redshifts for 21 galaxies of the 22 galaxies in the $B < 24$ sample (Cowie *et al.*, 1991). One galaxy remains unidentified, despite an attempt with a very long exposure (20 hours). Although our sample is small, we are complete at the 95% level. Figure 4.3 is our spectroscopic sample, with redshift plotted against B magnitude, along with the data from Broadhurst *et al.* (1988), and Colless *et al.* (1990). The data fits the no-evolution model, and the lack of high redshift objects rules out the strong evolution explanation for the excess B band number counts which are already a large effect at $B = 24$.

We can combine the redshift data with the apparent K magnitude to determine what the population producing the B band excess actually is. That is, the absolute K magnitude, plotted in Figure 4.4 against apparent B magnitude, should give a good estimate of the galaxy mass, except for the most extreme starbursting case where it is an upper limit. At the brighter magnitudes the absolute K magnitudes center around K^* for an elliptical galaxy. At the fainter end, however, which is where the excess B counts appear, we begin to see galaxies that are as much as 4 magnitudes fainter in K. This is unexpected in a magnitude-limited sample where we expect the counts to be dominated by the near-L^* galaxies which can be seen to the limits of largest volumes. Roughly 2/3 of the faintest galaxies appear to be dwarfs of this type. If we try to turn this into a luminosity function we find that the total K luminosity density is 8.1×10^8 L_{sol}/Mpc^3 with roughly half the light coming from the dwarfs and half from normal galaxies.

The blue dwarf population contains an equal amount of K band light as the normal population. Since they are likely to contain more gas than stars, this population could dominate the baryonic mass in the universe. In particular, if dwarfs contain four times as much mass in gas as in stars, then their baryonic density is $\rho_B = 1.4 \times 10^{-31}$ gm cm^{-3}. This is very approximate, but can be compared to the homogeneous Big Bang nucleosynthesis model of Yang *et al.* (1984.) which predicts $\rho = 2\text{-}9 \times 10^{-31}$ gm cm^{-3}

Looking back at the number counts in Figure 4.1 it is possible to see the impact of the blue dwarf galaxies. The population is very blue so it appears as an excess in the B counts, but does not appear in the K counts until we reach fainter levels. Thus these galaxies, instead of being an excess at the K = 18 to 22 level, does not appear until the K = 20 to 24 level, where they fit the models much better.

The observed K^* of the dwarfs is similar to that of the local dwarf spheroid population, but the local density of such objects is far too low to be the same population. Even in the Virgo cluster the ratio of dwarfs to normal galaxies is too low. There are several explanations for where these blue dwarfs are at the present epoch which we must consider. The dwarfs detected in our survey are relatively compact objects, and it is unlikely that they have spread out to become too low surface brightness to be detected nearby.

The galaxies could have merged to form larger galaxies, and this would explain the baryonic density of the dwarfs. However, neither present day ellipticals, because of their colors, nor spirals, because of the fragility of their disks, are the likely result of merging at $z \approx 0.4$.

Two proposals which seem most likely are that the blue dwarfs are either biased away from the local population, or that they have disrupted themselves during the starbursting process. Both of these explanations imply that there is significant biasing of matter away from the light of normal galaxies.

IV. Conclusion

All of our conclusions are model dependent and are yet to be confirmed by other groups. However, our K band number counts indicate that we are living in a $q_0 = 0.5$, $\Lambda = 0$ universe. The B band counts indicate that there is a population of blue dwarfs which flourished at $z \approx 0.4$ but has now burnt out and destroyed itself, or in some other way is no longer counted in the present galaxy population.

If we accept the presence of the blue dwarf population then it contains at least as much baryonic mass as the present day normal galaxies and may account

for the missing baryon problem which is suggested by primordial nucleosynth

models.

The material in this chapter has been published in *The Early Observable Univ*
From Diffuse Backgrounds, edited by B. Rocca-Volmerange, J.M. Deharveng a
Tran Thanh Van, (Cedex:Editions Frontieres), 1991.

References for Chapter 4

Broadhurst, T.J., Ellis, R.S., and Shanks, T., 1988, *M.N.R.A.S.*, **235**:827.

Colless, M., Ellis, R.S., Taylor, K., and Hook, R.N., 1990, *M.N.R.A.S.*, **244**:408.

Cowie, L.L., Gardner, J.P., Lilly, S.J., and McLean, I., 1990 *Ap. J.*, **360**:L1.

Cowie, L.L., Songaila, A., and Hu, E.M., 1991, *Nature*, **354**:460.

Cowie, L.L., Gardner, J.P., Hu, E.M., Wainscoat, R.J., Hodapp, K.W., 1992, *Ap. J.*, *submitted.*

Glazebrook, K., 1991, private communication.

Jenkins, C.R., and Reid, I.N., 1991, *A. J.*, **101**:1595.

Lilly, S.J., Cowie, L.L., and Gardner, J.P., 1991, *Ap. J.*, **369**:79.

Maddox, S.J., Sutherland, W.J., Efstathiou, G., Loveday, J., and Peterson, B.A., 1990, *M.N.R.A.S.*, **247**:1P.

Metcalfe, N., Shanks, T., Fong, R., and Jones, L.R., 1991, *M.N.R.A.S.*, **249**:498.

Tyson, J.A., 1988, *A.J.*, **96**:1.

Yang, J., Turner, M.S., Steigman, G., Shramm, D.N., and Olive, K.A., 1984, *Ap. J.*, **281**:493.

Yoshii, Y., and Takahara, F., 1988, *Ap. J.*, **326**:1.

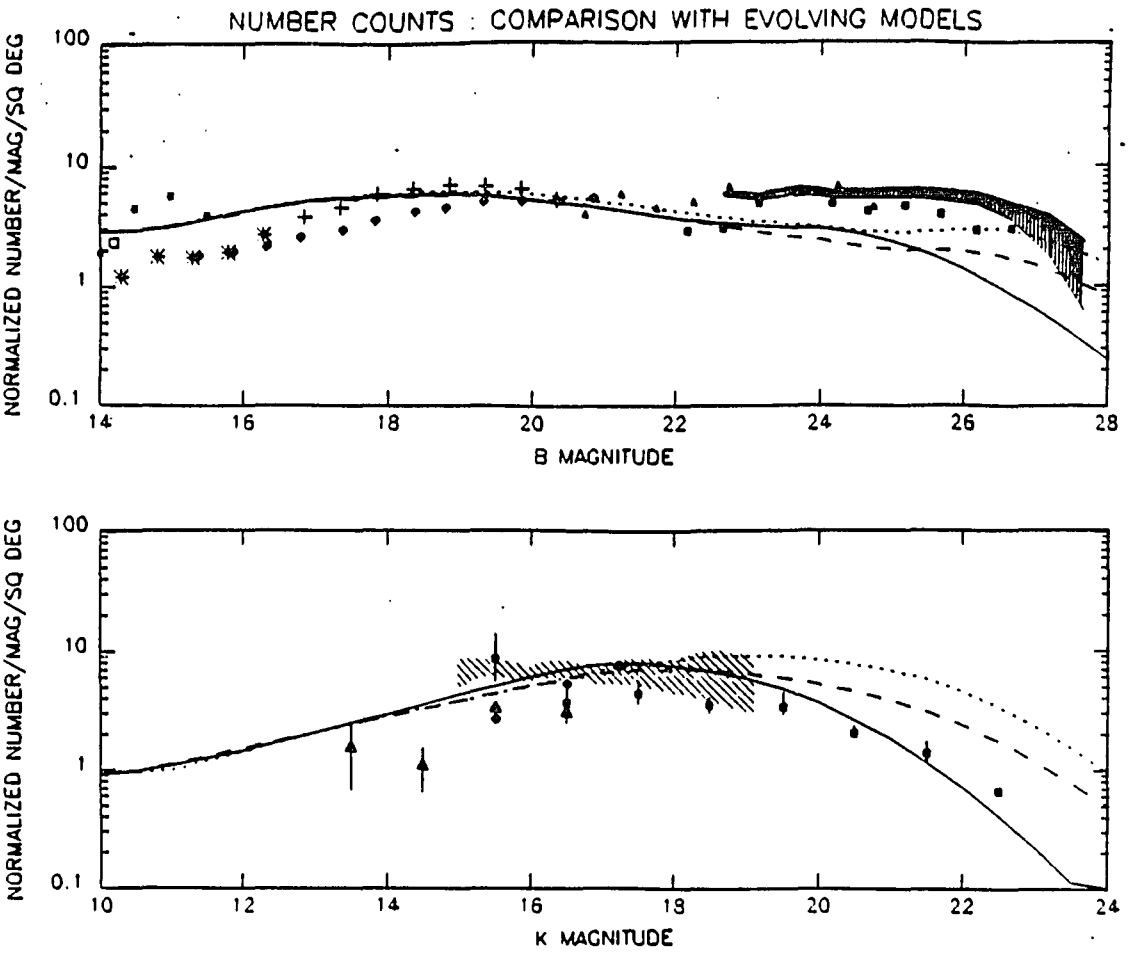

Figure 4.1: A comparison of blue and infrared galaxy counts with model predictions. The blue number counts are taken from the compilation of Metcalfe *et al.* (1991), Tyson (1988; shaded region), Lilly *et al.* (1990; solid squares), and the APM survey (diamonds; Sutherland *et al.* 1990). The infrared counts are taken from Glazebrook (1991; triangles), Jenkins and Reid (1991; shaded region), and our data, reported in Cowie *et al.*, (1992; squares). The models follow those of Yoshii and Takahara, (1988), except that the luminosity function is extended to 10 magnitudes below L^*. The counts have been normalized to power laws of slope 0.45 normalized at B = 16 and K = 11 in order to show the full dynamic range of the data. The models correspond to three geometries, $q_0 = 0.5$ (solid line), $q_0 = 0.02$ (dashed line), and flat with $\Lambda = 0.9$ and $\Omega = 0.1$ (dotted line).

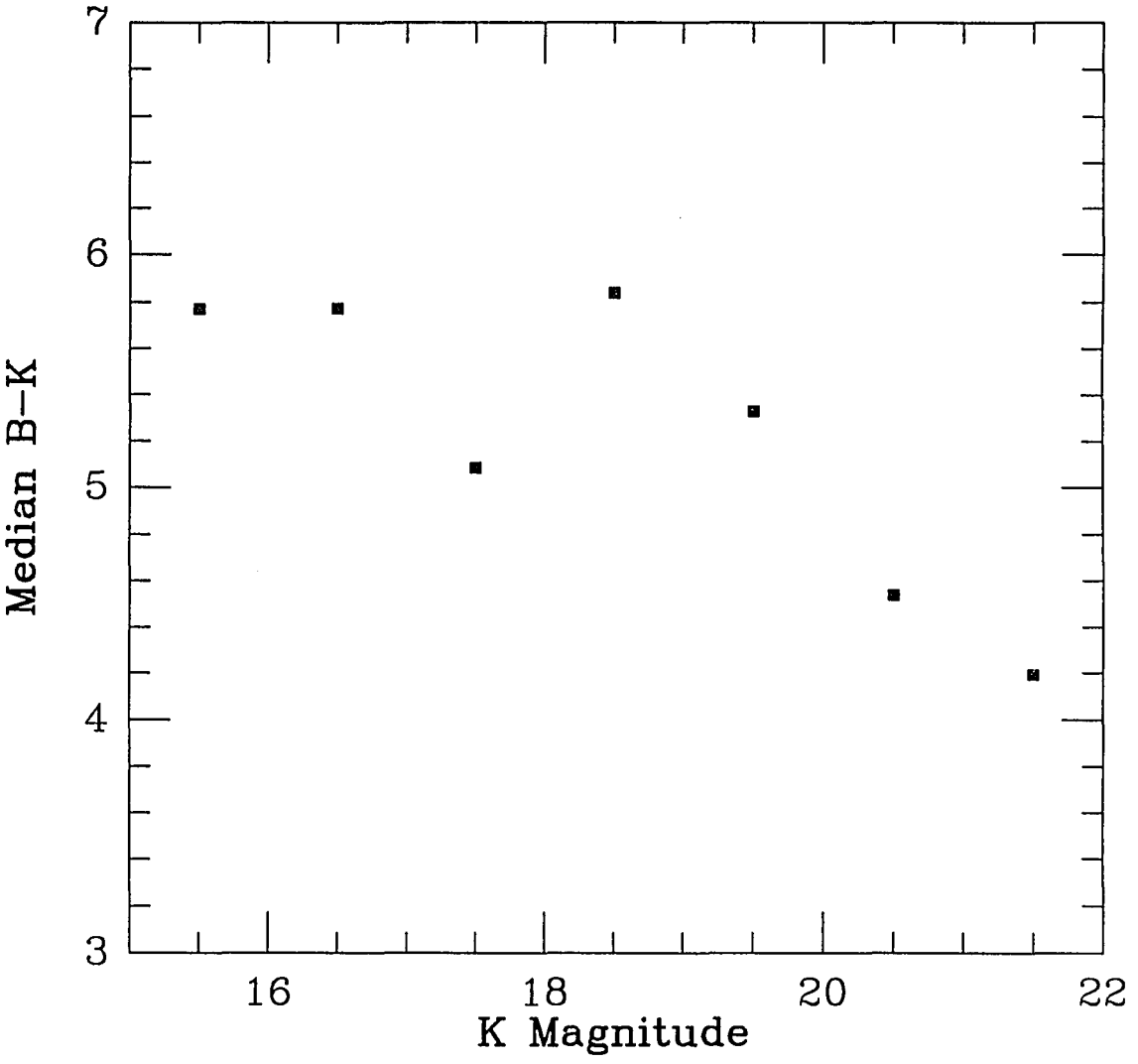

Figure 4.2: Median B-K vs. K magnitude for the HDS K selected sample. While at bright magnitudes B-K is around 5 to 6, typical for a nearby galaxy population, at the faint end B-K has fallen to 4, which is as blue as a local irregular.

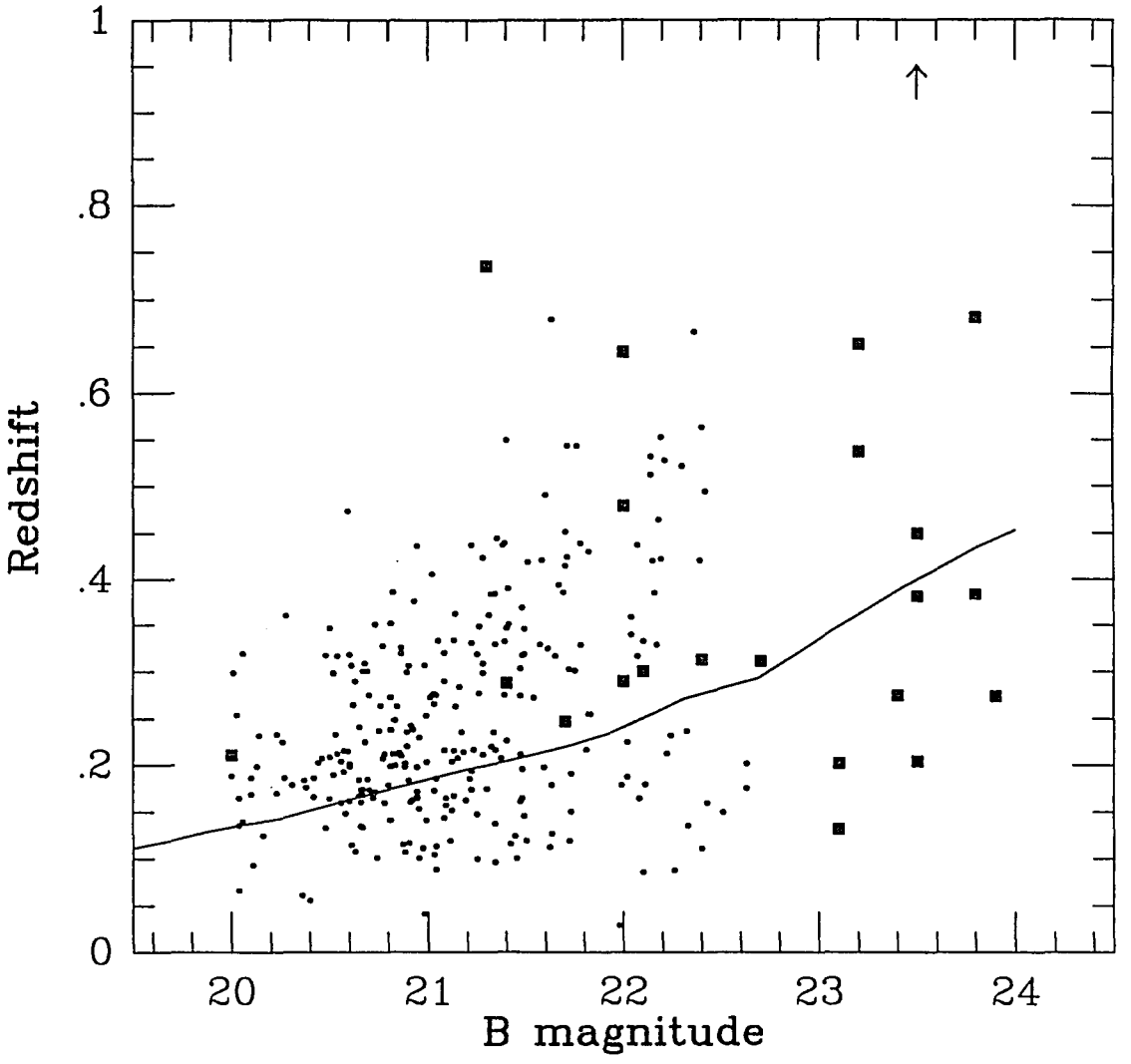

Figure 4.3: Spectroscopic redshifts for B magnitude selected samples. The dots show the B < 21 and B < 22.5 samples of Broadhurst *et al.*, (1988) and Colless *et al.* (1990). They are 85% and 81% complete, respectively. The solid squares show our data (Cowie *et al.*, 1991) which is 95% complete to B = 24. One object at B < 24 remains unidentified despite attempts and could be at any redshift (upward pointing arrow.) The line shows a predicted mean redshift for a model with no galaxy evolution; it provides a remarkably good fit.

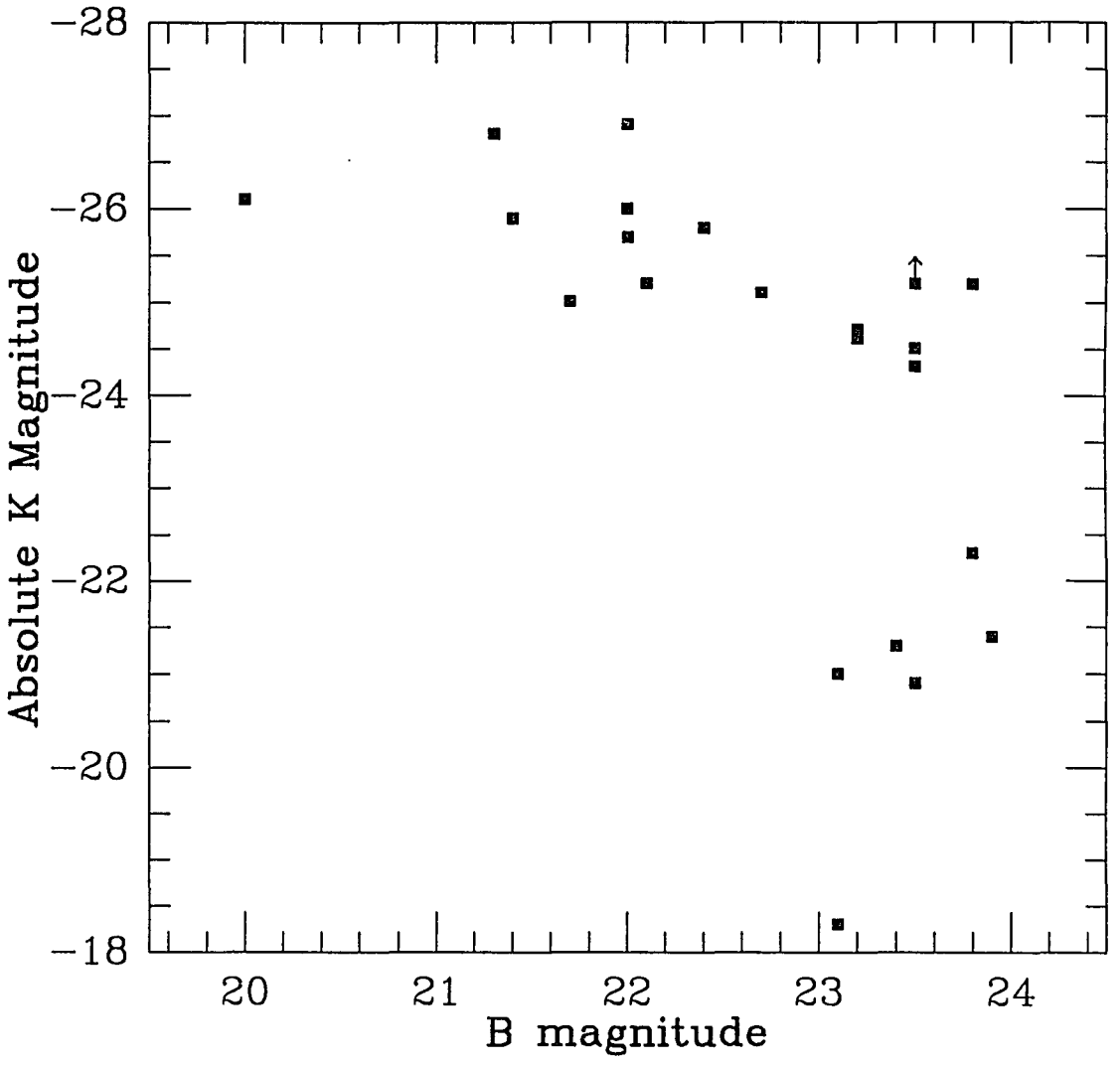

Figure 4.4: Absolute K magnitude vs apparent B magnitude for $H_0 = 50$, $q_0 = 0.5$. The object with an arrow remains unidentified despite a 20 hour exposure. It has been placed arbitrarily at a redshift of 1.5, but could be any absolute magnitude. At B < 23, most galaxies are approximately $K^* \approx -26$. At B > 23, a population of dwarf galaxies appears.

Chapter 5: Number counts

In this chapter we present the K band galaxy number counts from four surveys of the extragalactic sky. Each survey was designed with an optimal balance between exposure time and areal coverage to address a particular range of magnitudes. Each survey is limited at the faint end by the magnitude at which galaxies can be detected, and at the bright end when the number of galaxies per magnitude becomes small because of limited sky coverage. The results of the survey at the faintest magnitudes have been reported elsewhere (Cowie *et al.*, 1992) and will be discussed here only in relation to the new data. This survey, the Hawaii Deep Survey (HDS) was done with IRCAM on UKIRT and the NICMOS3 256^2 HgCdTe device on the University of Hawaii's 2.2 meter telescope and CFHT. The HDS covers 16 square arcminutes to varying depths and reaches a limit of K' = 22.5 in a 1.6 square arcminute region. Images were obtained in the U' (3400 Å ± 150 Å), B, V, I and K' broad band filters. The K' filter covers the wavelength range 2.0 microns to 2.3 microns and was designed to reduce the thermal component of the background (Wainscoat and Cowie, 1992).

The next survey, the Hawaii Medium Deep Survey (HMDS), covers 160 square arcminutes to a depth of K' = 18. The HMDS consists of 1 hour exposures with the NICMOS3 camera on the UH 2.2 meter telescope with the K' filter, and 1.5 hour exposures in B and I with a CCD camera. The third survey, the Hawaii Medium Wide Survey (HMWS) covers 580 square arcminutes to a depth of K' = 17. It consists of 3 minute exposures in K' and 5 minute exposures in B and I. The brightest survey, the Hawaii Wide Survey (HWS), covers 1.58 square degrees and reaches a depth of K' = 15. It was done with 4 minute exposures with the NICMOS3 camera in K' on the University of Hawaii's 60 centimeter telescope, and 4 minute exposures in B and I on this telescope. We present galaxy number counts as bright

as K = 12, and compare them to counts compiled from the survey of Mobasher *et al.* (1986), the survey of Glazebrook (1991), and the analysis of Jenkins and Reid, (1991).

I. Data Reduction

The data reduction was described in detail in chapter 3. In brief, the K' band data were dark subtracted, flattened with domeflats, and a median pixel response technique was used to obtain a sky image for subtraction. The data were calibrated using standard stars from the list of Elias *et al.* (1982). The optical data were dark subtracted, flattened with domeflats, further flattened with median pixel response flats, and calibrated with standard stars from the list of Landolt (1983). We consider our photometry to be good to 0.1 magnitudes, except where larger formal errors are quoted. Colors are good to 0.2 magnitudes.

The problem of star/galaxy separation is not an easy one, but is critical at these magnitudes. Misidentification can have a very serious effect upon the number counts even when it is random and not systematic, because of the great preponderance of stars at the bright magnitudes. We have confined ourselves, for the most part, to areas in which we have data in B, I, and K, so that we can use a combination of morphology and color to positively identify each object. We have found that using morphology alone results in high galaxy counts because of the presence in the data of just barely resolved double stars, which appear morphologically to be galaxies. In addition, in the intermediate magnitudes, any morphological criteria has an area of ambiguity, and the cutoff between stars and galaxies has a tendency to be arbitrary. There is similarly a region of ambiguity on the color-color plot, particularly at relatively low signal-to-noise, and therefore we

have used color to identify objects, except when the distinction between stars and galaxy colors are ambiguous, and we have used morphological criteria.

At the brightest levels, this is not a critical issue, for the galaxies are very large, and morphology is sufficient. At the faintest levels, the number of galaxies is far greater than the number of stars, and misidentification does not have as large of an effect. Thus we will limit this discussion to the HMWS and the HMDS. To determine morphology we have used the Kron r_{-2} criteria discussed in Kron (1980). We expanded the .75 arcsecond pixels by a factor of 8 in each direction, calculated the centroid for each object and then calculated the inverse second moment in five annuli within a 6.4 arcsecond radius. Because of the large expansion factor, excluding the center pixel (necessary because the data is discrete) had little effect. The measurement is small for stars and large for extended objects.

To determine star/galaxy separation in color, we used the criteria between the two regions on the B-I/I-K diagram corresponding to $2.5(I-K)-(B-I) \geq 2.0$. This criteria is true for galaxies, and false for stars. When the morphological and color criteria disagree, we have used the color criteria where it is unambiguous, and the morphological criteria otherwise. Finally, the star/galaxy separation was tested by obtaining spectra of a number of ambiguous objects in the HWS and HMDS fields, as part of a redshift survey. This data will be reported elsewhere (Cowie *et al.*, in preparation.)

II. The Data

The galaxy number count data are listed in table 5.0 and plotted in figure 5.1. (The star counts will be discussed elsewhere, Gardner, in preparation, Cowie *et al.*, in preparation.) In addition to our data, we have plotted the data from Glazebrook, (1991), a compilation of the K band number counts from Mobasher *et*

al., (1986), and the results of Jenkins and Reid (1991). Mobasher *et al.* (1986) measured the K magnitude of galaxies selected at B < 17. They did not compile the K band counts, however, the reddest object in the HWS has a B-K = 4.86 at K < 13, and assuming that there are no objects redder than this in the Mobasher *et al.* (1986) data, it is possible to compile K band counts to a limit of K = 12. Fainter than this, there is incompleteness because objects fainter than B = 17 are not being counted, and continuing to compile the counts fainter than this shows a drop-off just as is expected. However the counts are accurate in the K = 10 to K = 12 range, which provides considerable overlap with the HWS. We have also compiled the counts in the K = 12 to K = 12.5 under the assumption that the incompleteness due to the B limit is very small for this last half magnitude bin.

Magnitudes for the galaxies in the HWS were measured within an isophotal contour, and extrapolated using the surface brightness profile to correct to total K magnitudes. The faint end cutoff for the HWS was set at K' = 15, where the signal to noise dropped low enough that it was no longer feasible to compute isophotal magnitudes. In the other three surveys, aperture magnitudes were used, and these were in each case corrected to a larger aperture. For the HMWS and the HMDS, a 6 arcsecond aperture was used, and was corrected to 10 arcseconds. For the higher resolution HDS data, where at the fainter magnitudes surveyed the galaxies are expected to be smaller, a 3.5 arcsecond aperture was used, corrected to 6 arcseconds. The photometry of objects which lie in the overlaps between the surveys, and are therefore common to more than one survey are consistent within 0.1 magnitudes.

Table 5.1 contains the compiled number counts for the four surveys reported in this letter, as well as the surveys of Mobasher *et al.*, (1986), Glazebrook, (1991), and Jenkins and Reid, (1991). The high and low errors are based upon Poisson

statistics, compiled in Gehrels, (1986), except where the Poisson errors are dominated by other errors. The HMWS and HMDS errors contain, at the faintest magnitudes, a component based upon uncertain star/galaxy separation. The Jenkins and Reid (1991) counts were based upon a statistical process of fitting a power law number count relation to variations in the night sky. This process yielded a range of values at each magnitude, with no preferred value, and thus is presented as an envelope of the range.

For each magnitude bin in each survey, the area covered is presented in table 5.1. The HWS, HMWS, and HMDS data have no incompleteness correction, because the faintest magnitude levels are still at the 5 σ level. The effects of surface brightness variation upon the completeness are discussed in chapter 6. The incompleteness corrections for the HDS are discussed in Cowie *et al.*, (1992).

When the number counts are plotted, a turnover in slope is evident at around K' = 17. This is in contrast to the B band counts, plotted in figure 5.3, which nearly follow a power law of slope 0.44 with no turnover to the faintest levels observed, B = 27. Taking the turnover to be at K' = 17, and not using the data for one magnitude on either side, it is possible to fit the K band counts with two separate power laws, with slope 0.67 from K = 10 to K = 16, and with slope 0.26 from K = 18 to K = 22.5. The power laws were fit to all of the data plotted, and the reduced chi-squares are 1.45 and 0.50 respectively. These are plotted in figure 5.1, and the two lines intersect at K = 17.0.

Figure 5.2 contains the K band number counts plotted against the models of Yoshii and Takahara, (1988). A power law of 0.45*(K-12) has been subtracted in order to show the variation in the data. In addition the models are normalized so that the no-evolution model is tied to the HWS point at K = 14.5, thus removing the

uncertainty in the local luminosity function. This normalization corresponds to a Schechter type luminosity function with $\phi^* = 1.12 \times 10^{-3}$.

Figure 5.4 is a plot of the B-K colors of the galaxies in the Mobasher *et al.*, (1986) survey and the four Hawaii surveys. In each bin the median B-K color is plotted for the survey with the best statistics (i.e. the greatest number of galaxies.) One sigma error bars are calculated for the median by the median sign test, and are plotted. The median sign test determines the probability, for each point in the distribution, that the true median lies above or below that point. The upper error bars are those points for which the probability that the true median lies below that point is 0.84, and likewise the lower error bars are those points for which the probability that the true median lies above it is one sigma. These errors thus depend both upon the number of galaxies in the bin, and upon their distribution.

III. Discussion

Much attention has been paid recently to the excess over the models in the B band number counts, and the corresponding lack of an excess in the K band counts. (Tyson, 1988, Lilly *et al.*, 1991, Cowie *et al.*, 1992) This excess begins to appear at B = 20 (Maddox *et al.*, 1990), rising to a factor of 4-5 by B = 24, and continues unabated to the faintest levels observed, at B = 27. Despite these excesses, the redshift distribution of spectroscopic survey data is best fit by the no-evolution model even at the faintest level, at B = 24. (Broadhurst *et al.*, 1988, Colless *et al.*, 1990, Cowie *et al.*, 1991) The lack of a high redshift tail in the redshift distribution rules out normal luminosity evolution, and the lack of an excess in the K band counts rules out explanations based upon an open cosmological geometry, or non-zero cosmological constant. Broadhurst *et al.*, (1988) proposed luminosity dependent luminosity evolution, where low luminosity galaxies go through a

bursting phase at moderate redshift ($z \approx 0.4$), which high luminosity galaxies do not go through. Lilly *et al.*, (1991) argued that there is evolution in ϕ^* rather than evolution in L^*, that is, number evolution rather than straight luminosity evolution. Broadhurst *et al.* (1992) more recently proposed that the explanation involves large amounts of merging at intermediate redshifts.

Cowie *et al.*, (1992) analyzing the HDS K band number counts and the results of a spectroscopic survey of a small but complete sample selected at B = 24 (Cowie *et al.*, 1991) argued that the K band counts show that the universe is flat with $\Lambda = 0$. The turnover in the number counts appearing at K = 17 is caused by the fact that at these magnitudes we are ceasing to observe galaxies at greater distances, but are instead working our way down the luminosity function. The excess in the B band counts are the result of a population of faint blue dwarf galaxies which appear at intermediate redshifts ($z \approx 0.4$), but are not counted in the local population. The data reported in this chapter support this conclusion.

The K band number counts can be fit by two power laws of slope 0.67 between K = 10 and K = 16, and of slope 0.26 between K = 18 and K = 22.5, as is indicated in figure 5.1. The B band number counts are fit by a power law of slope 0.44 from the bright end to as faint as has been observed, at B = 27 (Lilly *et al.*, 1991 measures 0.38 at the faint end; Tyson, 1988, measures 0.45). The B band counts are plotted against the power law in figure 5.3.

The median B-K color, shown in figure 5.4 shows three separate regions. At $K < 13$, the B-K color is essentially flat. At these bright magnitudes the galaxies are at low redshift, and have essentially no *K* correction due to redshift. Their K magnitudes are determined by their distance, with little cosmological correction. Between K = 13 and K = 17, the B-K color becomes progressively redder, peaking at approximately K = 17. This is primarily due to the *K* correction; as the galaxies

become progressively more distant the redshift in spectrum become more imp
Fainter than K = 18 the B-K color rapidly becomes bluer.

Thus the discrepancy between the K band number counts and the B b
number counts is due to a color effect. While there are still (subject to the limi
magnitudes of the B band observations) a number of very red objects at the fa
levels in K, the B-K colors become dominated by very blue galaxies.

That the B band counts and the K band counts, while dramatically dif
are sampling the same population can be shown by convolving the K band co
with the B band counts and comparing the result with the B-K colors. Fitting
power law to the B band counts gives a slope of 0.44 all the way from B = 18 t
B = 27. Convolving this power law with the two power laws fit to the K band c
and correcting for the difference in luminosity functions, produces the dotted
in figure 5.4, which are comparable to the fit to the median, indicated by the s
lines.

In the K band, for non-starburst galaxies, the light is produced mainly
near-solar mass stars, and thus the absolute K magnitude is a measure of th
of the galaxy. There is not yet any direct evidence as to the redshifts of the fai
galaxies making up the K band counts. However, the Cowie *et al.* (1991) redshift
survey is limited at B = 24. The median B-K color at K = 18 is 6.0, and thus almost
all galaxies bluer than the median would be sampled at B = 24. Similarly, bec
the trend towards blue galaxies is so pronounced, the galaxies bluer than the
median at K = 19.5 would nearly all be brighter than B = 24. Thus if the blue
population of galaxies, which appears at K = 18 and comes to dominate at K =
were at high redshift, one would expect to see some high redshift objects in a
selected at B = 24.

Cowie *et al.*, (1991), while measuring redshifts for only a small sample of 22 objects, were nonetheless 95% complete. Their highest measured redshift was $z = 0.735$. Similar surveys reaching $B = 24$, while still in the initial phases and far from complete, have similarly failed to turn up any galaxies more distant than $z = 0.9$ (Allington-Smith *et al.*, 1992, Colless *et al.*, 1992.) It appears from this that the blue galaxies which dominate at the faintest levels in the K band are at low redshift, and therefore are small starbursting galaxies. This population either undergoes large amounts of merging to become the present population, or becomes too faint to be counted locally.

IV. Conclusion

We have presented K band galaxy number counts from four surveys stretching from $K = 12$ to $K = 22.5$. We have shown that the slope of the counts turns over at $K = 17$ from 0.67 to 0.26. Similarly we have shown that the median B-K color turns over at $K = 17$, and the population of galaxies fainter than $K = 18$ rapidly becomes bluer. We have shown that the discrepancy between the excess numbers of galaxies seen in the B band and the deficiency of galaxies seen in the K band is due to this color effect. Because no population of high redshift galaxies have been detected in redshift surveys to $B = 24$, this population must be nearby, and consist of small blue starbursting galaxies.

References for Chapter 5

Allington-Smith, J., Ellis, R., Glazebrook, K., Shaw, G., Tanvir, N., Webster, J., Breare, M, Gellatly, D., Jorden, P., MacLean, J., Oates, P., Taylor, P., Worswick, S., and Taylor, K., 1992, *Gemini*, **36**:4.

Broadhurst, T.J., Ellis, R.S., and Shanks, T., 1988, *M.N.R.A.S.*, **235**:827.

Broadhurst, T.J., Ellis, R.S., and Glazebrook, K., 1992, *Nature*, **355**:55.

Colless, M., Ellis, R.S., Taylor, K., and Hook, R.N., 1990, *M.N.R.A.S.*, **244**:408.

Colless, M., Ellis, R.S., Taylor, K., and Shaw, G., 1992, preprint.

Cowie, L.L., Songaila, A., and Hu, E.M., 1991, *Nature*, **354**:460.

Cowie, L.L., Gardner, J.P., Hu, E.M., Wainscoat, R.J., Hodapp, K.W., 1992, *Ap. J.*, *submitted.*

Elias, J.H., Frogel, J.A., Matthews, K., and Neugebauer, G., 1982, *A.J.*, **87**:1029.

Gehrels, N., 1986, *Ap. J.*, **303**:336.

Glazebrook, K., 1991, *private communication.*

Heydon-Dumbleton, N., Collins, C.A., and McGillivray, H., 1989, *M.N.R.A.S.*, **238**:379.

Jenkins, C.R., and Reid, I.N., 1991, *A. J.*, **101**:1595.

Kron, R.G., 1980, *Ap. J. Supp.*, **43**:305.

Landolt, A.U., 1983, *A.J.*, **88**:439.

Lilly, S.J., Cowie, L.L., and Gardner, J.P., 1991, *Ap. J.*, **369**:79.

Maddox, S.J., Sutherland, W.J., Efstathiou, G., Loveday, J., and Peterson, B.A., 1990, *M.N.R.A.S.*, **247**:1P.

Metcalfe, N., Fong, R., Shanks, T., and Kilkenny, D., 1989, *M.N.R.A.S.*, **236**:207.

Metcalfe, N., Shanks, T., Fong, R., and Jones, L.R., 1990, *M.N.R.A.S.*, **249**:498.

Mobasher, B., Ellis, R.S., and Sharples, R.M., 1986, *M.N.R.A.S.*, **223**:11.

Peterson, B.A., Ellis, R.S., Efstathiou, G., Shanks, T., Bean, A.J., Fong, R., and Zen-Long, Z., 1986, *M.N.R.A.S.*, **221**:233.

Shanks, T., 1990, in *The Galactic and Extragalactic Background Radiation, Proc. IAU Symp. No. 139*, eds. S. Bowyer and C. Leinert, (Kluwer:Dordrecht), p. 269.

Tyson, J.A., 1988, *A.J.*, **96**:1.

Wainscoat, R.J., and Cowie, L.L., 1992, *A.J.*, **103**:332.

Yoshii, Y., and Takahara, F., 1988, *Ap. J.*, **326**:1.

Survey	K	raw	low	high	area	perdeg	low	high
Mob	10.25	3	1.37	5.92	84% of	0.17	0.07	0.33
Mob	10.75	5	2.84	8.38	41.56	0.28	0.16	0.47
Mob	11.25	13	9.44	17.70	sq	0.74	0.53	1.00
Mob	11.75	19	14.68	24.44	deg	1.08	0.83	1.39
Mob	12.25	49	42.02	57.05		2.79	2.39	3.25
HWS	10.50	2	0.71	4.64	1.58	1.26	0.45	2.94
HWS	11.50	1	0.17	3.30	sq	0.63	0.11	2.09
HWS	12.50	5	2.84	8.38	deg	3.16	1.80	5.30
HWS	13.50	23	18.24	28.87		14.56	11.54	18.27
HWS	14.50	124	106.00	142.00		78.48	67.09	89.87
Glz	13.50	3	1.37	5.92	592.3	18.23	8.33	35.98
Glz	14.50	6	3.62	9.58	sq	36.47	22.00	58.23
Glz	15.50	50.8	43.20	58.40	arc	308.76	262.57	354.96
Glz	16.50	131.5	116.80	146.20	min	799.26	709.91	888.60
HMWS	12.75	2	0.70	4.63	582.03	24.74	8.75	57.37
HMWS	13.75	1	0.17	3.30	sq	12.37	2.14	40.82
HMWS	14.25	3	1.36	5.91	arc	37.11	16.91	73.20
HMWS	14.75	11	7.73	15.42	min	136.07	95.67	190.75
HMWS	15.25	22	17.34	27.76		272.15	214.61	343.52
HMWS	15.75	45	38.31	52.76		556.67	470.07	652.71
HMWS	16.25	89	79.58	99.47		1100.97	816.45	1230.53
HMWS	16.75	158	145.44	171.59		1954.53	1484.45	2127.72
HMDS	13.75	2	0.70	4.63	167.68	85.87	30.40	199.15
HMDS	14.75	1	0.17	3.30	sq	42.93	7.42	141.69
HMDS	15.25	5	2.84	8.38	arc	214.69	121.94	359.91
HMDS	15.75	21	16.45	26.66	min	901.71	706.67	1144.91
HMDS	16.25	28	22.74	34.36		1202.29	976.57	1475.46
HMDS	16.75	48	41.09	55.98		2061.06	1764.72	2403.81
HMDS	17.25	73	64.47	82.58	119.19	4409.76	3894.94	4988.94
HMDS	17.75	108	97.62	119.42	s.a.m.	6524.03	5195.06	7214.39
HMDS	18.25	87	77.69	97.37	62.07	10091.80	9012.17	11294.40
HMDS	18.75	21	16.46	26.66	12.99	11639.70	9122.05	14779.00
JR	15.00				39.24	417.50	305.00	530.00
JR	16.00				sq	1129.50	954.00	1305.00
JR	17.00				arc	3059.50	2537.00	3582.00
JR	18.00				min	8613.50	6027.00	11200.00
JR	19.00				equiv	24400.00	11900.00	36900.00
HDS	15.50	5	2.84	8.38	16.5	1090.00	619.12	1827.27
HDS	16.50	6	3.62	9.58	sq	1308.00	789.16	2089.31
HDS	17.50	19	14.68	24.44	arc	4142.00	3200.24	5327.91
HDS	18.50	43	36.47	50.61	min	9374.00	7950.62	11034.00
HDS	19.50	69	60.71	78.35		17829.00	15688.00	20245.00
HDS	20.50	84	74.85	94.20		37010.00	32981.00	41507.00
HDS	21.50	62	54.14	70.92		72890.00	63661.00	83379.00
HDS	22.50	18	13.80	23.32		99586.00	76349.00	129019.00

Table 5.1: The compiled K band number counts. The surveys are (Mob), Mobasher *et al.*, (1986), (Glz), Glazebrook, (1991), (JR), Jenkins and Reid, (1991), and the remainder are from this thesis.

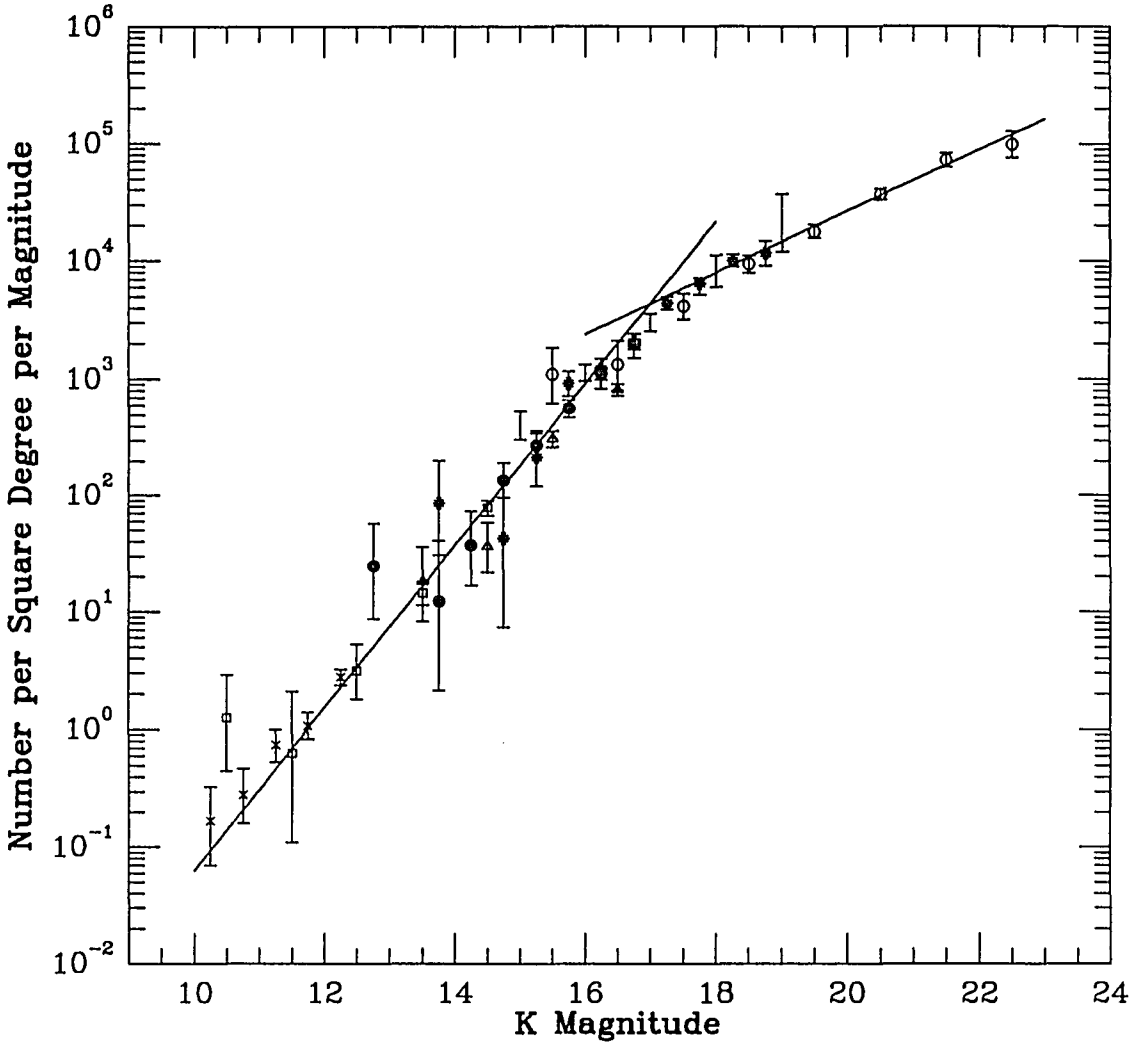

Figure 5.1: The K band number counts. The counts are fit by two separate power laws, with an exponent of 0.67 between K = 10 and K = 16, and an exponent of 0.26 between K = 18 and K = 22.5. The data are a compilation from Mobasher *et al.*, (1986), (exes), the Hawaii Wide Survey (open boxes), Glazebrook, (1991), (triangles), the Hawaii Medium Wide Survey (solid circles), the Hawaii Medium Deep Survey (starred circles), Jenkins and Reid (1991), (error bars without points), and the Hawaii Deep Survey, (open circles).

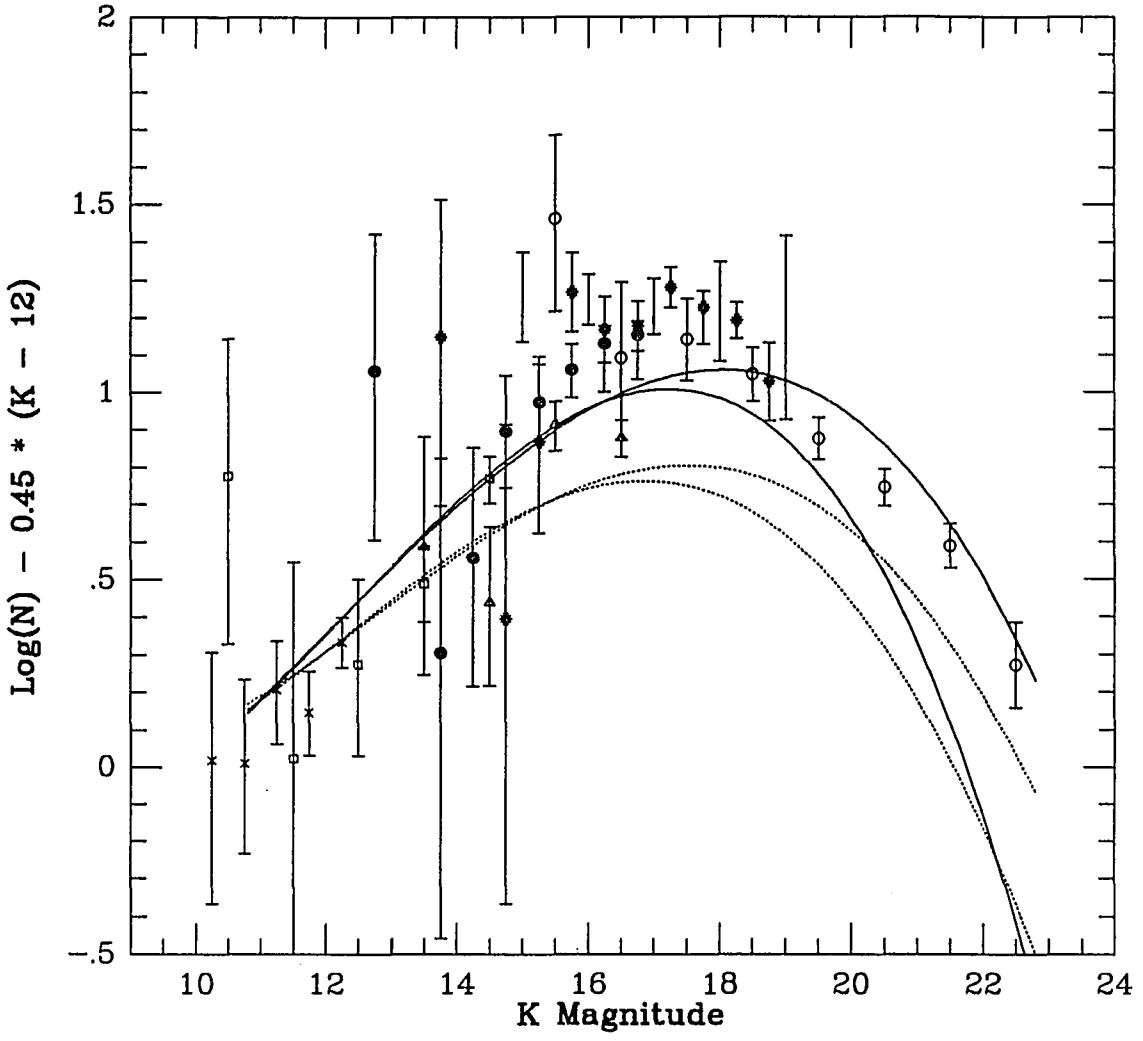

Figure 5.2: The K band number counts with an expanded ordinate plotted against the models of Yoshii and Takahara, (1988). The models have been normalized to the Mobasher *et al.* (1986) point at K = 12.25.

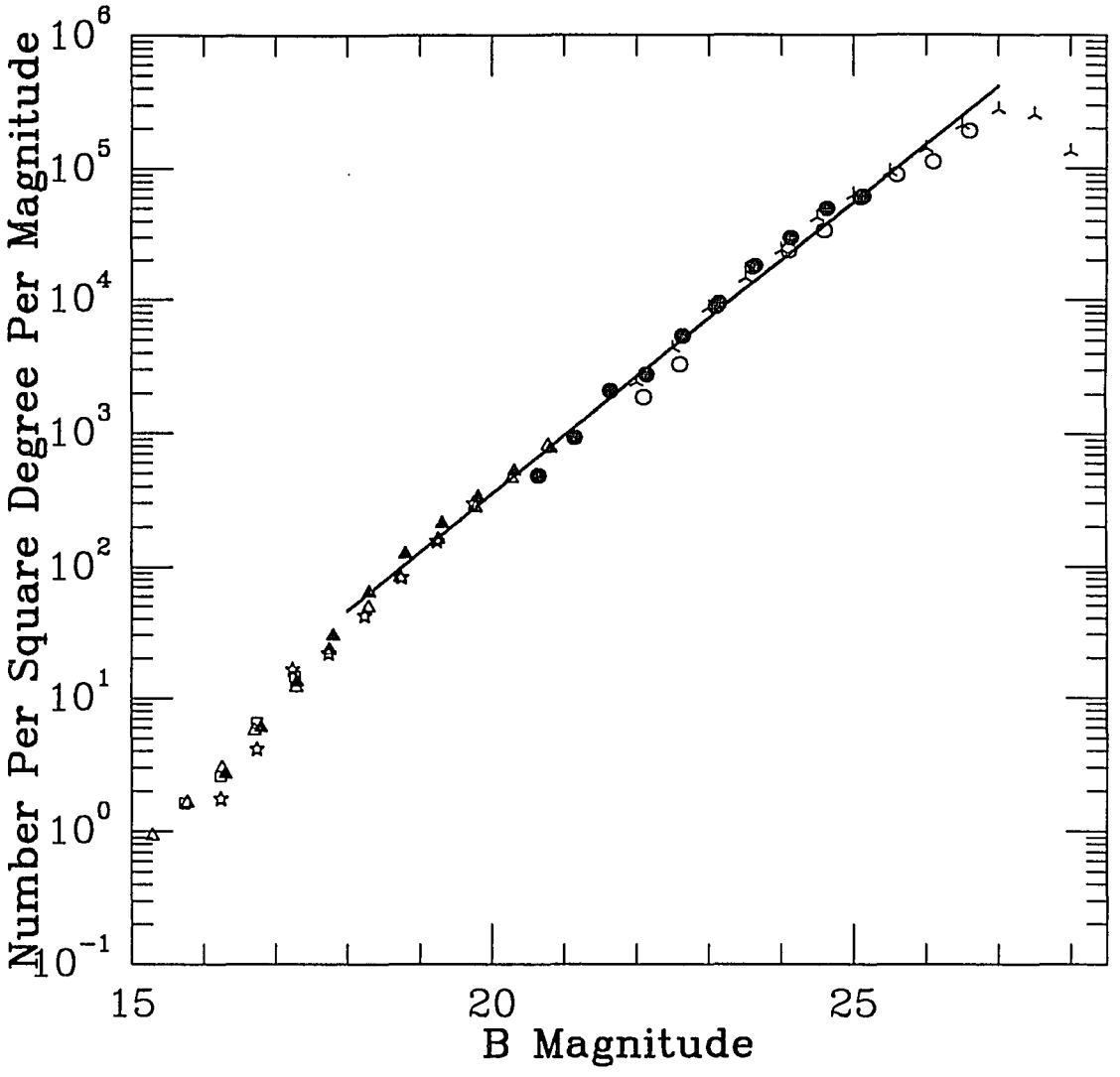

Figure 5.3: The B band number counts with a power law fit. The data are Metcalfe *et al.*, (1989), (open boxes), Shanks, (1990), (filled triangles), Heydon-Dumbleton *et al.*, (1989), (stars), Metcalfe *et al.*, (1990), (filled circles), Maddox, *et al.*, (1990), (open triangles), Tyson, (1988), (skeletal triangles), and Lilly *et al.*, (1991), (open circles.)

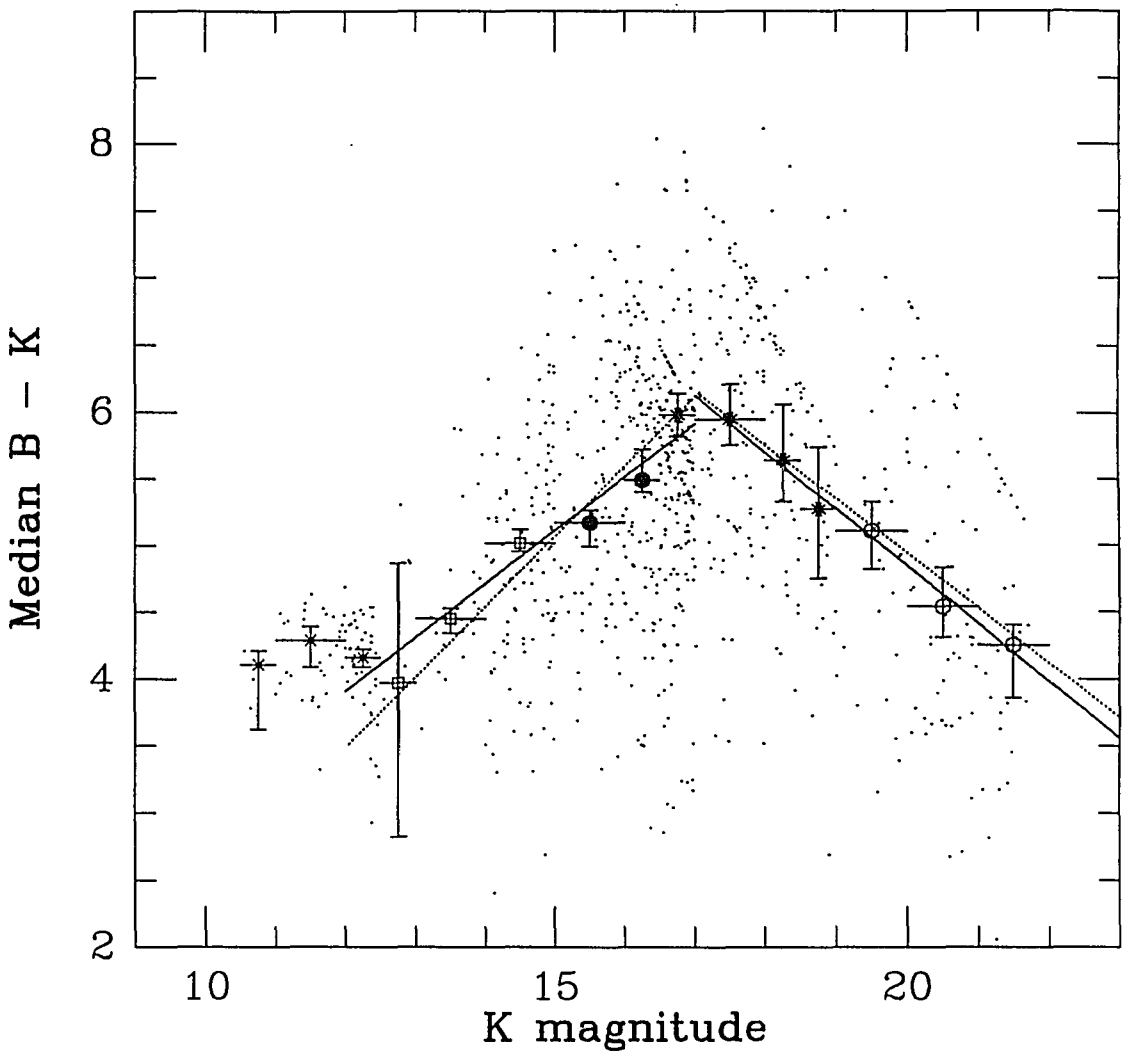

Figure 5.4: A plot of the B-K color as a function of K magnitude for the Mobasher *et al.* (1986) data and the four Hawaii surveys. The dots represent individual galaxies. The horizontal lines are the median B-K for each bin, plotted with 1 sigma error bars based upon the median sign test. The solid lines are fits to the data between K = 12.5 and K = 16, and between K = 18 and K = 22. The dotted lines are the B-K colors inferred from the number counts.

Chapter 6: Analysis

In this chapter I will compare the data of the HWS, the HMWS, the HMDS, and the HDS to several theoretical models of galaxy evolution. The standard approach to galaxy evolution has been to invoke pure luminosity evolution, or evolution in L^*, within a $\Lambda = 0$ Friedmann universe. While there have been several different approaches to this, (Tinsley and Gunn, 1976; Bruzual, 1983,) I will primarily take the models of Yoshii and Takahara (YT; 1988) as the standard model with which to compare the more exotic models. As has been discussed elsewhere in this thesis, it has already been necessary to consider alternatives to the standard model to explain the data. One alternative is to invoke a cosmology with a non-zero cosmological constant Λ, (Fukugita *et al.* 1990). Another is a merging model, in which galaxies at intermediate and high redshift merge to form the local population. (Rocca-Volmerange and Guiderdoni, 1990, Broadhurst *et al.*, 1992.) And finally, there is a model in which there are two separate populations of galaxies; the local population, and an additional population of small blue starbursting galaxies at intermediate redshifts. (Cowie *et al.*, 1991, 1992.)

In this chapter I will begin in section I by presenting the data of the HWS, the HMWS, the HMDS, and the HDS in color-magnitude and color-color form, and discuss the general characteristics of the data. In section II, I will discuss the effects of surface brightness on the selection of the objects, and the effects that this can have on the data. In section III, I will discuss the models and show how the data fits them. And finally, in section IV, I will summarize the testable predictions of the models and discuss potentially useful follow-up studies.

I. The Data

The K band number counts were presented in 5, and were discussed there in the context of the B band counts and the median B-K color as a function of K magnitude. Figure 6.1a is a plot of the I-K color as a function of K magnitude for the HWS. Also plotted are a no-evolution model for an elliptical galaxy at K^*, for $q_0 = 0.02$ and $q_0 = 0.5$ ($\Lambda = 0$), and a model of this galaxy type with YT luminosity evolution. The models are the reddest that galaxies can normally be expected to get, although the data does show some scatter around this line. A brightest cluster member CD galaxy, or a starbursting galaxy such as IRAS 05189-2524 is as red as I-K = 5.0 at K = 10.2. (Sanders *et al.*, 1988). In addition, Annis, (1992), has identified several ultra-red objects, with R-K > 6.3 at K = 18 in the field of the gravitational lens system MG 1131-0456. However, in a random survey covering 1.58 square degrees one would expect to see neither IRAS galaxies nor gravitational lens systems of that type. Figures 6.1b, 6.1c, and 6.1d, are plots of the I-K color vs. K magnitude for the HMWS, the HMDS, and the HDS, respectively, with the same YT models. Figure 6.1e is a plot of I-K vs. K for all of the galaxy data.

There are several features of the I-K vs K plot that should be noted. The stars (plotted as filled symbols in figures 6.1b-d) separate reasonably well from the galaxies. This separation, however, is more dramatic when the B-I color is included, and the star/galaxy separation was done on the B-I/I-K plot, as was discussed in chapter 3. At the faint limit of each survey there is a turn-up in the data where the I-K color rises above the models. This, however, is merely due to noise. While each survey sample was selected to be greater than 5 σ in the K band, the I magnitudes for the K selected objects were measured down to 2 σ. Objects fainter than 2 σ in I are plotted as lower limits set at I = 2 σ.

Elston *et al.* (1988) surveyed 10 square arcminutes of the extragalactic sky to a galaxy detection limit of K = 18. They detected two objects at K = 16.6 and K = 16.8 with R-K > 5. They first suggested that these were Partridge and Peebles (1967) type primeval galaxies at redshift z > 6, but spectroscopy of a similar object from the same survey, done by Lilly *et al.* (1988), revealed it to be a normal elliptical galaxy at z = 0.3. Elston *et al.* (1989) then did spectroscopy on the two objects, and on the basis of, in one case just the 4000 Å break, and in the other case this break and a very low signal-to-noise OII 3727 Å line, they identified these two objects as elliptical galaxies at z ≈ 0.8. These galaxies thus have a K band excess of 0.3 to 0.5 over the reddest model.

The discovery of two such objects in 10 square arcminutes implies a density on the sky of 720 per square degree. However, the failure in the HMDS to find similar objects implies a 1 σ upper limit of 39.5 objects per square degree, and the HMWS limit is more stringent, although that survey has some objects undetected in I at the K = 16 to K = 17 level. The HMDS limit is sufficient to rule out the presence of this population at greater than the 99.95% confidence level. A population of 720 per square degree would result in the detection in the HMDS of 34 objects. Clearly these objects do not appear in figure 6.1c. In addition, the redshift surveys which have been begun on K selected samples do not show objects at z = 0.8 at the K = 16 to 17 level. Thus, the Elston *et al.* (1989) data is highly atypical.

The general trend of the I-K colors of the galaxies is to follow the models for elliptical galaxies at the bright end. This becomes even more clear in the B-I/I-K diagram (figure 6.3), but it is evident even in the I-K color. Photometric surveys of this type generally pick out the intrinsically brightest galaxies at each apparent magnitude, since they are the most distant, and therefore sample the largest volume. Thus one expects, in K selected surveys, to be dominated by L^* elliptical

galaxies, and this is evident in the HWS and HMWS data. At the faint end of the HMDS, and more dramatically in the HDS, however, these L^* unevolved elliptical galaxies are no longer seen. This deficiency of elliptical galaxies is also seen in the B-I/I-K diagram in figure 6.3, and in the spectroscopic redshift information (Cowie, private communication). Essentially, non-evolved L^* elliptical galaxies at a redshift of $z \approx 1$ do not appear in the data.

Brown dwarf stars would appear in figure 6.1 as very red objects at bright magnitudes. While they would be morphologically compact, the method used in the HMWS and HMDS of star/galaxy separation in color would misidentify them as galaxies. However, in these figures, morphologically compact objects which were nonetheless identified as galaxies are plotted as open triangles, rather than squares. (Likewise, morphologically diffuse objects which had stellar colors are plotted as filled triangles.) In addition, at the faint end of each survey, the signal to noise level drops below the point where it is reasonable to identify objects morphologically. That is, when the total photometry of the object is at the 5 σ level, the signal to noise in annuli around the object is much lower. There are several objects in the HMWS and in the HMDS which are worthy of further study, particularly high resolution J, H, and K photometry. This would determine whether the objects are indeed compact, and if their near-infrared colors match those of brown dwarfs.

The B-K color as a function of K magnitude for the surveys was discussed in chapter 5. The data is plotted again in figures 6.2a-f, this time separated as to survey, so that the effects of noise at the faint end of each survey can be separated from the behavior of the data. The trend is similar to the trend in I-K. At the very bright end, in the Mobasher *et al.*, (1986) data, the galaxies are generally elliptical and Sa galaxies at low redshift. Their B-K color does not vary, since they are not at large enough redshift for the *K* correction to change their color. Their apparent

magnitude is simply a function of their distance. Beginning in the HWS, in figure 6.2b, and continuing through the HMWS data, in figure 6.2c, the B-K color gets redder, because the *K* correction begins to dominate the colors. The data is plotted against a no-evolution model of the median B-K color. In this magnitude range the no-evolution model is a good fit to the data, and the effects of evolution are neither expected to be nor seen to be large. However, beginning at the faint end of the HMDS in figure 6.2d, the no-evolution model is redder than the majority of the objects, and is no longer a good fit to the median color. This effect appears more dramatically in the HDS, in figure 6.2e, as the B-K color rapidly gets bluer. Figure 6.2f is a plot of all of the galaxies B-K color, the median color in each magnitude bin, and the no-evolution model for the median color. The model fits the data reasonably well until the turnover in the colors at K = 17, when the data rapidly becomes bluer.

Figure 6.3a is a plot of the B-I color against the I-K color for the HWS galaxy data. From this figure, it is evident that the majority of the galaxies detected are ellipticals and Sa galaxies. This is expected in a K band selected sample. Figure 6.3b is B-I vs I-K for the HMWS data at K < 16. The galaxies in this plot are mostly unevolved elliptical and Sa galaxies at low to moderate redshift. Figure 6.3c is B-I vs I-K for the HMWS data at 16 < K < 17. The large number of galaxies undetected in B makes it difficult to interpret this figure. Figure 6.3d is B-I vs I-K for the HMDS data at K < 17. The majority of the galaxies are still elliptical and Sa galaxies at moderate redshift. No evidence for evolution is seen. Figure 6.3e is B-I vs I-K for the HMDS data at 17 < K < 18. The large number of galaxies undetected in B makes it difficult to interpret this figure. However, we begin to see some objects with the colors of unevolved high redshift spirals.

Figure 6.3f is B-I vs I-K for the HDS data at K < 20. The galaxies at this magnitude level are no longer clustering around the elliptical and Sa galaxy line. There are several objects with the colors of unevolved high redshift spirals, and few with the colors of unevolved high redshift ellipticals. Figure 6.3g is B-I vs I-K for the HDS data at 20 < K < 21. The trend away from the colors of unevolved ellipticals is dramatic, as there are almost no galaxies on that line. Nearly every galaxy has the colors of unevolved high redshift spiral and irregular galaxies. It should be noted, however, that this does not mean that the galaxies are actually at high redshift, as clearly there is some form of evolution operating. Figure 6.3h is B-I vs I-K for the HDS data at 21 < K < 22. At the faint limit of the HDS, the trend to bluer galaxies is most extreme. The small number of detected objects makes it difficult to interpret this figure, but there are clearly very few red objects, even when the lower limits are taken into account.

In summary, all of the data, both the K band number counts discussed in chapter 5 and the color information presented in figures 6.1-3 show a turnover at K = 17 from a no-evolution model to something quite different. The slope of the number counts changes from 0.67 to 0.26. The I-K colors drop away from the K^* elliptical line. The median B-K color stops getting redder with fainter K magnitude and begins to get dramatically bluer. The B-I vs I-K color plots show the galaxies dropping away from predominantly having the colors of unevolved elliptical and Sa galaxies and show the colors of high redshift spiral galaxies. Although it is unlikely that they actually are at high redshift, the colors show that no-evolution models, and even simple luminosity evolution models are not sufficient to explain the data. The redshift survey on a sample selected from the HDS at K < 20, while still incomplete, has detected no galaxies with z > 0.8. (Cowie, private communication.)

II. Surface Brightness Effects

The method used to identify objects in each survey is highly dependent upon the surface brightness of the objects. At the faint end of each survey, this effect can possibly bias the sample. The method used for object identification is to examine pixels which lie above some threshold, usually chosen to be between 1 and 2 σ above the background level. The local maxima within this contour are examined, and positions where the total photometry in an aperture exceeds the catalog limit are kept. These positions are then examined further, and double identifications are eliminated. In addition, where real objects are close enough together that they affect each other's photometry, some correction for this is made. The result is then compiled into a catalog, and the photometry is done in the other filters.

When number counts are compiled to levels that are below 5 σ, a correction must be made for failure to identify all of the objects. This is done by placing the brighter galaxies, suitably reduced in magnitude, back on the images. The object identification programs are run again, and the number counts are corrected for the percentage of the placed objects which the programs fail to find. This procedure must be repeated many times, as one cannot place too many new objects on the images without introducing false confusion. This technique is suitable for correcting object finding algorithms which fail to find all of the galaxies, but it does not correct for algorithms which find too many galaxies -- that is, which identify noise spikes as objects.

When these corrections are made, it becomes clear that the object finding routines go quickly from finding almost all of the objects at 5 σ, to finding almost no objects at 2 σ. (Tyson, 1988, Cowie *et al.*, 1992). Of course, this is because the initial contour in the finding routines are typically set to 2 σ, and an object at this limit is only found if it has all of its flux in a single pixel, or if noise pushes the

central pixel above the threshold. This difference, between 5 σ and 2 σ, is approximately 1 magnitude.

It is possible, to examine the expected behavior analytically. Figure 6.4 is a plot of the surface brightness per square arcminute vs total magnitude within the 6 arcsecond aperture (corrected to 10 arcseconds). The stars have (with some scatter due to noise) the same ratio of surface brightness to total magnitude (which of course appears as a constant difference in the magnitudes.) The galaxies have intrinsic scatter. This intrinsic scatter passes through the object finding routine limits at the faint end in the course of about 1 magnitude. When the stellar line reaches the initial contour limit, almost no objects are found. In this plot, it is clear that there are very few objects missing from the excluded region above and to the right of the object detection limit. However, if the data had been pushed to fainter than 5 σ at K = 18, there would begin to be many objects missing.

The correction to the number counts is a simple function of the noise levels, as has been discussed above, as long as there are no evolutionary effects on the surface brightness. Cosmologically, the surface brightness is $\mu \propto l/d_e^2$ where l is the apparent luminosity and d_e is the apparent angular diameter, $d_e \propto (1+z)^2/d_L$ where d_L is the luminosity distance. The difference, in magnitudes, between the surface brightness and the apparent magnitude (the quantity plotted in figures 6.4 and 6.5) goes as $(1+z)^4/d_L^2$, which is plotted for objects 10 kpc in diameter with constant surface brightness in figure 6.6. This figure, is the upper limit in each cosmological geometry for objects which are 10 kpc in diameter. Even this upper limit is lower than the detection limit in the HMDS and the HMWS. In the redshift ranges sampled by the HMWS and the HMDS, these cosmological effects are small. The large difference seen at low redshift is a result of the fact that surface brightness is

constant in Euclidean (i.e. local) geometry, and the HWS used isophotal magnitudes rather than aperture magnitudes for this reason.

The theoretical models of the number counts focus on the chemical and spectral evolution of the galaxies without considering the dynamical history. The surface brightness, however, depends upon total luminosity and angular size. While effects of the cosmological geometry upon the surface brightness is incorporated into the models through the total luminosity, if galaxies are significantly bigger in the past than they are at present, they would have a lower surface brightness relative to their total luminosity. This would introduce a bias against high redshift objects due to the method of selecting the objects. Partridge and Peebles (1967) developed a model of galaxy formation in which large, low surface brightness, ultrared objects are the progenitors of the current galaxy population.

At the fainter end, figure 6.4 shows that galaxies have roughly the same surface brightness profile independent of magnitude. The potential problem comes from the use of aperture magnitudes, and the limit of detection is in an aperture magnitude is a constant surface brightness object that fills the entire aperture. This is plotted in figure 6.4. If galaxies were (because of dynamical evolution, for example), significantly larger in the past, over and above the cosmological geometry effect, the aperture magnitude would not include the total flux, and thus might fail to detect these objects. There are several ways to check this, in the higher signal-to-noise levels of the data. One way is to smooth the images, and run the object detection programs with larger apertures. In the HMDS and the HDS, there is an upper limit to the size at which a galaxy would be detected, because the median flat fielding technique described in chapter 3 destroys information on scales larger than the offset size. In the HMDS this was typically 20 arcseconds, in the HDS it was 10 arcseconds. However, the HMWS used 60 arcsecond offsets and only observed each

point on the sky 3 times while using 12 images in the flat fielding procedure. Thus all large-scale information remains intact in the final images.

Another way to check the data to see if there are any large, low surface brightness objects is demonstrated in figure 6.7. This figure is a plot of the number of objects detected in the magnitude range K = 16 to K = 17 in the HMDS as a function of the initial contour level used in the object detection program. When the contour level is lower than K = 17.5 no objects are detected. As the contour level passes through a magnitude range 2 to 3 magnitudes fainter than the object magnitude range of interest, the number of objects detected goes from 0 to 100%. Then as the contour level goes fainter yet, no further objects are detected. It is this which indicates that there are no large, low surface brightness objects in this magnitude range. This figure is the reverse of figure 6.4 in that it shows the effects of varying the detection contour level for a given magnitude bin, rather than showing the effects of varying the magnitude for a given contour level.

For this type of object detection program to fail to detect a large, low-surface brightness galaxy at the K = 16 to K = 17 level, the galaxy would have to be larger than the 6.375 arcsecond aperture used. The lowest surface brightness possible is a constant surface brightness. For an object to be at K = 16.5 with a constant surface brightness lower than 20.37, it would be larger than the 6.375 aperture used in the survey. However, figure 6.4 shows that all of the galaxies detected have a peak surface brightness at least a magnitude brighter than the constant surface brightness upper limit to detection.

While having a primeval galaxy be much larger than the local population is not excluded by the models of dynamical galaxy formation, (and, in fact is predicted,) the large primeval galaxies would then need to collapse to form the current population. This intermediate stage would happen on a time scale

comparable to the age of the galaxies, and would be visible in the data. That we do not see these intermediate stages argues against large low-surface brightness primeval galaxies of the type proposed by Partridge and Peebles (1967). A similar analysis of the HDS data has revealed that there are no detected galaxies of this type in the K = 18 to K = 19 magnitude range. (Cowie, private communication).

Baron and White (1987) proposed a model of galaxy formation within the Cold Dark Matter scenario, in which primeval galaxies take the form of the radio galaxy 3C326.1. While Lilly and McLean (1989) have since then shown that this galaxy has high emission in the near-infrared, and thus has an old stellar population, nonetheless we must consider whether primeval galaxies appear as Baron and White (1987) predicted. The galaxy 3C326.1 has extended, non-symmetric lumpy structure. Within this model, primeval galaxies would be misidentified as a small group of several objects, rather than a single object. However, they could be identifiable by the fact that the colors of the objects would be similar. If they were at high redshift (i.e. $z > 3$, although within the CDM scenario, galaxy formation is more recent than this), they would have very red B-I colors as Lyman α would have been redshifted out of the B band. Figure 6.8 is a plot of the B-I/I-K colors of the galaxies within the HMDS which have neighbors within 6 arcseconds. Objects are connected by lines to their neighbors. Within this sample, there are 4 sets of 3 objects. Contour plots of these objects in B, I and K, along with their colors are plotted in figures 6.9a-d. In each case, the objects are more clearly separated than the components of 3C326.1. In figures 6.9b, c and d, the brightest component is clearly identifiable as a foreground star, and in the remaining figure, 6.9a, the components appear as separate galaxies. The radio galaxy 3C326.1 has a K magnitude of K = 18.95, and we would not expect objects at this high redshift to be significantly brighter than this. Therefore, it is unlikely that we would detect a

Baron and White (1987) type primeval galaxy at high redshift in the HMDS or the HMWS, and indeed, we see no evidence for them.

If galaxies were much more compact at high redshift than locally, they would appear as point sources. In a survey with star/galaxy separation based upon morphology alone, they would be identified as stars. In the HMDS and the HMWS, however, star/galaxy was based upon a combination of color and morphology, with color usually taken to be predominant. It is unlikely that high redshift compact primeval galaxies would have the same colors as stars, and thus they would be counted among the galaxies.

There is evidence, however, in the color data, in figures 6.1a-e, figures 6.2a-f, and figures 6.3a-h, that there is a dependence of Hubble type upon redshift. That is, color evolution causes the population of galaxies to appear to be dominated by later types at fainter magnitudes. If there were a systematic dependence of peak surface brightness upon Hubble type, and if this dependence carried through to the evolutionary effects seen in the data, this could potentially bias the object selection. However, because there is such a great distance between the bulk of the data and the detection limits at the brighter levels, this is unlikely to have a large effect.

III. The Models

The theoretical models used to analyze the number count and color data typically have the following form. The apparent magnitude at which an object of absolute magnitude M_λ appears is given by:

$$m_\lambda = M_\lambda + K_\lambda(z) + E_\lambda(z) + 5 \log(d_L / 10 \text{ pc})$$

where M_λ is the absolute magnitude, $K_\lambda(z)$ is the *K* correction, $E_\lambda(z)$ is an evolutionary correction, and d_L is the luminosity distance. This equation provides the Hubble diagram, or magnitude as a function of redshift, when applied to

standard candle galaxies. It can then be convolved with a luminosity function, summed over galaxy types, and integrated over the volume-redshift relation out to a redshift z_{form} to provide the number counts. Similarly, this equation can be calculated in two different bandpasses to provide color as a function of redshift. (Yoshii and Takahara, 1988).

The models which produce the number counts all have several things in common. At low redshift, where the volume-redshift relation dominates the calculation, and the galaxy mix, the *K* corrections, and the luminosity function are all relatively constant, and where the evolutionary corrections are negligible, the slope of the number counts d log(n(m))/dm = 0.6. At fainter levels, the slope of the no-evolution model goes down, due to the *K* correction dimming, reaching 0.45 in the B band. In the K band, because of the flatness of the spectrum, the *K* corrections are much smaller, so this does not have as great of an effect. Finally, at the faintest levels the diagram begins to be dominated by the choice of parameters such as q_0 and z_{form}. The counts will eventually turn over as the end of the galaxy occupied volume is reached. This occurs, nominally, at the magnitude bin in which an M^*+K+E galaxy at z_{form} occurs. At this point evolution dominates the diagram, and the number and magnitude in which the counts turn over is very sensitive to the choice of model parameters. (Yoshii and Takahara, 1988.)

Figure 6.10 is a plot of the K band number counts against the models of Yoshii and Takahara (1988). The model has been normalized at the bright end to the K = 12.25 point from the Mobasher *et al.* (1986) data, to correct for the uncertainty in the local luminosity function. The dotted lines are the no-evolution model for $q_0 = 0.5$ and $q_0 = 0.02$. The solid lines include the effects of pure luminosity evolution. The best fit to the data is the $q_0 = 0.02$ evolution line, although even this has a slight undercount in the K = 15 to K = 18 region. This model, however,

underpredicts the B band counts at the faint end. In addition, the results of the redshift surveys (Broadhurst *et al.*, 1988, Colless *et al.*, 1990, Cowie *et al.*, 1991) show that to B = 24, the median redshift fits the no-evolution model, contrary to the predictions of the YT model. And finally, the I-K colors, plotted in figures 6.1a-e against the red envelope from the YT evolution model, show that pure luminosity evolution is not sufficient.

Two deviations from this standard model involve a cosmological constant model, in which the geometry of the universe provides more volume at low redshift, and a model in which merging plays a significant role in producing the number counts. The cosmological constant model was put forth by Fukugita et al. (1991), in which they determined the effects of a non-zero Λ on the number count models of YT. The motivation for this model is that it fits the B band number counts and the redshift distributions. By providing greater volume at low redshift than the convention cosmological geometries, the number counts are high, but the redshift distribution (normalized to the number counts) remains similar to the no-evolution model. The K band number count predictions of this model are plotted in figure 6.11. While the no-evolution model fits the data at the faint end, it underpredicts the counts in the K = 15 to K = 18 region where the effects of luminosity evolution are most likely to be seen. In addition, it is the model with luminosity evolution that fits the B counts, and this model overpredicts the K counts at the faint end. This model, by basing its deviation from the standard model solely on cosmological geometry, predicts that the galaxies making up the excess seen in the B band counts are at low redshift, and are very similar to the local population. The change in color with magnitude seen in figures 6.1-3 would not be seen in this model.

Broadhurst *et al.*, (1992) constructed a model in which the excess in the B band counts is caused by large amounts of merging. Their simple model assumed

that all galaxies merge, but that the proportions of different types, their *K* corrections, and their luminosity function shapes are maintained with time. The characteristic mass, M^* decreases with increasing look-back time, and the number density ϕ^* increases accordingly, with the product $M^*\phi^*$ remaining constant. M^* and ϕ^* each have an exponential dependence upon time, with

$$\phi^*(\delta t) = \exp(\mathcal{Q}\delta t/\beta t_0) = \exp(-\mathcal{Q}/\beta((1+z)^{-\beta}-1) \approx 1+\mathcal{Q}z \quad (z < 1)$$

where $\mathcal{Q}$ is parameter representing the merger rate and $\beta \equiv 1+(2q_0)^{0.6}/2$. This formalism is preferable to a merging rate exponential in (1+z) (Rocca-Volmerange and Guiderdoni, 1990) in that it avoids the problem of an unrealistically high merging rate at high redshift. The parameter $\mathcal{Q} = 4$ implies that a present-day galaxy is the result of the merging of 4-6 galaxies at $z = 1$, depending upon q_0.

This model, with $\mathcal{Q} = 4$ fits well the B band counts and the B selected redshift survey data. It is plotted in figure 6.12 against the K band counts. As Broadhurst *et al.*, (1992) modified the no-evolution model of Bruzual (1983) rather than that of YT, I have plotted for comparison the prediction of that model for an open universe with luminosity evolution. From this figure it can be seen that the merging model with $\mathcal{Q} = 4$ (the best fit to the B counts and the redshift data) fits the counts at the faint end, but does not fit the counts in the intermediate range, addressed by the HMWS and the HMDS, from K = 15 to K = 18. However, this model is a modification of a no-evolution model, and this region is where luminosity evolution is likely to have the largest effect. In addition, the assumptions of this model are too simplistic. This model assumes that colors do not evolve, but change only due to the *K* correction. However, merging models are likely to change the colors of the galaxies, in just the way that is seen in the data. The merging process induces star formation, and thus the galaxies which are merging are likely to be

bluer and brighter than the current population. This is seen in the data, in figures 6.1-3.

Cowie *et al.*, (1991), and Cowie *et al.*, (1992) proposed that the number count data indicate a separate population of faint blue galaxies existing alongside the current population, which is present up to a redshift of $z \approx 0.4$, but is not seen locally. This model is also discussed in chapter 4. The difference between this model and the merging model is difficult to see, as the components undergoing merging are faint blue galaxies. However, this difference is seen in figures 6.1a-e and in figures 6.3a-h. These figures show very few unevolved, or pure luminosity evolution, elliptical galaxies at a redshift of $z = 1$. A K^* galaxy at this redshift would be at $K = 17.8$ if unevolved, or $K = 17.1$ with YT luminosity evolution (for $q_0 = 0.5$, for $q_0 = 0.02$, these would be approximately 0.4 magnitudes brighter). At these magnitudes, the blue dwarf population is not just dominating the progenitors of the local population, they must be the progenitors of the local population, for there is nothing else there.

IV. Summary and Future Observations

In any field, as the data gets better and more comprehensive, the models used to fit the data must become more complicated. In this chapter, I have discussed the no-evolution model, the pure luminosity evolution model, the non-zero cosmological constant model, the faint blue dwarf model, and the merging model. Each of these models focuses on one aspect that can affect the number counts, while making simple assumptions about the other aspects. The data, however, has now become good enough that a more complex model is needed, such as one with both merging, or number evolution, and luminosity evolution. It can be seen that one, but not the other, is not sufficient to explain the data.

The specifics of a model combining number and luminosity evolution that would explain the data are not as clear as the fact that such a model is needed. In the absence of redshift information, there is a limit to what is contained in the number count and color data. Most redshift surveys done to date (Broadhurst *et al.*, 1988, Colless *et al.*, 1990, and Cowie *et al.*, 1991) have selected the objects for study in the B band, as this provides an *a priori* indicator of the feasibility of obtaining redshifts. However, the redshifts of the K band selected population now need to be known. Only this way can the effects of luminosity evolution and number evolution be separated. Cowie *et al.*, (1992) have begun two K band selected redshift surveys, covering the HWS at $K < 15$, and the HDS at $K < 20$. The bright end is suitable for determining the local luminosity function, and calibrating the no-evolution redshift prediction. The deep survey results show that the median redshift even at $K = 20$ is very low, of order $z = 0.5$, with no objects detected at $z > 1$. While the sample is small, this is confirmation of the indications in figures 6.1-3 that there are few galaxies at $z > 1$ at $K < 20$. Redshift information in the intermediate region, from $K = 15$ to $K = 18$, is needed as this is the region that is difficult to fit to the models, and is the region where luminosity evolution would have the largest effect.

There are two ways to go about constructing a K band selected redshift survey. One way, of course, is simply to begin obtaining redshift on a K band selected sample. The other way takes advantage of pre-existing spectroscopic data. By obtaining K band photometry of the fields of a B band selected redshift survey, some of the objects will have already been observed with a spectrograph. When this is done, there is the immediate benefit of absolute K magnitudes for the B selected sample. For non-starbursting galaxies the K band light comes from near-solar mass stars and so the absolute K magnitude is a good indicator of the mass of the galaxy. It was the low absolute K magnitude of the objects in their $B < 24$ redshift survey

sample which led Cowie *et al.*, (1991) to conclude there is a population of faint blue dwarf galaxies at moderate redshifts.

With K band photometry of a B selected redshift survey sample one immediately obtains a K band selected redshift sample that is complete to a limit determined by the reddest object in the sample. This was the strategy followed by Mobasher *et al.*, (1986) for it was very difficult to cover large areas of the sky with the K band single point detectors available at the time. Their survey data, which I have used extensively in this thesis contains a K band selected survey complete to approximately K = 12, and K band photometry of a B band redshift survey complete to B = 17. Work has begun on complete K band photometry of the Colless *et al.*, (1990) redshift survey, and indeed, three of the HMDS survey fields were selected to cover part of the area of that survey.

Having obtained K band photometry of the objects in a B selected sample, particularly if the entire field has been observed in K, one then constructs a K band selected sample, and begins to obtain spectroscopic redshifts of the objects redder than the B-K limit. The Mobasher *et al.*, (1986) could not do this, as they only observed the B selected objects in K, and did not observe the entire field. Unfortunately, it will also be difficult to construct a K band selected sample from K band photometry of the Colless *et al.*, (1990) fields. They selected their sample not only with a faint B band limit of B = 22.5, but also with a bright limit of B = 21. In addition, their sampling rate was only 1 out of every 3 objects, although they selected these solely by the geometric constraints of their spectrograph, and thus did not introduce any bias into their sample. Thus they obtained redshifts for 1/3 of the objects in $21 < B < 22.5$. It will be difficult to construct a complete K sample from this, as there will be both a blue and a red limit. However, the sample could be made complete at the blue end fairly easily by obtaining redshifts of the objects in

the K selected sample brighter than B = 21. The sample could then be made complete at the red end by the much more difficult task of obtaining redshifts for the objects within the K limit, but with B > 22.5.

One aspect of the data in the HMWS and the HMDS which I have not considered in this thesis are the stars. With color-magnitude and number count information it will be possible to discuss the density and luminosity function of the stars in the halo of our galaxy. This aspect of the data will be, perhaps, among the most exciting results of those surveys. The galaxy data fills in the important gap between the HWS and the HDS, but there are not very many important conclusions and trends in the data which were not already seen in the HDS. The HDS covers too small of an area to have statistical information on the stars. Thus the HMDS is the deepest K band survey of stars in the halo that has been done to date. It will be possible to compile a luminosity function of low-luminosity M dwarfs stars, and to investigate brown dwarf candidates. Follow-up high resolution J, H, and deeper K band photometry will be useful in identifying the reddest objects.

References for Chapter 6

Annis, J., 1992, *Ap. J. Lett.*, **391**:L17.

Baron, E., and White, S.D.M, 1987, *Ap. J.*, **322**:585.

Broadhurst, T.J., Ellis, R.S., and Shanks, T., 1988, *M.N.R.A.S.*, **235**:827.

Broadhurst, T.J., Ellis, R.S., and Glazebrook, K., 1992, *Nature*, **355**:55.

Bruzual A., G., 1983, *Ap. J.*, **273**:105.

Coleman, G.D., Wu, C.-C., and Weedman, D.W., 1980, *Ap. J. Supp.*, **43**:393.

Colless, M., Ellis, R.S., Taylor, K., and Hook, R.N., 1990, *M.N.R.A.S.*, **244**:408.

Cowie, L.L., Songaila, A., and Hu, E.M., 1991, *Nature*, **354**:460.

Cowie, L.L., Gardner, J.P., Hu, E.M., Wainscoat, R.J., Hodapp, K.W., 1992, *Ap. J., submitted.*

Elston, R., Rieke, G.H., and Rieke, M.J., 1988, *Ap. J. Lett.*, **331**:L77.

Elston, R., Rieke, M.J., and Rieke, G.H., 1989, *Ap. J.*, **341**:80.

Fukugita, M., Takahara, F., Yamashita, K., and Yoshii, Y., 1990, *Ap. J. Lett.*, **361**:L1.

Johnson, H.L., 1966, *Ann. Rev. Astron. Astrop.*, p. 193.

Lilly, S.J., and McLean, I.S., 1989, *Ap. J. Lett.*, **346**:L65.

Lilly, S.J., Gardner, J.P., Cowie, L.L., McLean, I.S., 1988, *Ap. J. Lett.*, **332**:L59.

Partridge, R.B, and Peebles, P.J.E., 1967, *Ap. J.*, **148**:377.

Rocca-Volmerange, B., and Guiderdoni, B., 1990, *M.N.R.A.S.*, **247**:166.

Sanders, D.B., Soifer, B.T., Elias, J.H., Madore, B.F., Matthews, K., Neugebauer, G., and Scoville, N.Z., 1988, *Ap. J.*, **325**:74.

Tinsley, B.M., and Gunn, J.E., 1976, *Ap. J.*, **203**:52.

Yoshii, Y., and Takahara, F., 1988, *Ap. J.*, **326**:1.

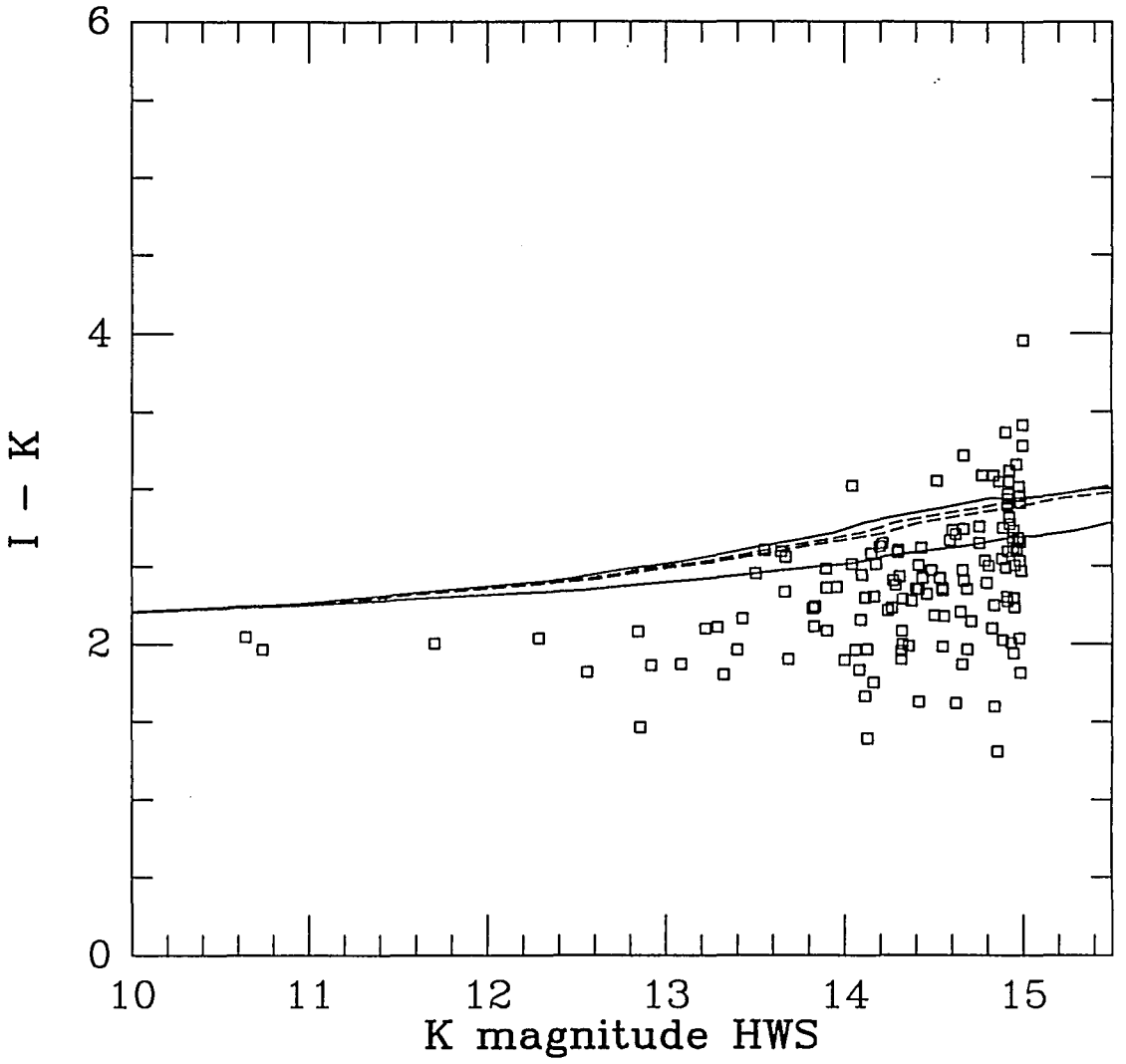

Figure 6.1a: I-K vs K -- the HWS data. Also plotted are a model for a K^* elliptical galaxy. The dashed lines are the no-evolution model, with the lower line being for $q_0 = 0.5$, and the upper line being for $q_0 = 0.02$. The solid lines include Yoshii and Takahara (1988) evolution. Most galaxies in this bright survey are elliptical and Sa galaxies at near K^*.

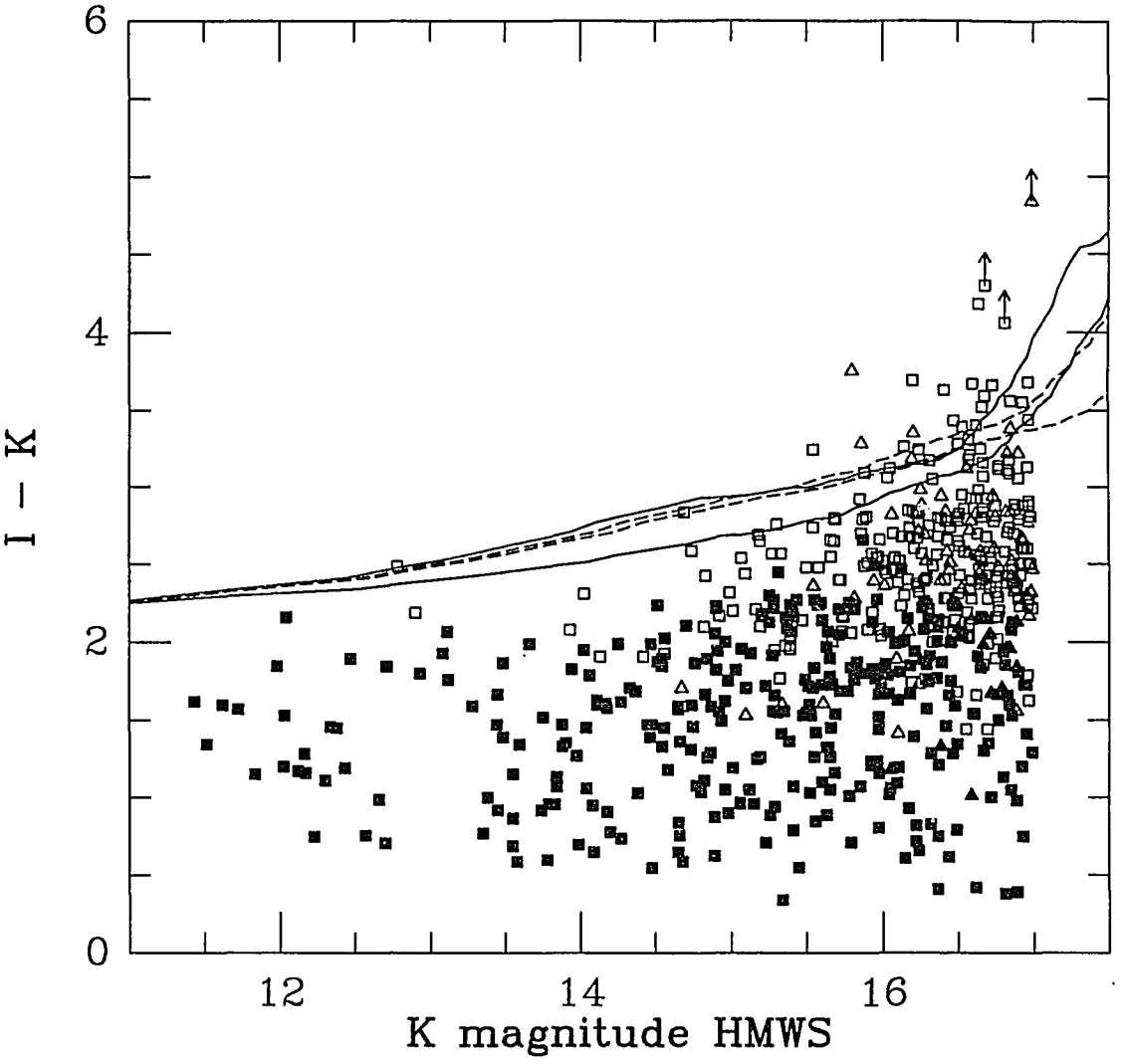

Figure 6.1b: I-K vs K -- the HMWS data. The models are the same as in figure 6.1a. The stars are represented by the filled symbols, and the galaxies are the open symbols. Compact objects with the colors of a galaxy are plotted as triangles; likewise, diffuse objects with stellar colors are plotted as triangles. Objects for which the morphological star/galaxy separation agreed with the color criteria are plotted as squares. Most galaxies in this figure cluster just below the K^* elliptical model lines.

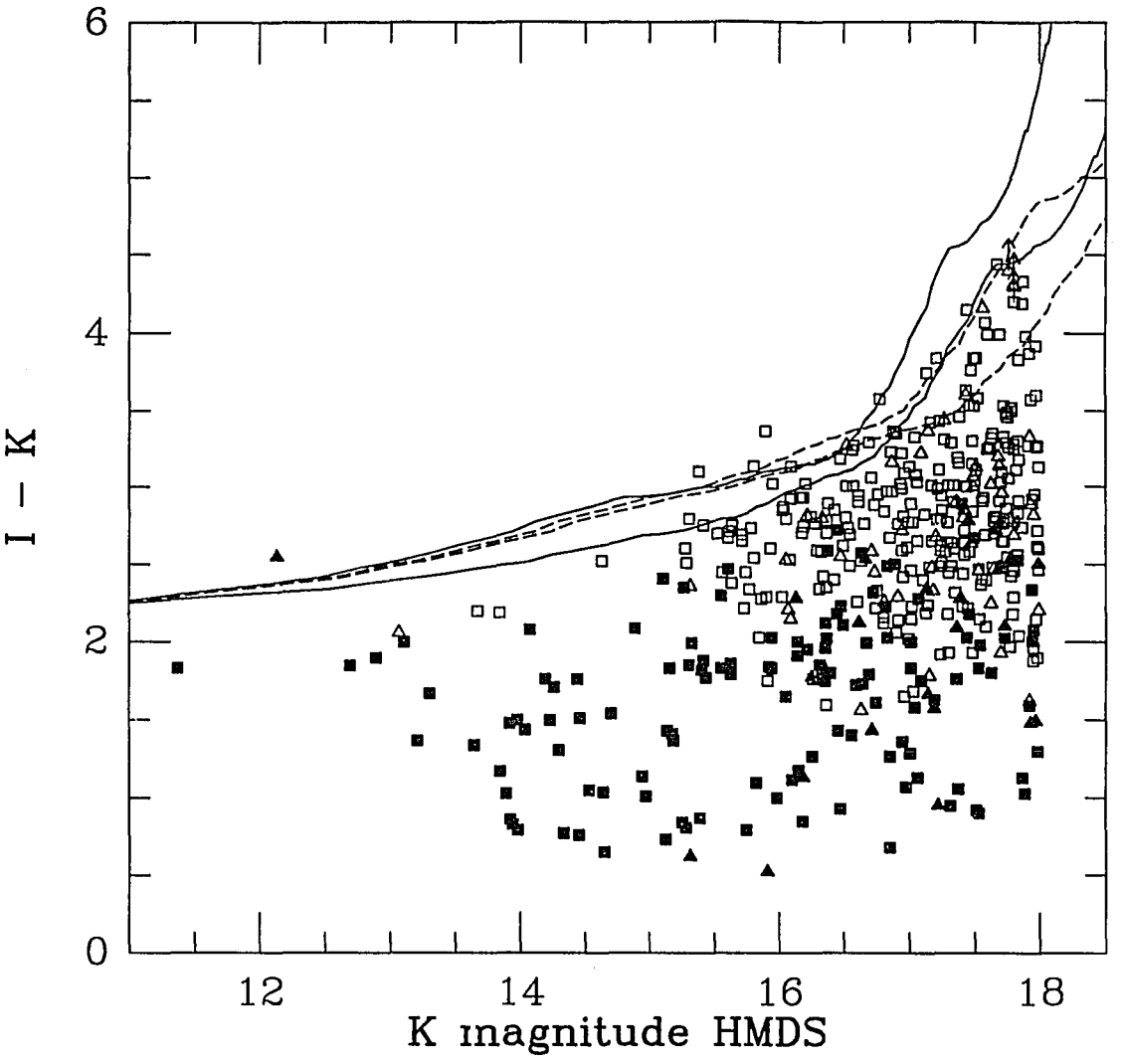

Figure 6.1c: I-K vs K -- the HMDS data. The models and symbols are the same as in figure 6.1b. In this figure, despite the high noise turnup at K = 18, the bulk of the galaxies are beginning to be bluer than the models. There are no bright, ultra-red objects of the type reported by Elston *et al.*, (1989).

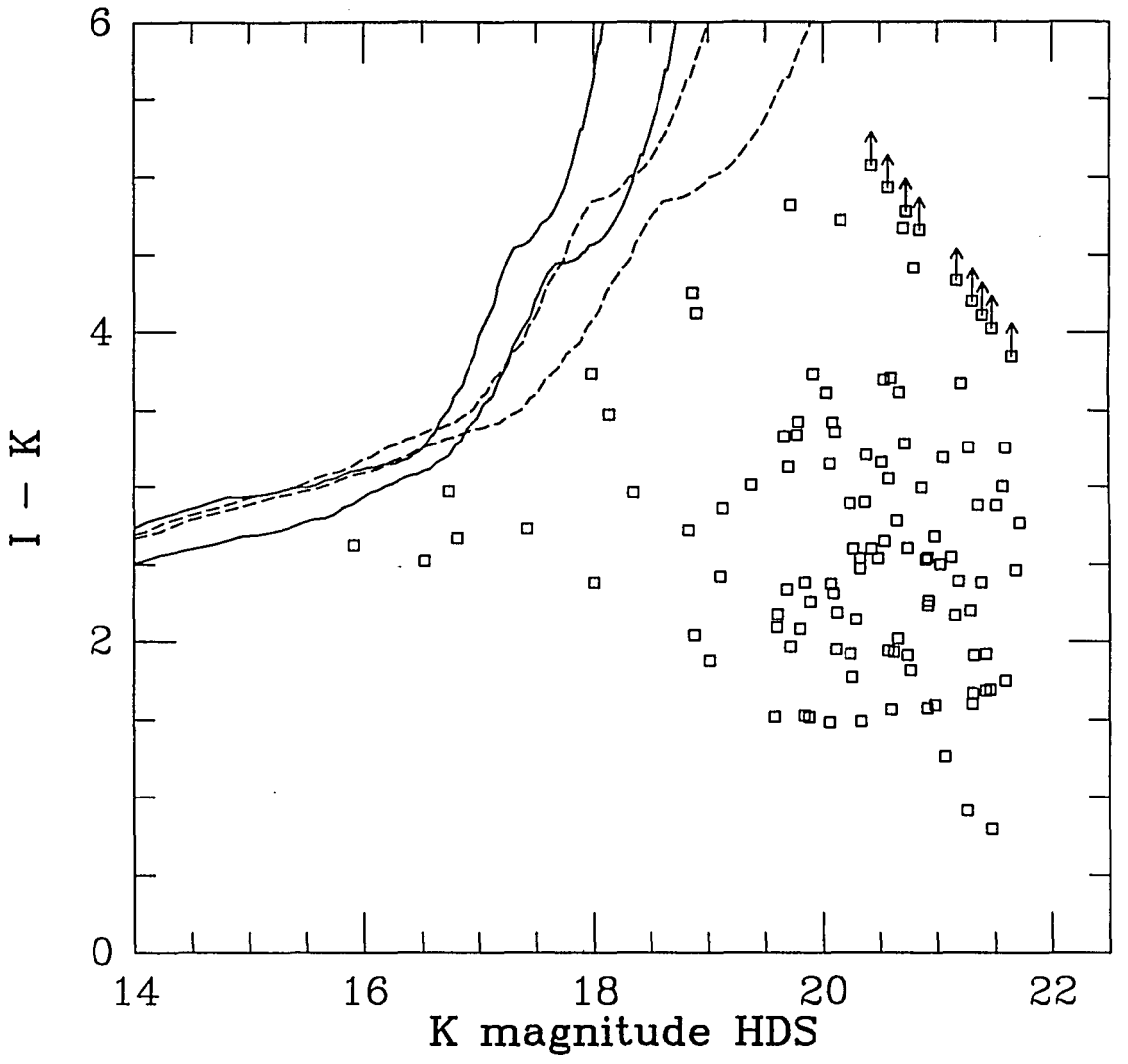

Figure 6.1d: I-K vs K -- the HDS data. In this figure the galaxies are much bluer than the models, indicating a near complete lack of K^* elliptical galaxies at redshifts of $z \approx 1$. Standard luminosity evolution, indicated by the solid lines, would tend to make galaxies redder, not bluer.

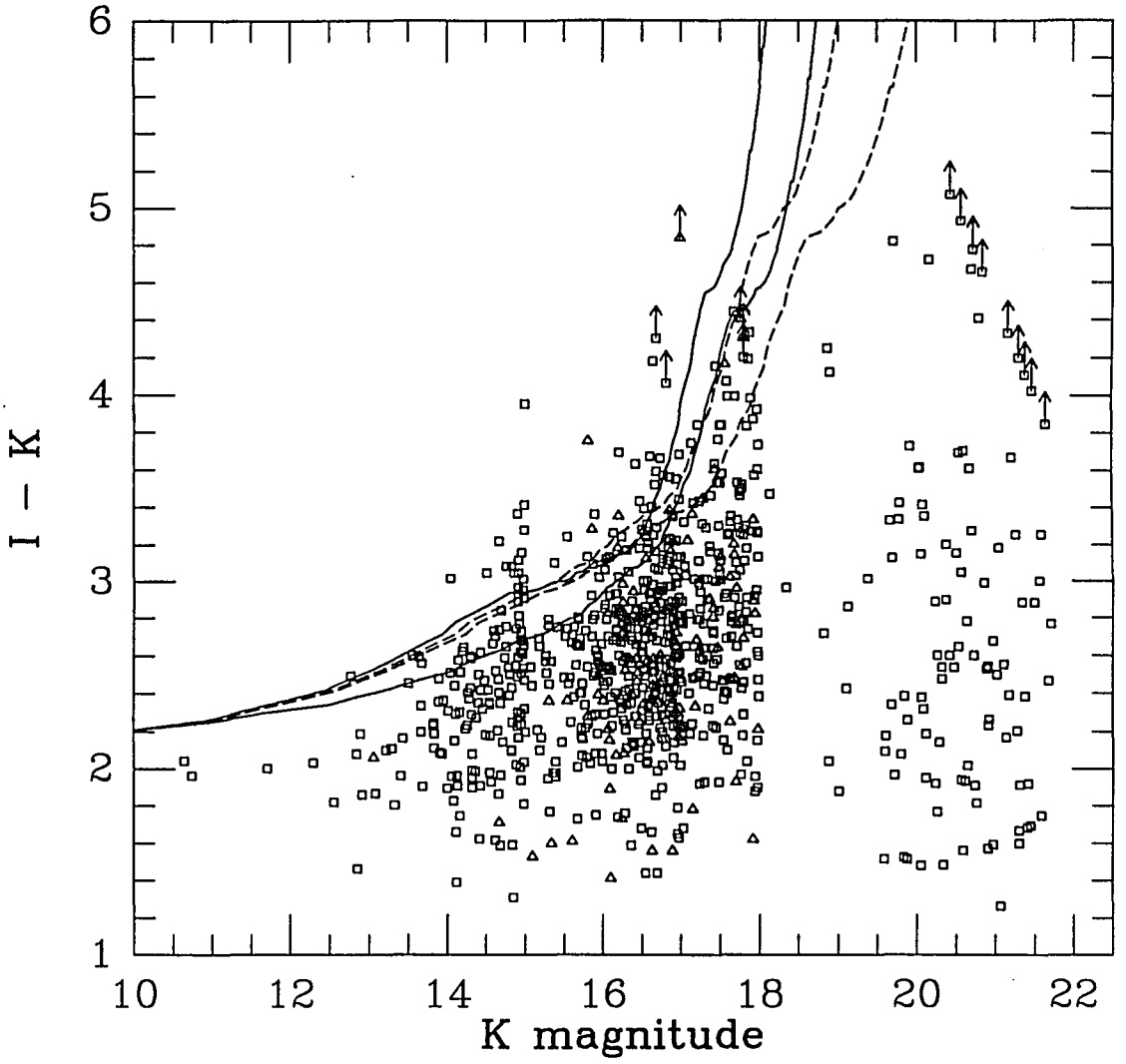

Figure 6.1e: I-K vs K -- all the galaxy data.

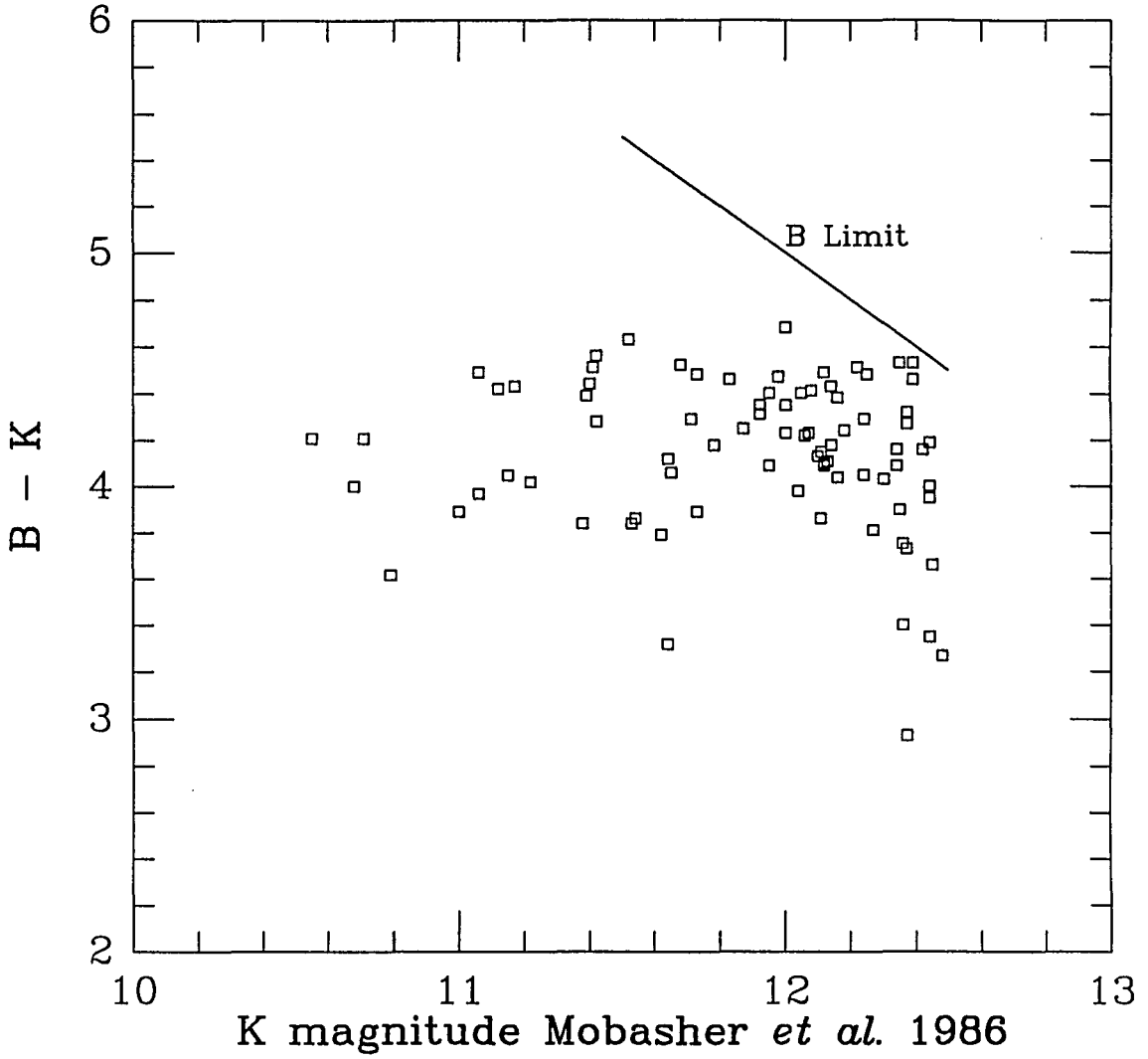

Figure 6.2a: B-K vs K -- the Mobasher *et al.*, (1986) data. The line represents the B = 17 limit of the survey. The data comprises a nearly complete survey to K = 12.5, but fainter than this the B = 17 limit would mean that the K band would be incomplete. The galaxies in this sample are at low enough redshift that their *K* corrections are negligible, thus the B-K color does not change as a function of K magnitude.

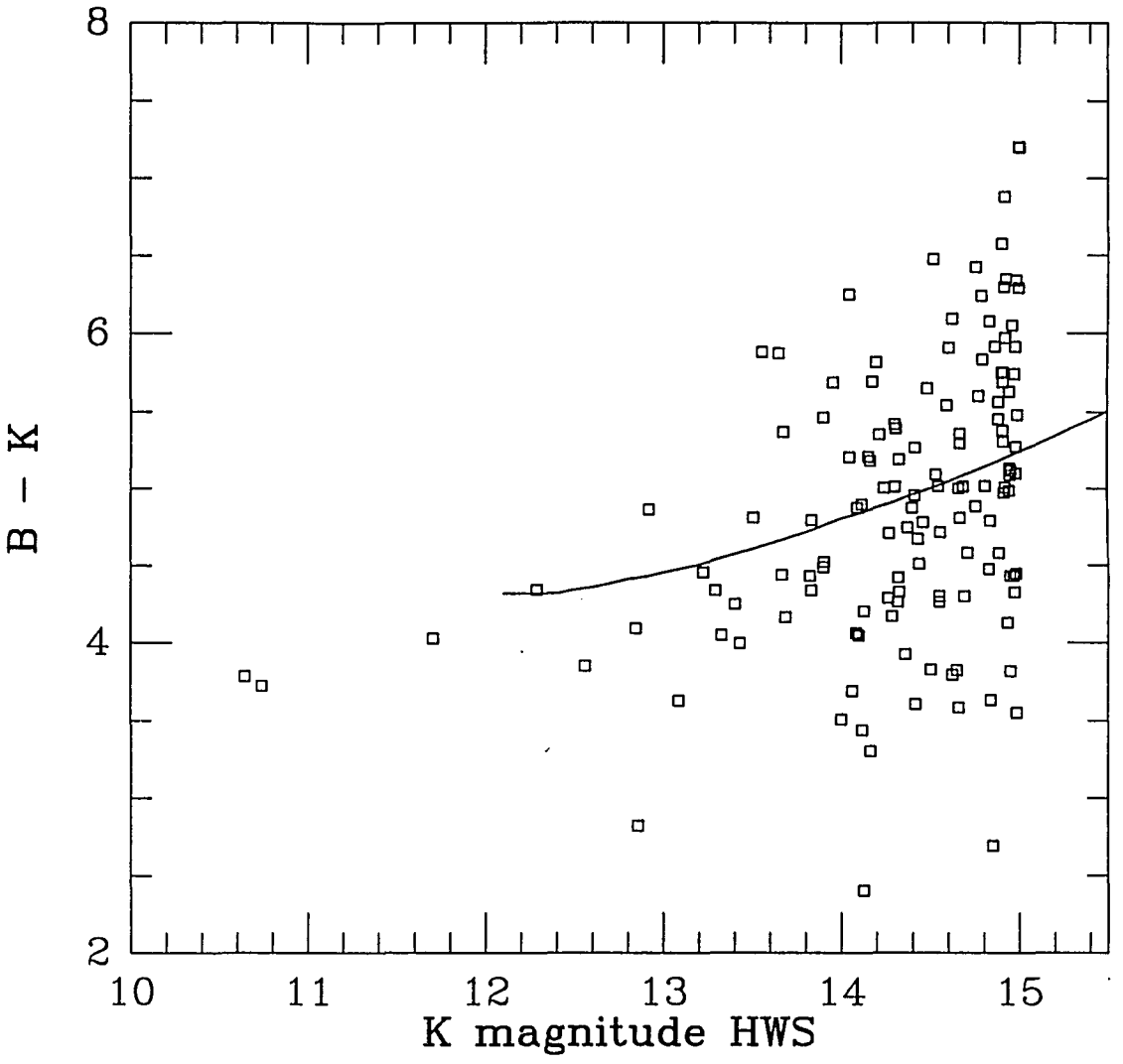

Figure 6.2b: B-K vs K -- the HWS galaxy data. The line is a no-evolution model for the median B-K color as a function of magnitude. In these data the galaxies get redder as they get fainter due to the *K* correction. No evolution is expected or seen.

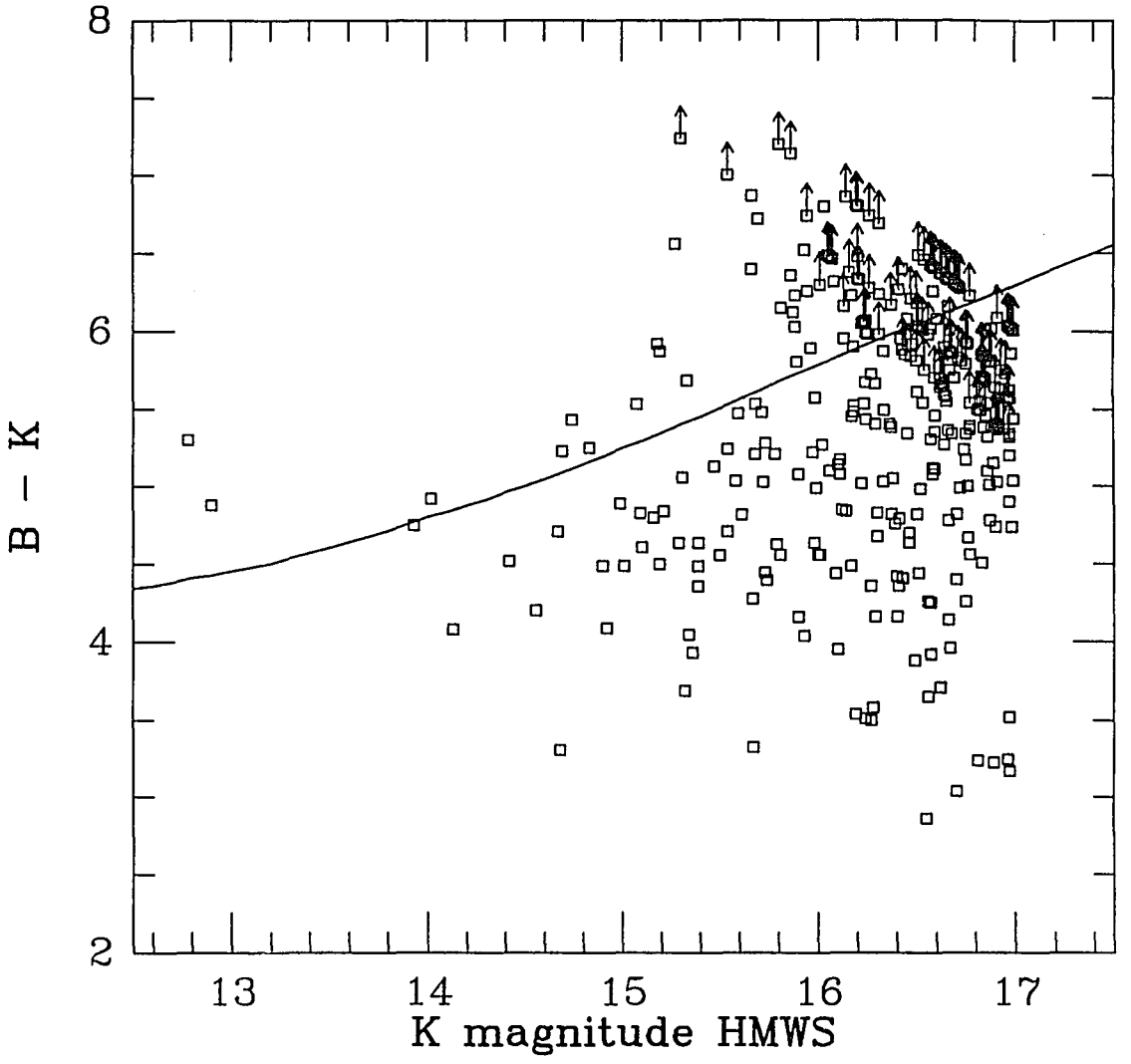

Figure 6.2c: B-K vs K -- the HMWS galaxy data. The model is the same as in figure 6.2b. Although it is difficult to see in this plot due to the large number of lower limits to the colors, the data generally follows the no-evolution model.

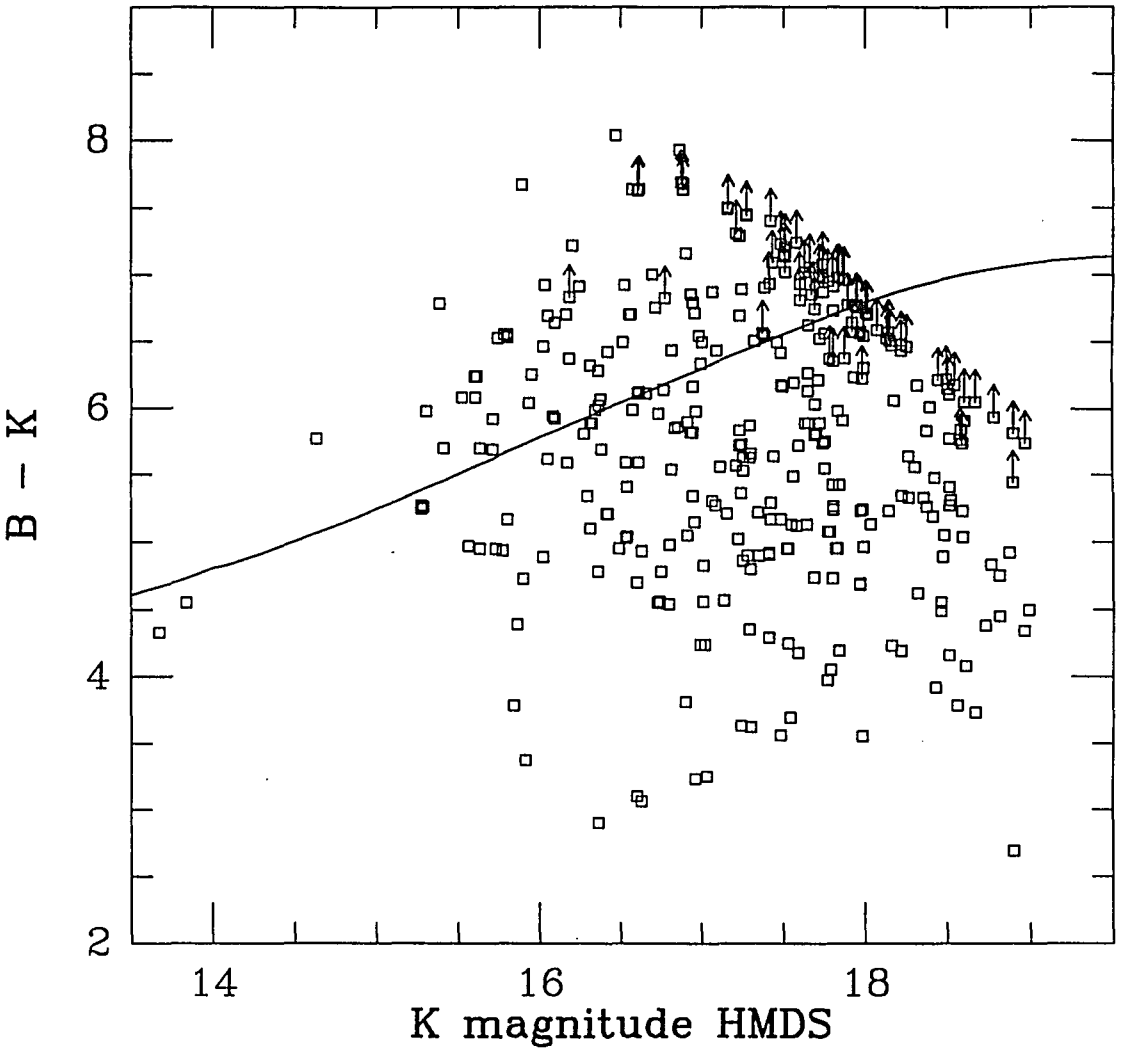

Figure 6.2d: B-K vs K -- the HMDS galaxy data. The model is the same as in figure 6.2b. The galaxies are starting to show a turnover in the B-K median color, getting bluer, while the no-evolution model continues to get redder.

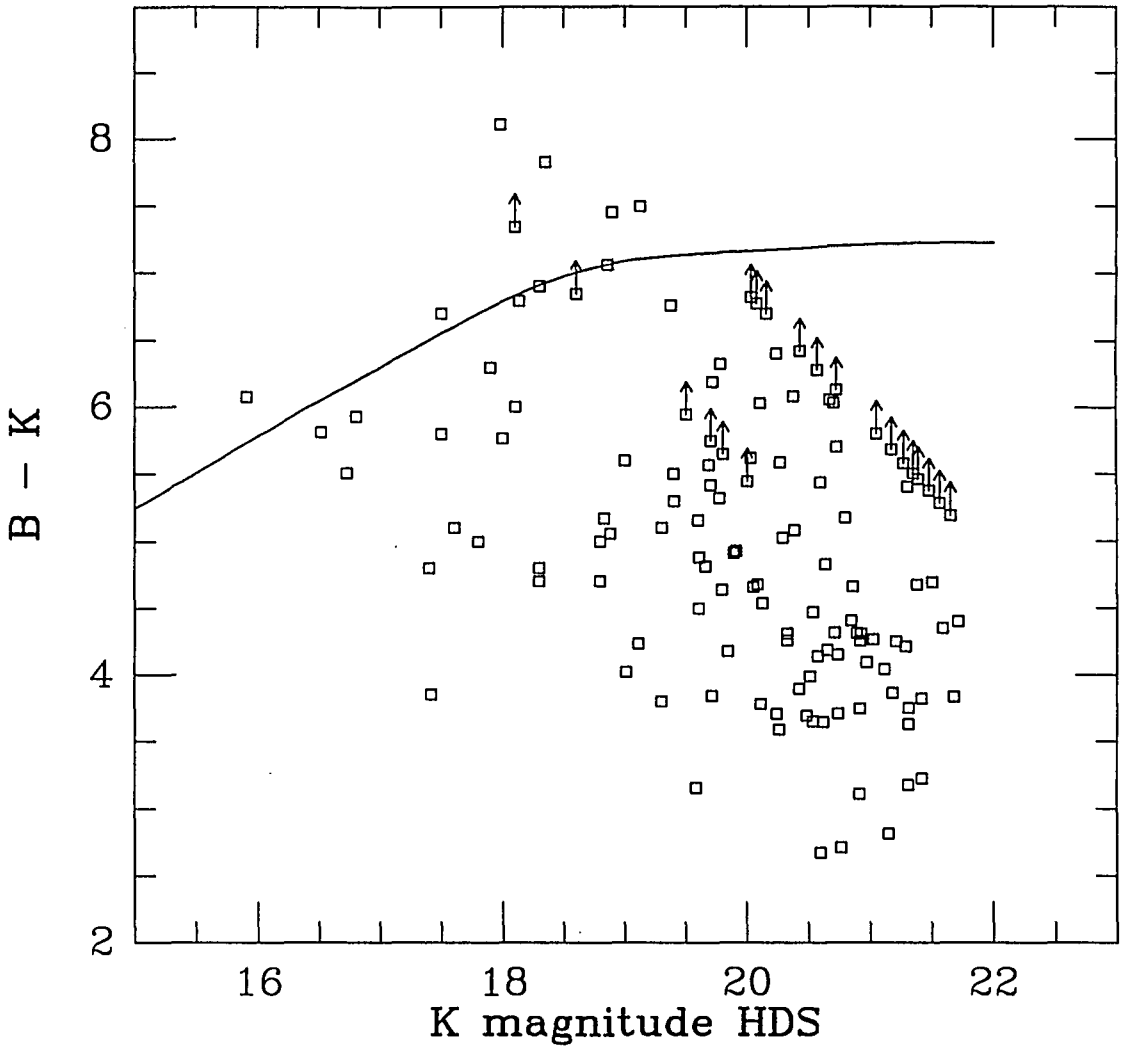

Figure 6.2e: B-K vs K -- the HDS galaxy data. The model is the same as in figure 6.2b. The data is much bluer than the median predicted by the no-evolution median model.

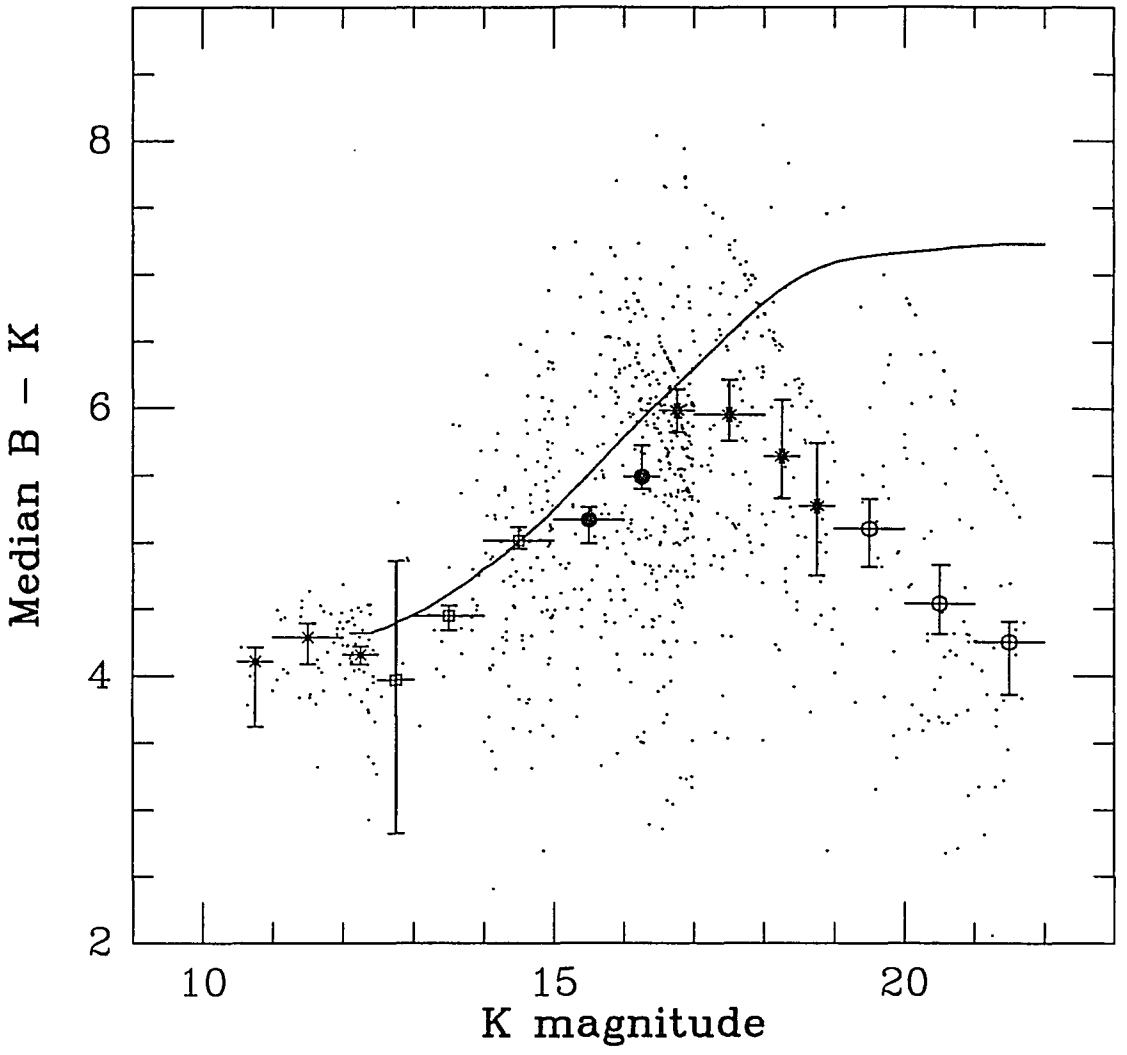

Figure 6.2f: B-K vs K -- all the galaxy data. The model is the same as in figure 6.2b. The points with error bars are the median B-K color in each bin, with the errors determined by the median sign test. The data follows the no-evolution model until about K = 17 when it turns over to rapidly become bluer.

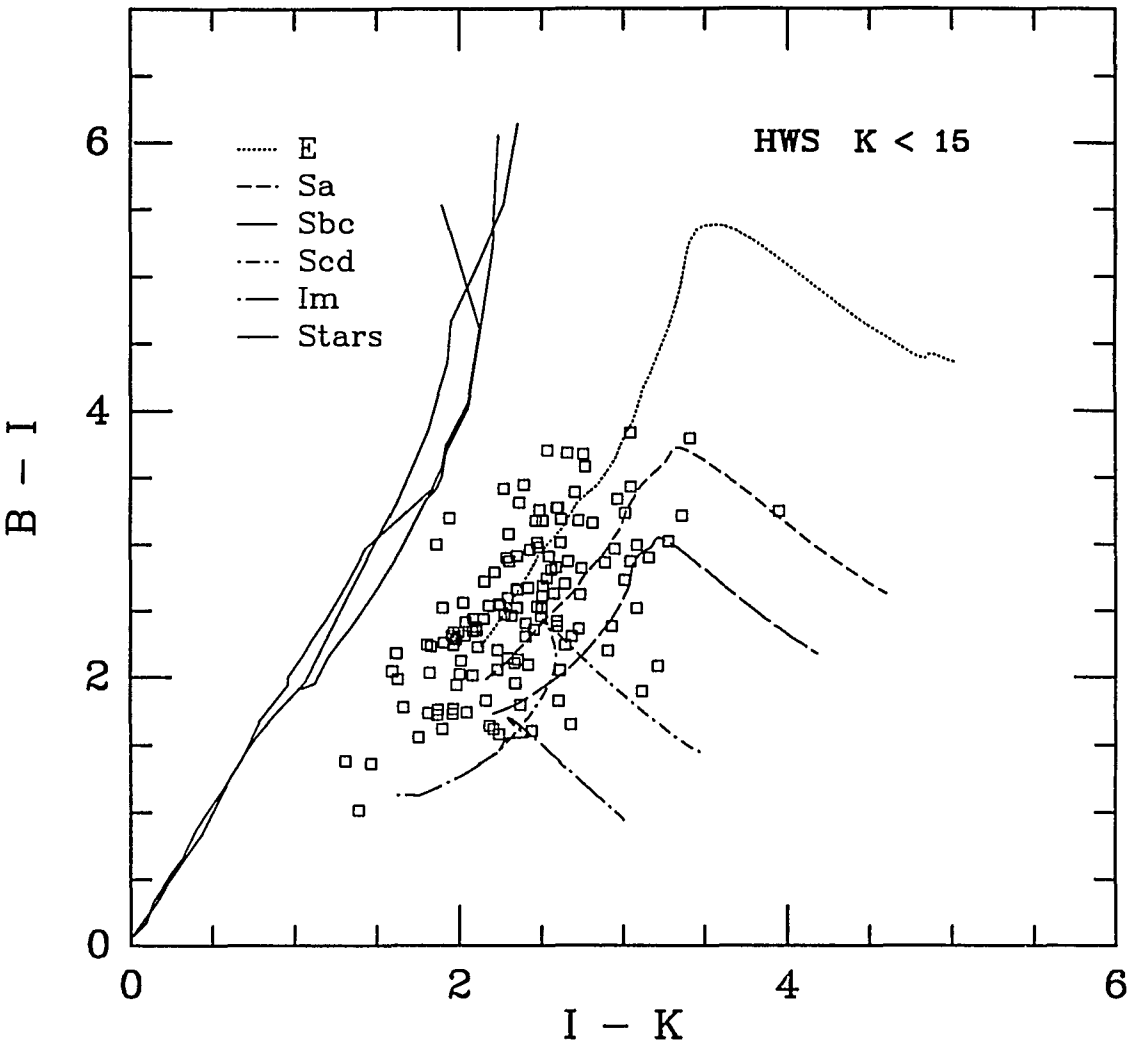

Figure 6.3a: B-I vs I-K -- the HWS galaxy data. The lines are no-evolution models of 5 types of galaxies plotted from z = 0 to z = 1.5, and for three types of stars, dwarfs, giants and super-giants. The galaxy models are based upon the spectral energy distributions of Coleman, *et al.*, (1980), and the stars are based upon Johnson, (1966). Both the galaxy and the star models are transformed into the filter set used in the Hawaii surveys. From this figure, it is evident that the majority of the galaxies detected are ellipticals and Sa galaxies. This is expected in a K band selected sample.

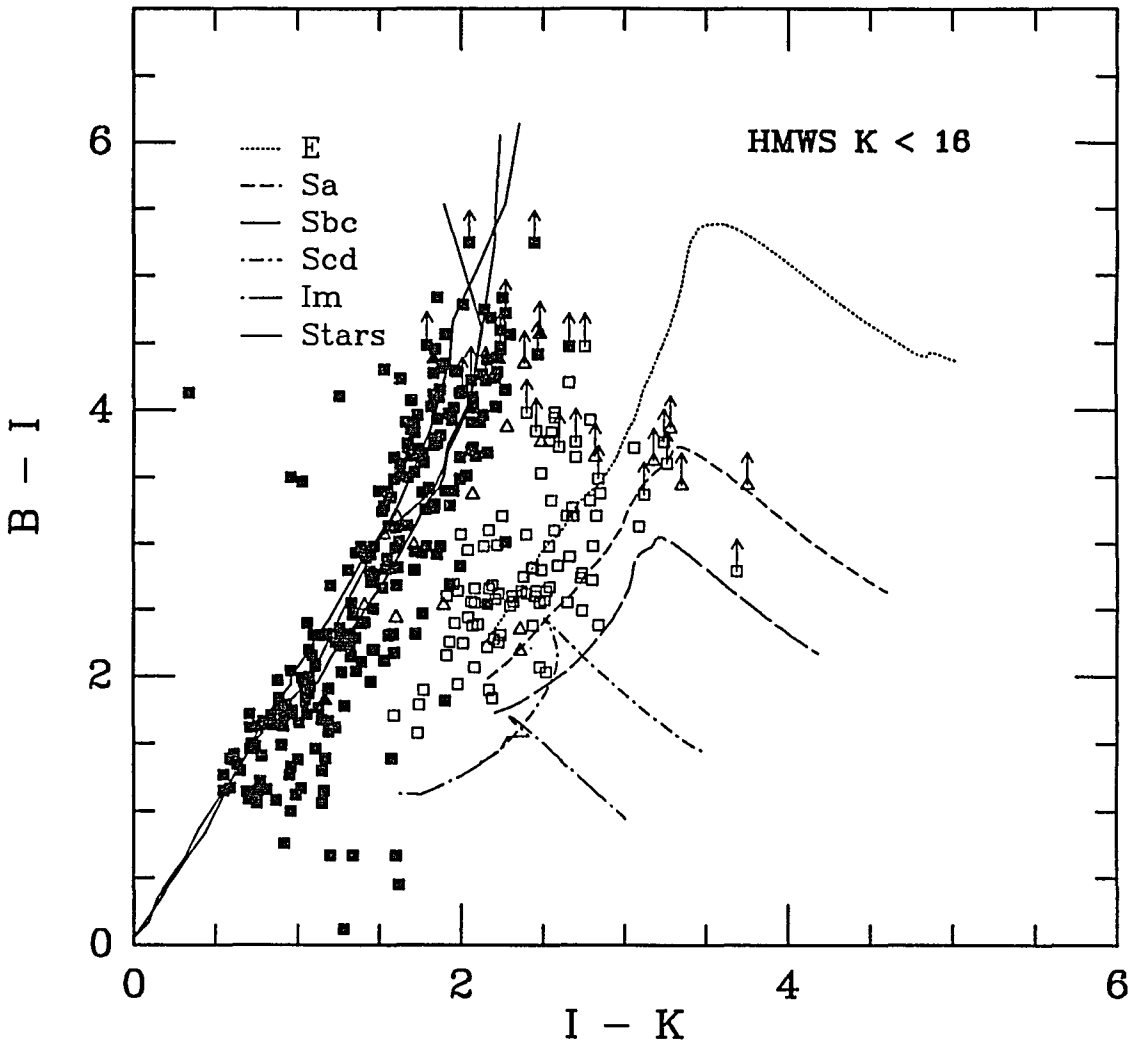

Figure 6.3b: B-I vs I-K - the HMWS data at K < 16. The models are the same as in figure 6.3a. The galaxies are plotted as filled symbols, while the stars are plotted as open symbols. The star/galaxy separation was done, for the most part, by this figure. Objects for which the morphological classification disagreed with the color classification are plotted as triangles; objects clearly identified are plotted as squares. The objects with upward pointing arrows are undetected at the 2 σ level in B, and are plotted as 2 σ lower limits to the B-I color. The stars in the far left are mostly objects whose colors are contaminated by nearby companions. The stars in the extreme lower left are mostly objects with saturated colors. The galaxies in this plot are mostly unevolved elliptical and Sa galaxies at low to moderate redshift.

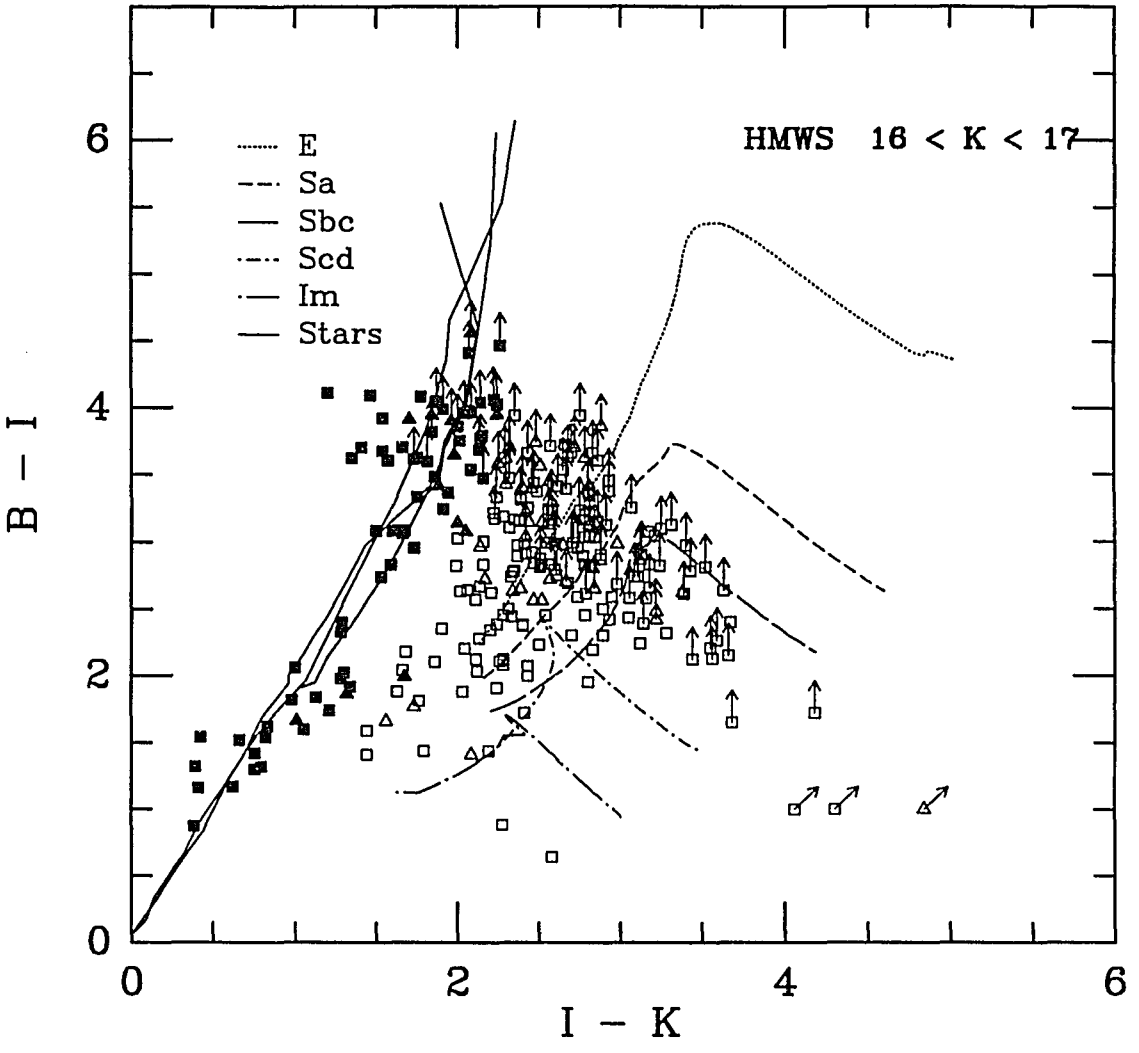

Figure 6.3c: B-I vs I-K - the HMWS data at 16 < K < 17. The models and symbols are the same as in figure 6.3b. Objects with diagonal arrows are undetected at the 2 σ level in both B and I, and are plotted as 2 σ lower limits to the I-K color, with the B-I color arbitrarily set to B-I = 1. The large number of galaxies undetected in B makes it difficult to interpret this figure.

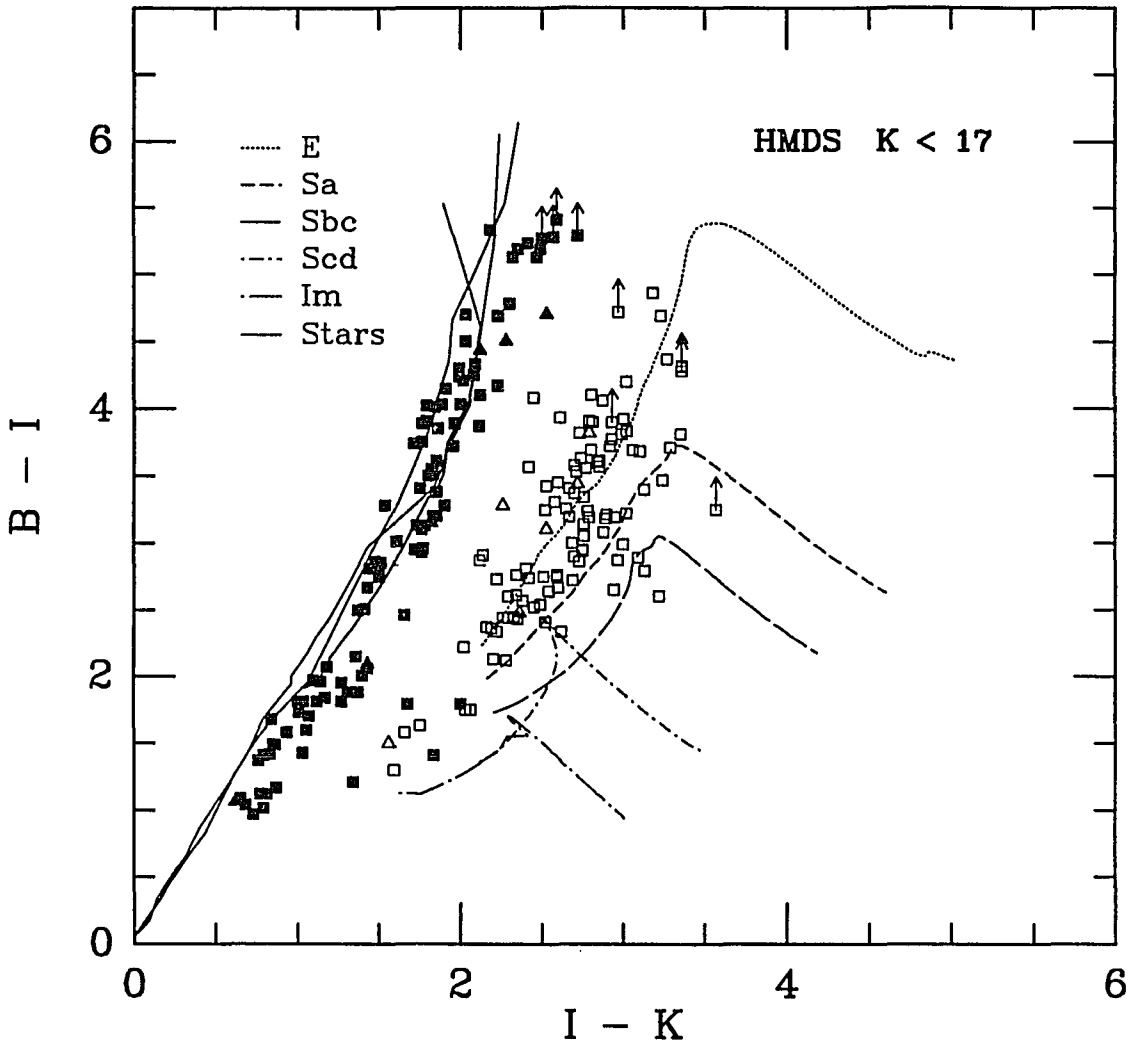

Figure 6.3d: B-I vs I-K - the HMDS data at K < 17. The models and symbols are the same as in figure 6.3b. The majority of the galaxies are still elliptical and Sa galaxies at moderate redshift. No evidence for evolution is seen.

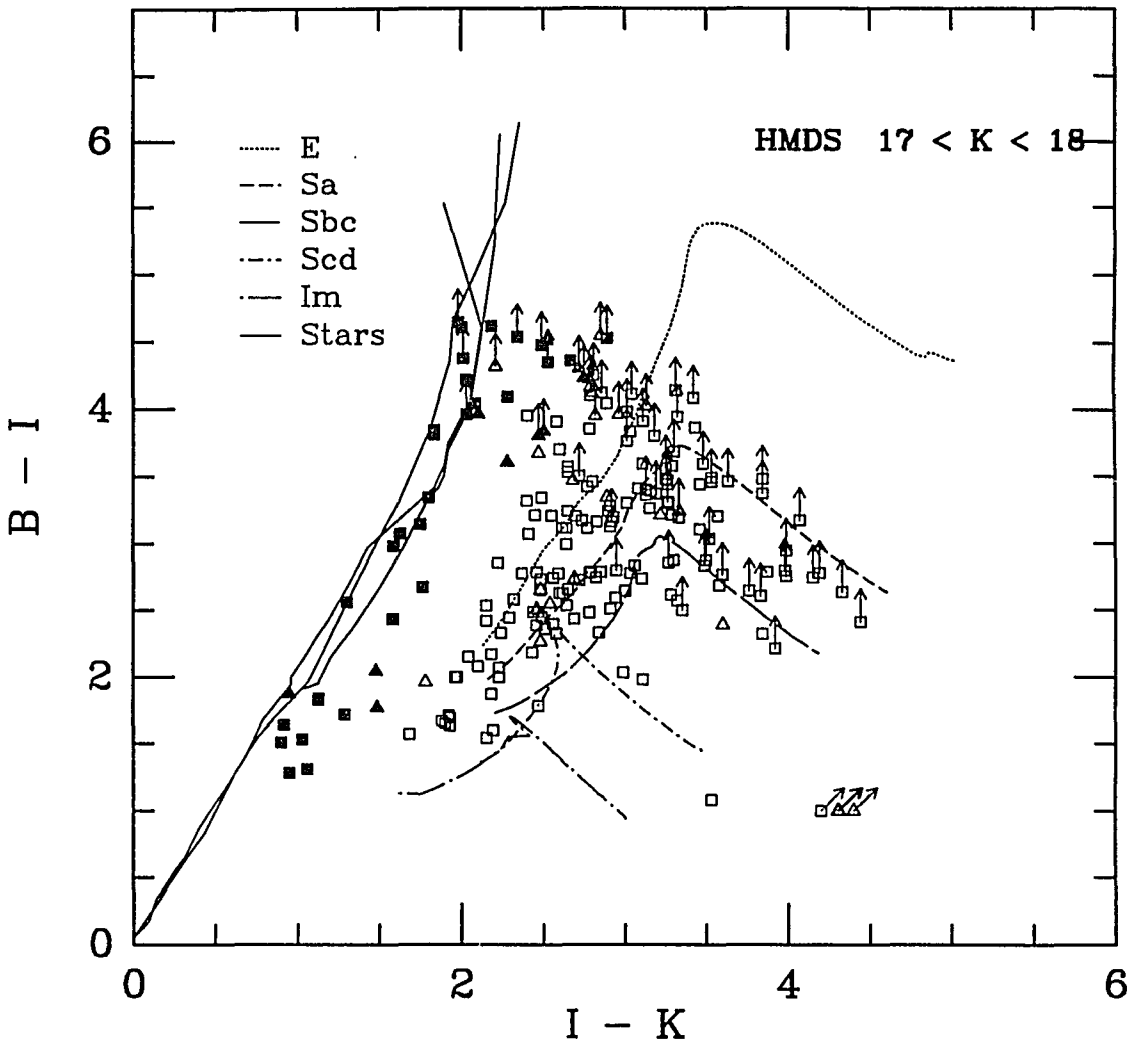

Figure 6.3e: B-I vs I-K - the HMDS data at 17 < K < 18. The models and symbols are the same as in figure 6.3b. The large number of galaxies undetected in B makes it difficult to interpret this figure. However, we begin to see some objects with the colors of unevolved high redshift spirals.

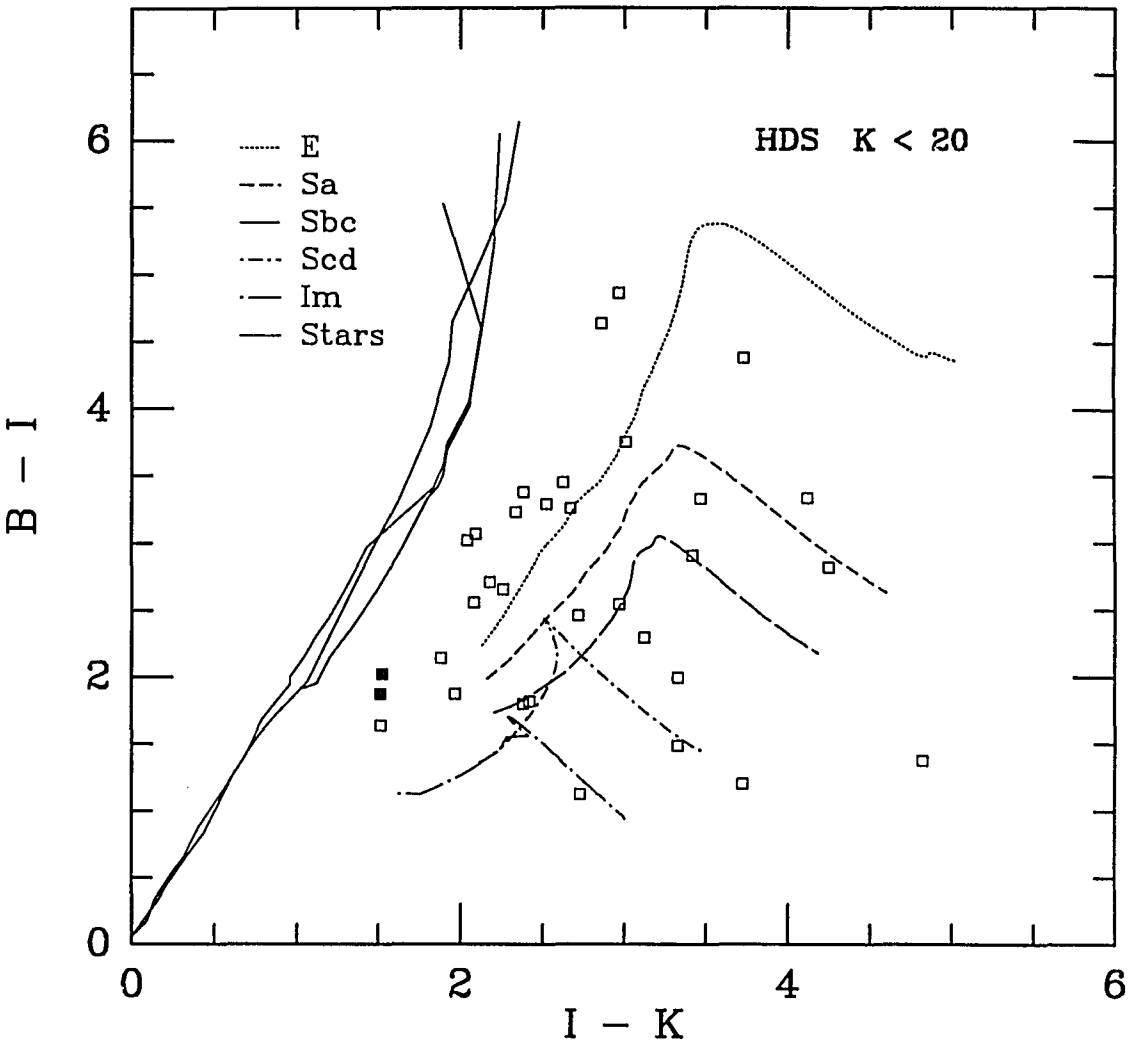

Figure 6.3f: B-I vs I-K - the HDS data at K < 20. The models and symbols are the same as in figure 6.3b. The galaxies at this magnitude level are no longer clustering around the elliptical and Sa galaxy line. There are several objects with the colors of unevolved high redshift spirals, and few with the colors of unevolved high redshift ellipticals.

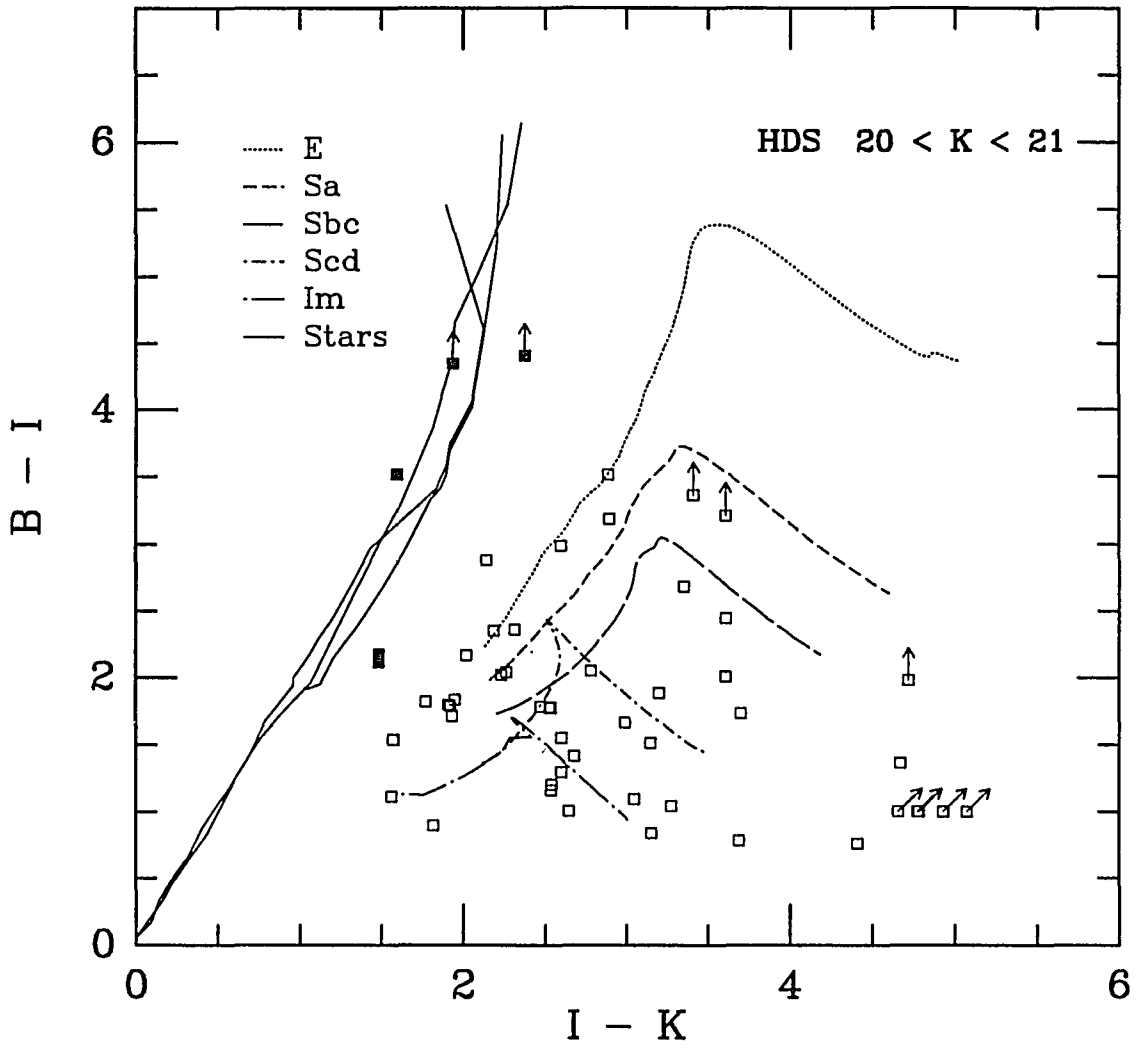

Figure 6.3g: B-I vs I-K - the HDS data at 20 < K < 21. The models and symbols are the same as in figure 6.3b. The trend away from the colors of unevolved ellipticals is dramatic, as there are almost no galaxies on that line. Nearly every galaxy has the colors of unevolved high redshift spiral and irregular galaxies. It should be noted, however, that this does not mean that the galaxies are actually at high redshift, as clearly there is some form of evolution operating.

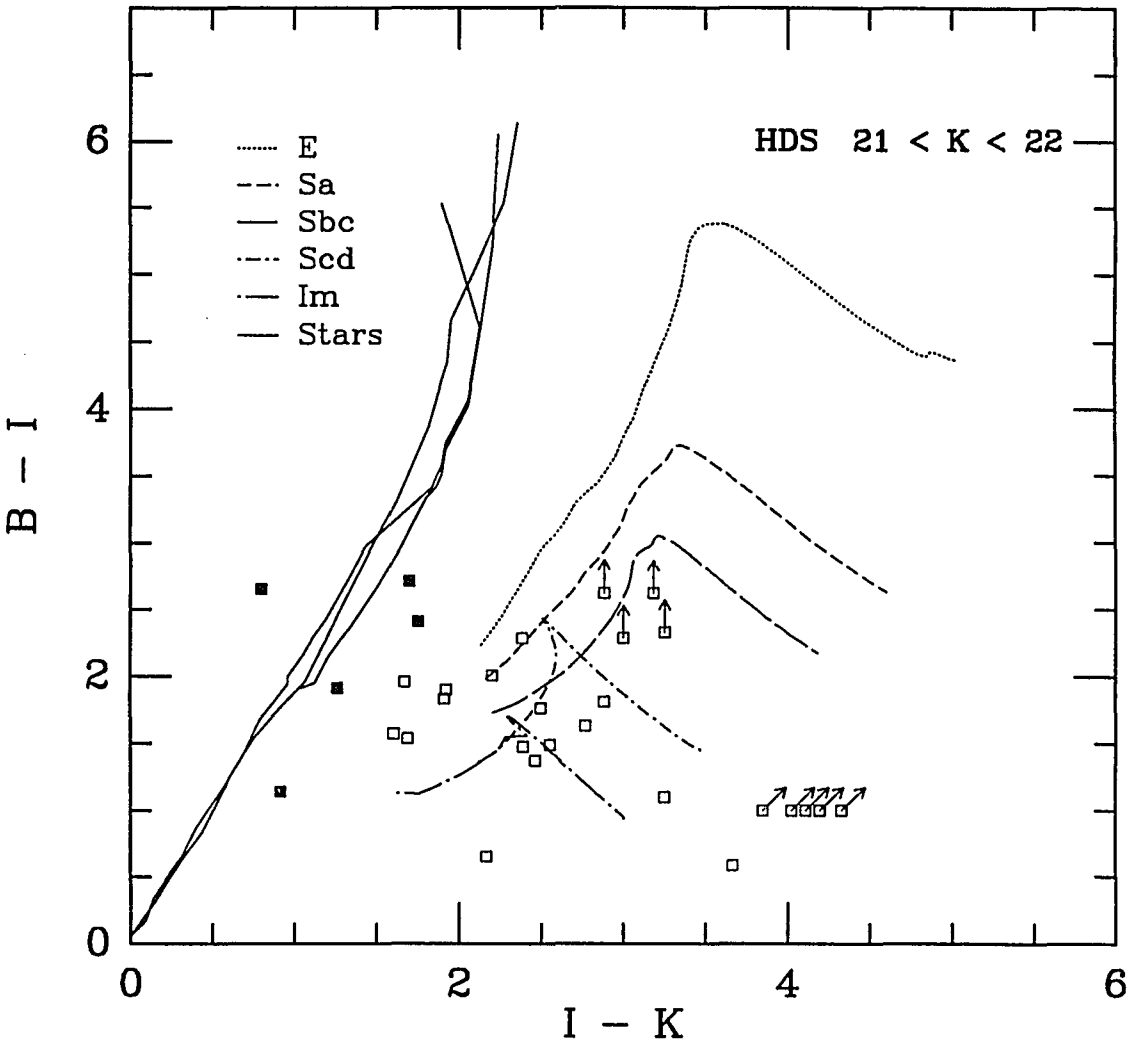

Figure 6.3h: B-I vs I-K - the HDS data at 21 < K < 22. The models and symbols are the same as in figure 6.3b. At the faint limit of the HDS, the trend to bluer galaxies is most extreme. The small number of detected objects makes it difficult to interpret this figure, but there are clearly very few red objects, even when the lower limits are taken into account.

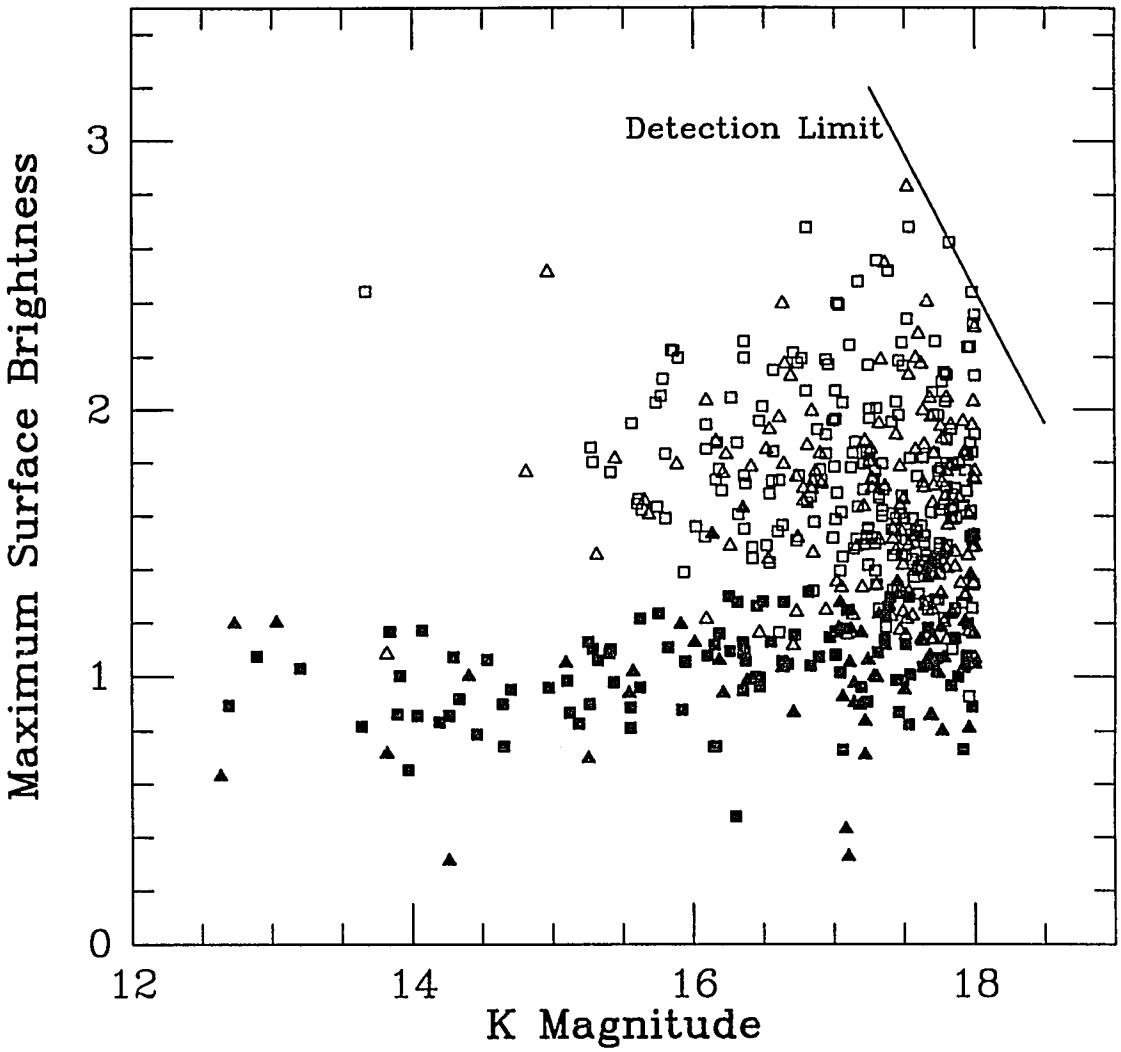

Figure 6.4: Surface brightness as a function of magnitude in the HMDS. The object finding programs were set with an initial contour limit of K = 20.37 magnitudes per square arcsecond, and a total photometry limit of K = 18. At the faint end, it can be seen that very few objects are missed by the program; however, going fainter would require corrections.

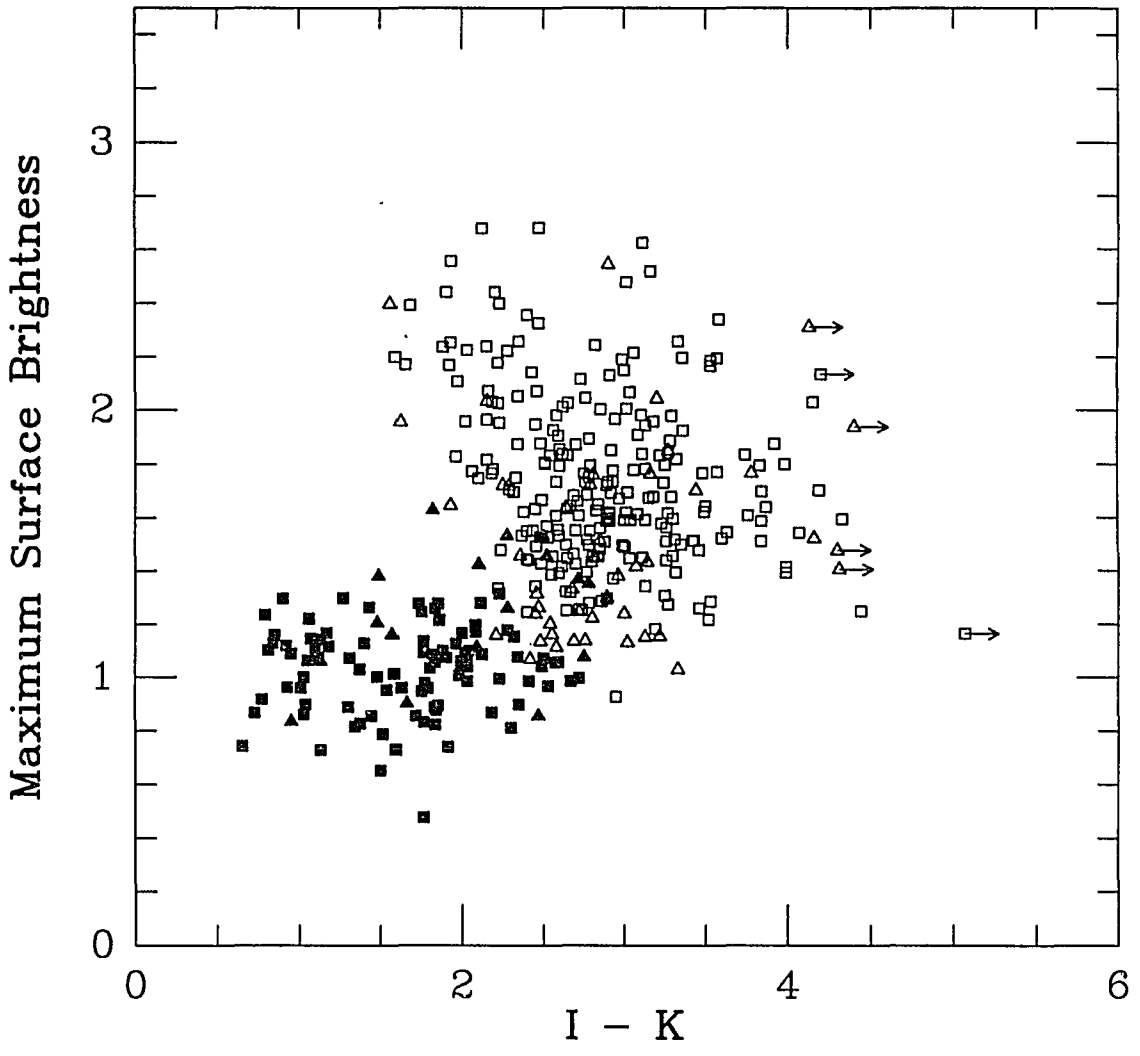

Figure 6.5: Surface brightness as a function of I-K color for the HMDS sample.

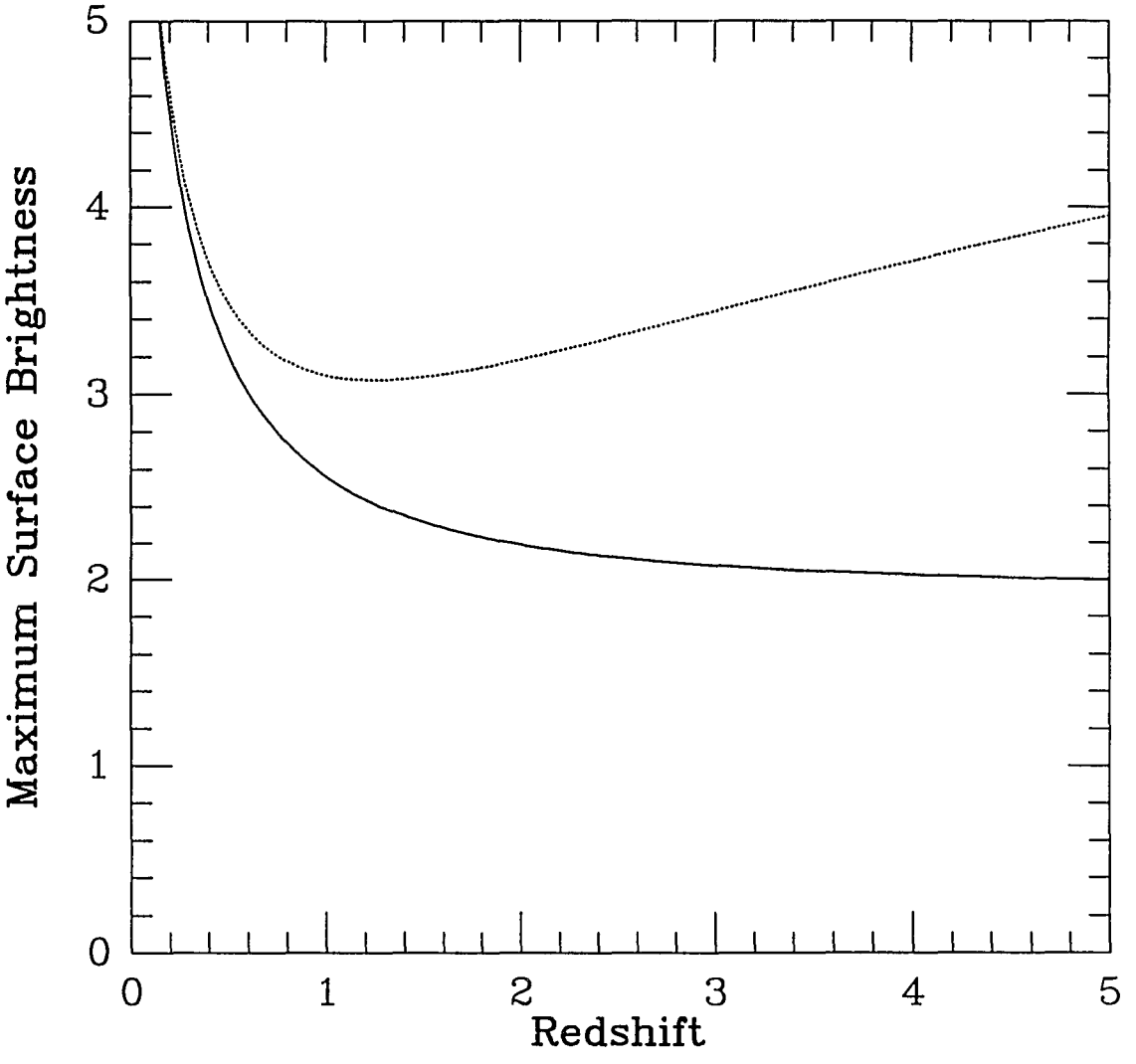

Figure 6.6: Functional dependence upon redshift of the quantities plotted in figures 6.4 and 6.5, for a constant surface brightness, constant galactic radius model. The solid line represents $q_0 = 0.02$, and the dotted line represents $q_0 = 0.5$.

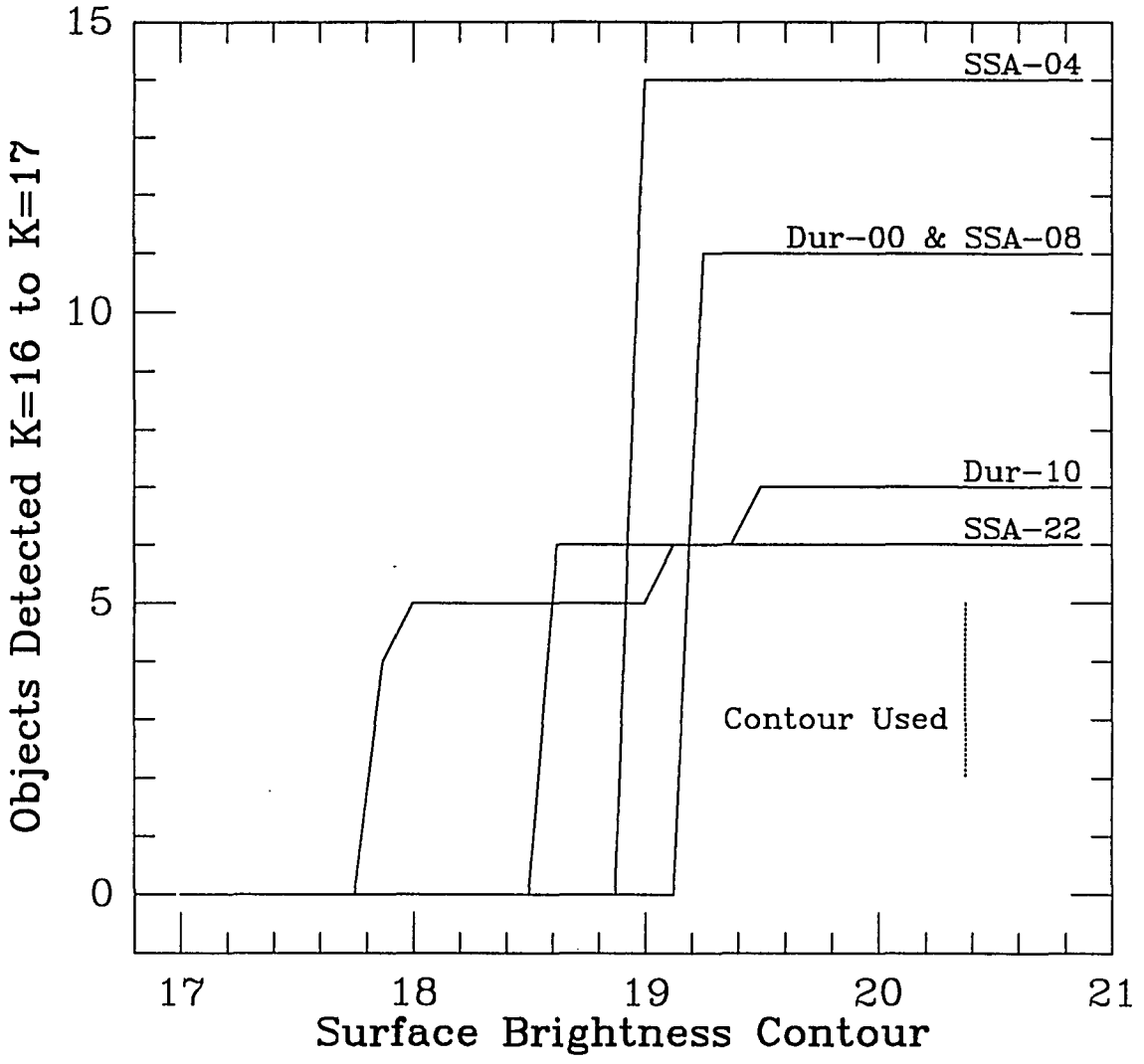

Figure 6.7: The number of objects detected in the HMDS between K = 16 and K = 17 as a function of the surface brightness contour level used in the image detection program.

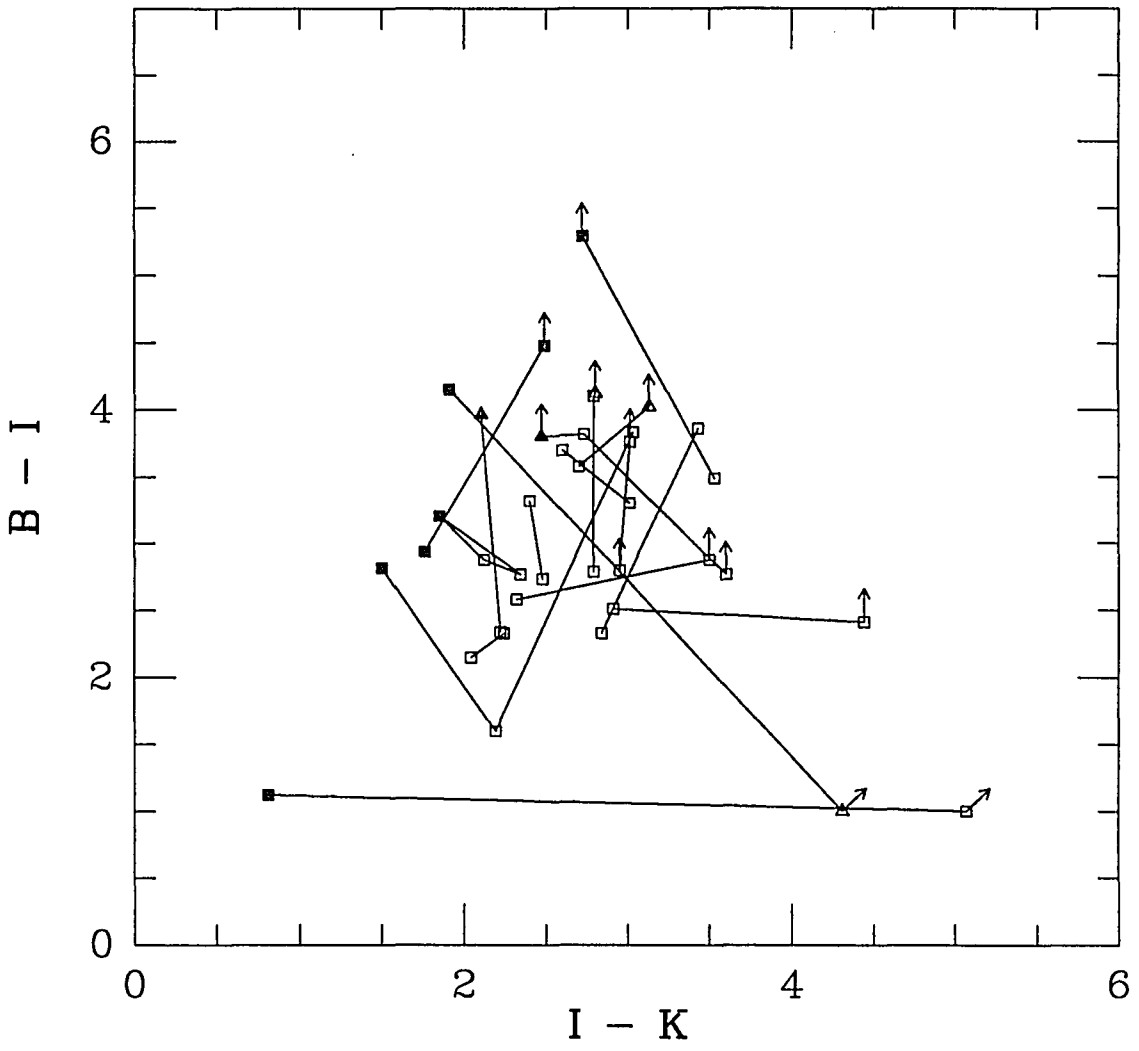

Figure 6.8: A plot of the I-K vs B-I colors for objects which have neighbors within 6.375 arcseconds. A Baron and White (1987) type of primeval galaxy would appear as a small group of galaxies with similar colors.

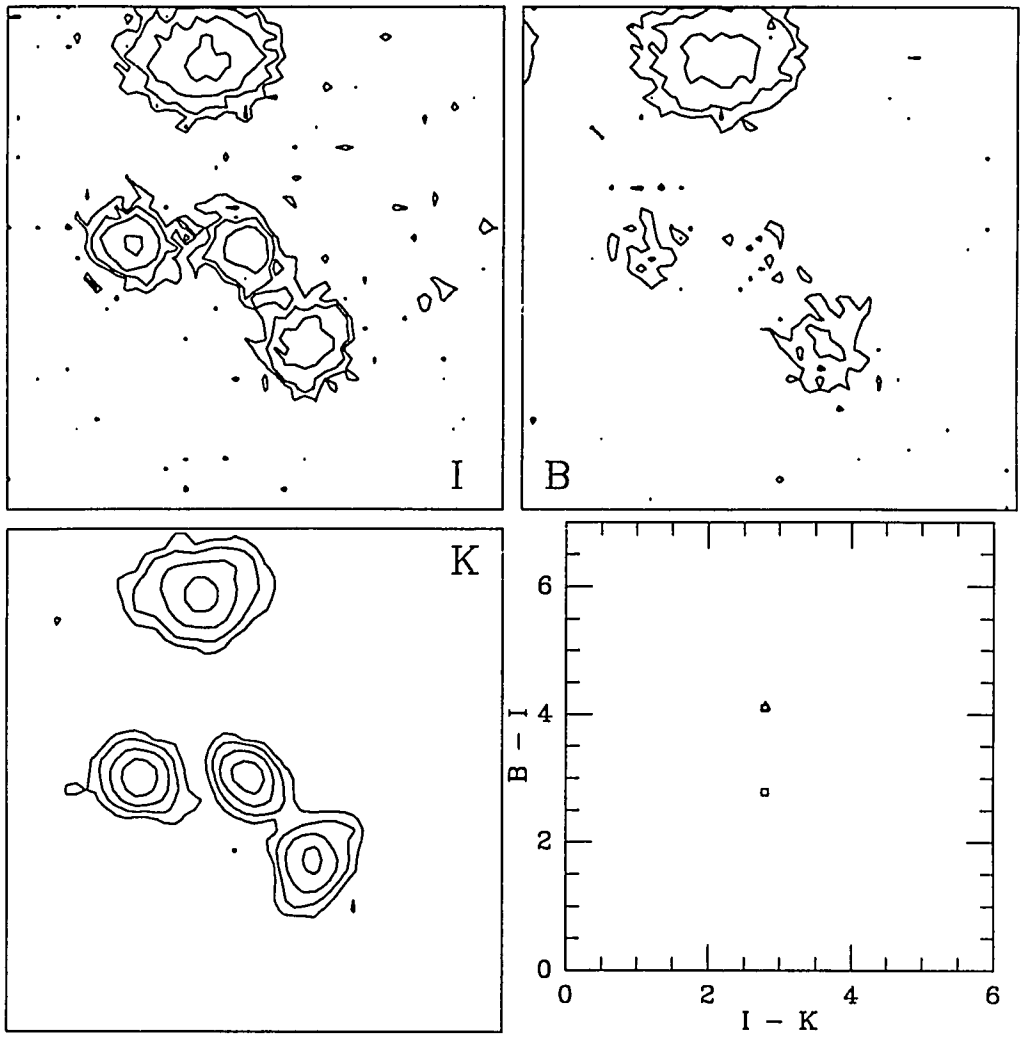

Figure 6.9a: Contour plots in K, I and B and a color diagram for multiple objects in the HMDS. This triple object appears to be three distinct galaxies, rather than a Baron and White (1987) type of primeval galaxy.

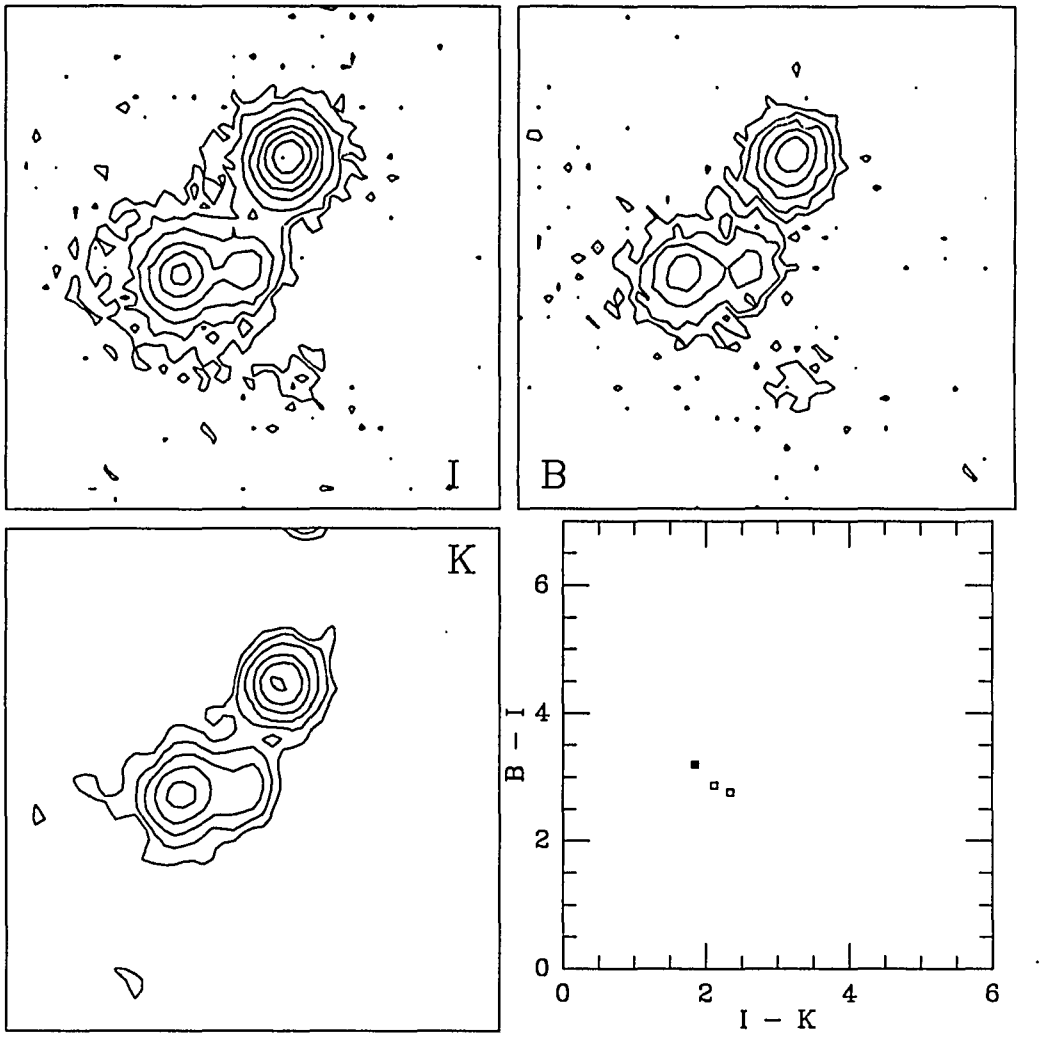

Figure 6.9b: A triple object in the HMDS. There is a clearly defined foreground star superimposed upon two galaxies.

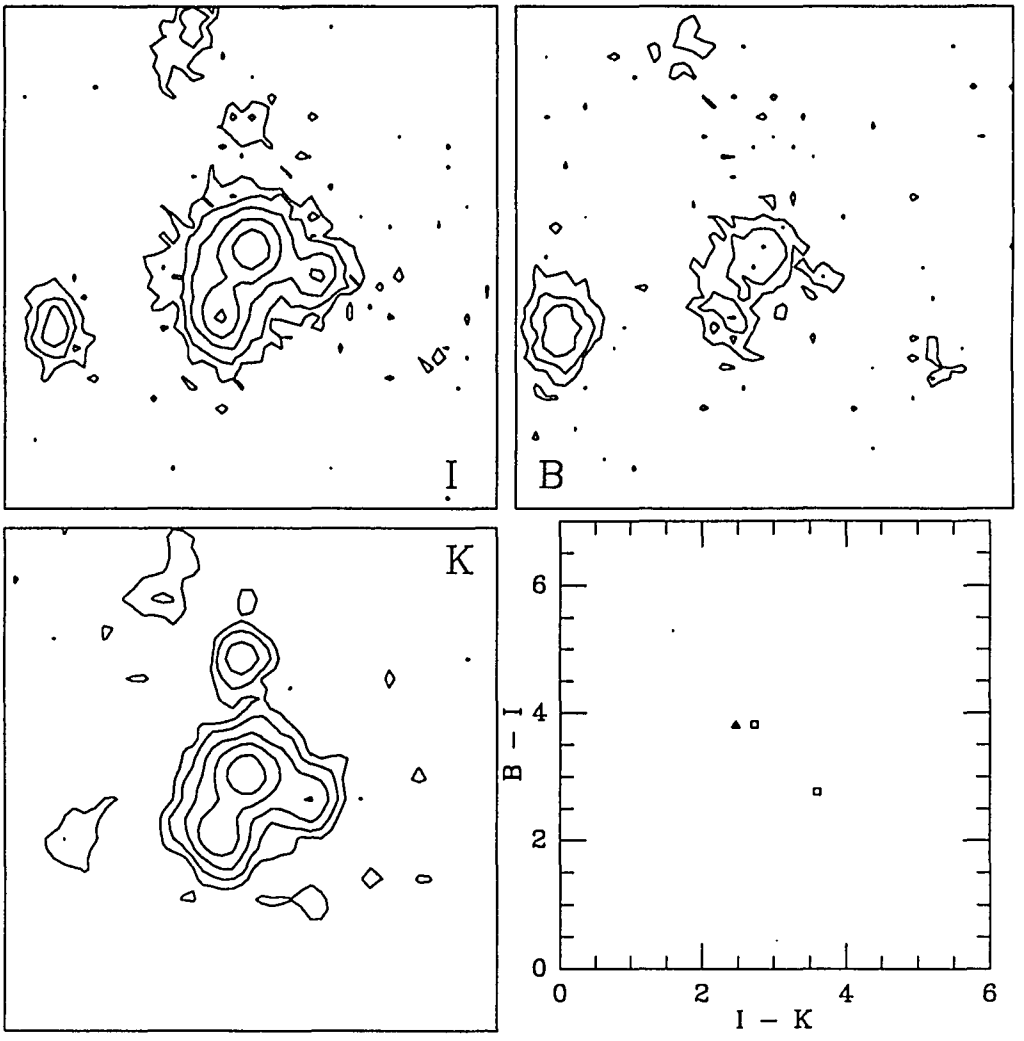

Figure 6.9c: A triple object in the HMDS. There is a clearly defined foreground star superimposed upon two galaxies.

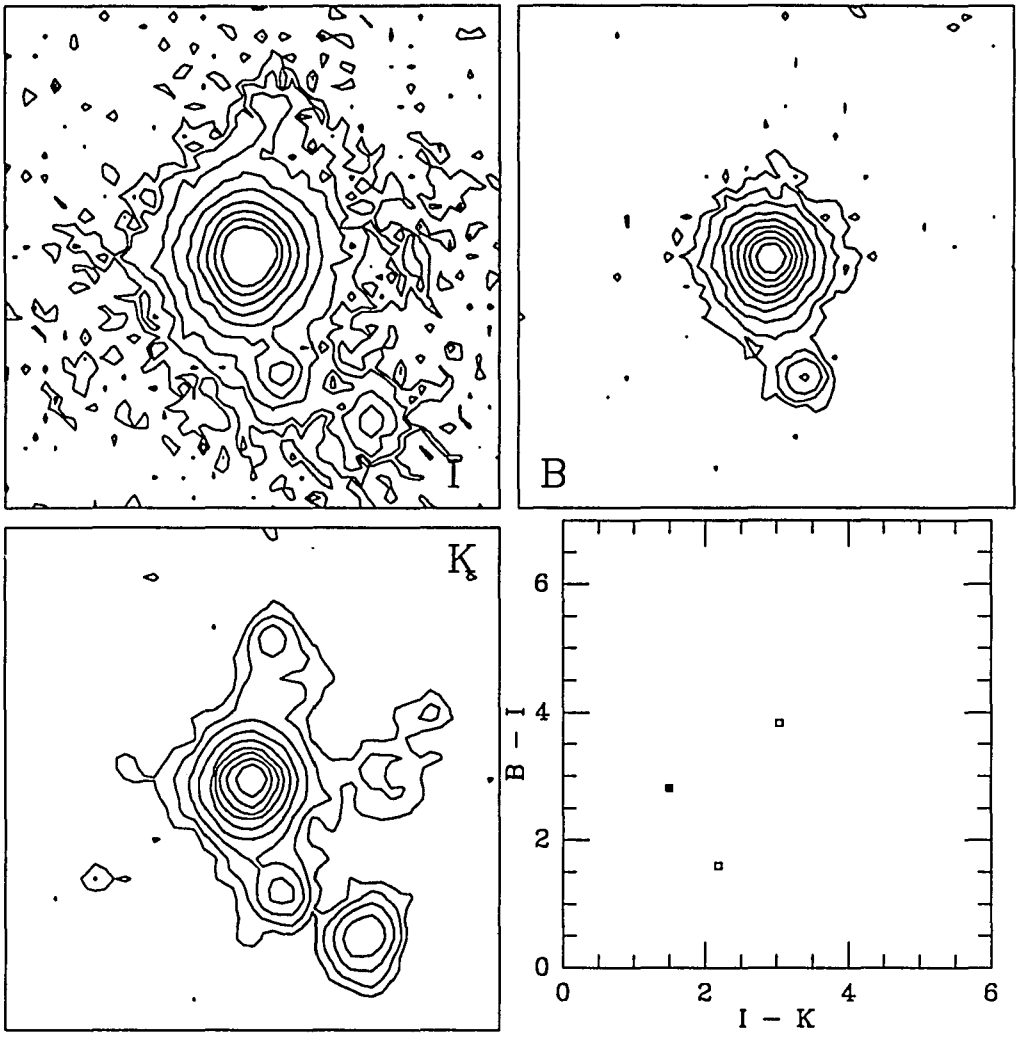

Figure 6.9d: A triple object in the HMDS. There is a clearly defined foreground star superimposed upon two galaxies.

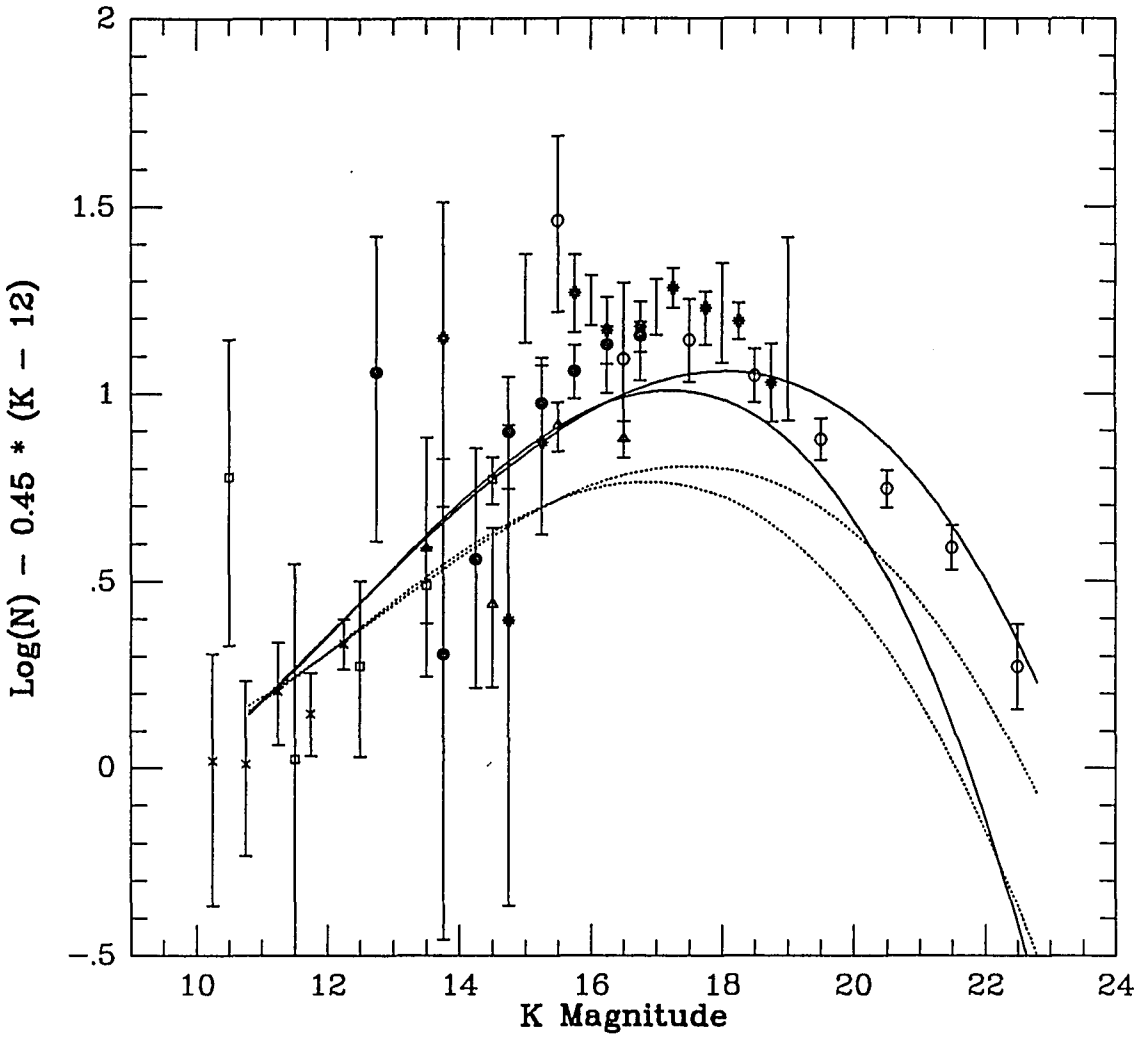

Figure 6.10: The K band number counts plotted against the models of Yoshii and Takahara (1988). The dotted lines are the no evolution model, with $q_0 = 0.5$ (lower line) and $q_0 = 0.02$. The solid lines include the effects of luminosity evolution with $z_{form} = 5$.

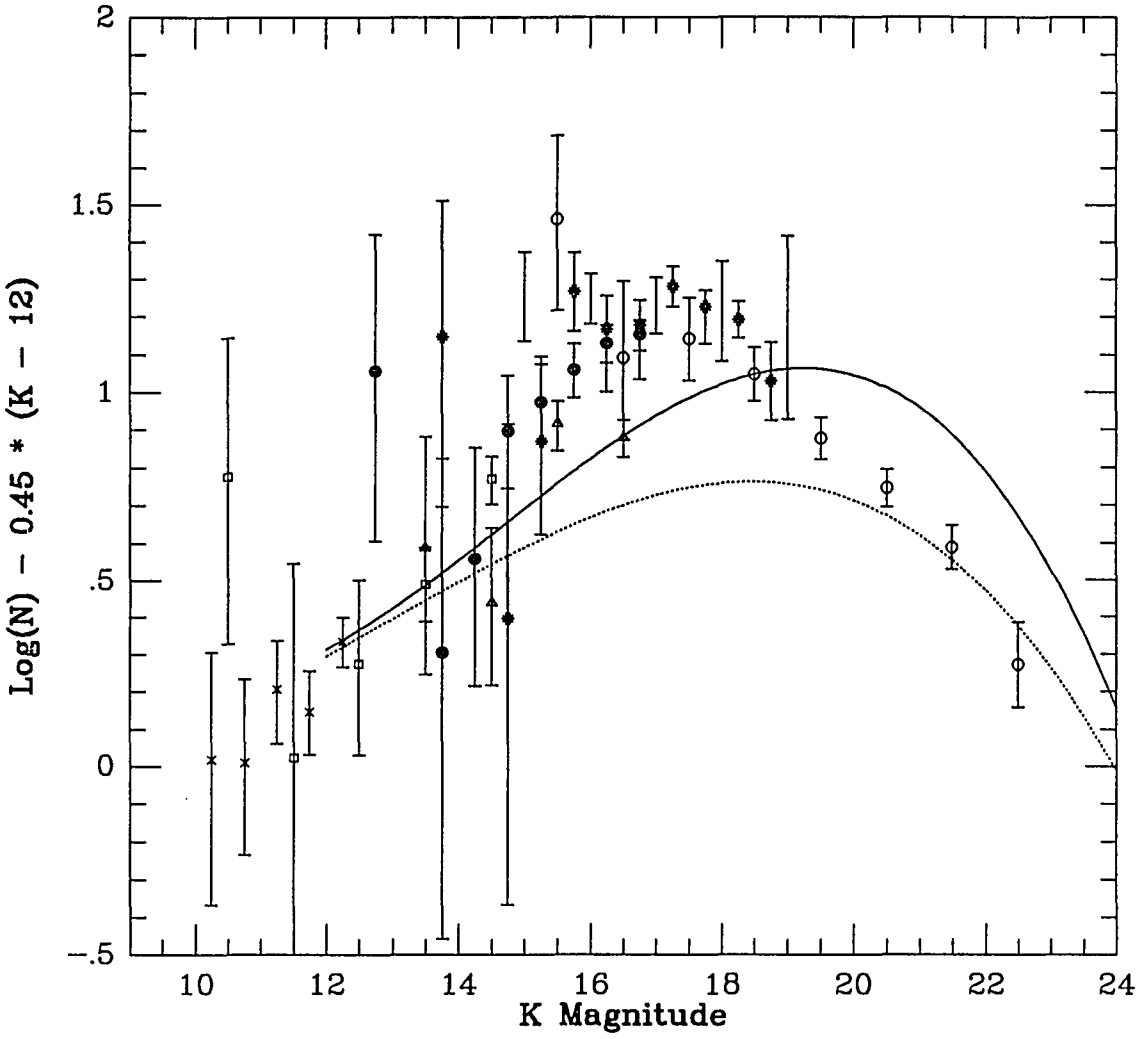

Figure 6.11: The K band number counts plotted against a model with $\Lambda = 0.9$, and $\Omega = 0.1$. The dotted line is a no-evolution model, while the solid line includes YT luminosity evolution. This model is attractive in that it predicts the B band counts, and redshift survey data accurately, however, it overpredicts the K counts at the faint end.

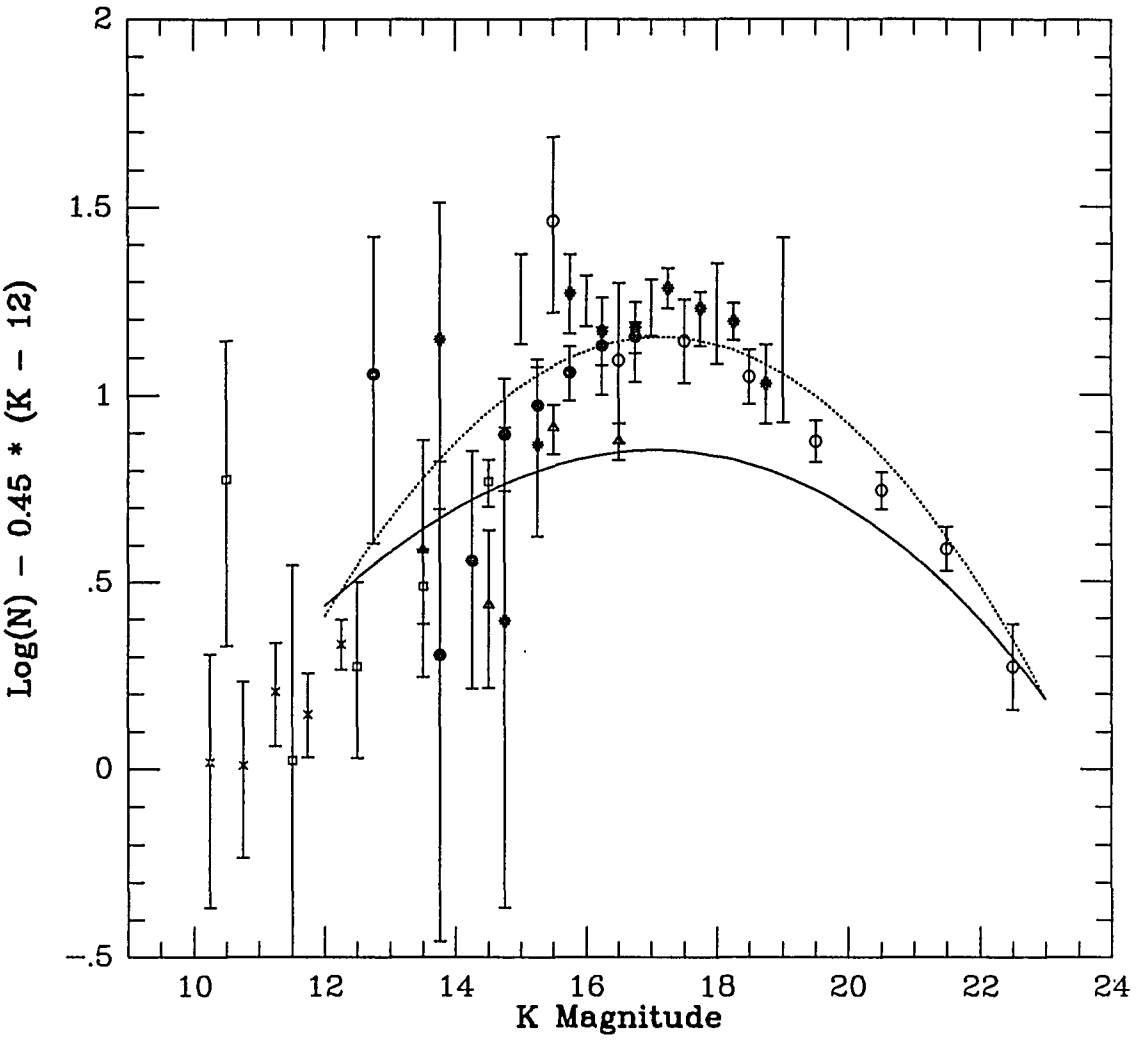

Figure 6.12: The K band number counts plotted against a model with merging. The dotted line is Bruzual luminosity evolution with $q_0 = 0.0$. The solid line is a model in which the product $M^*\phi^*$ is kept constant, but 4-6 galaxies at a redshift of $z \approx 1$ merge to form each present day galaxy. This model fits the B band counts and the redshift distribution at B = 21 to B = 22.5. In addition, the behavior seen in the color data, in which few galaxies with the colors of elliptical galaxies at $z \approx 1$, is consistent with this model.